

Dynamics of legged locomotion: Models, analyses, and challenges

Philip Holmes¹, Robert J. Full², Dan Koditschek³ and John Guckenheimer⁴

¹ Department of Mechanical and Aerospace Engineering,
and Program in Applied and Computational Mathematics,
Princeton University, Princeton, NJ 08544, U.S.A.

² Department of Integrative Biology,
University of California, Berkeley, CA 94720, U.S.A.

³ Department of Electrical Engineering and Computer Science,
University of Michigan, Ann Arbor, MI 48109, U.S.A.

⁴ Department of Mathematics and Center for Applied Mathematics,
Cornell University, Ithaca, NY 14850, U.S.A.

pholmes@math.princeton.edu, rjfull@socrates.Berkeley.edu
kod@umich.edu, gucken@cam.cornell.edu

March 19, 2004

Abstract

Cheetahs and beetles run, dolphins and salmon swim, and bees and birds fly with grace and economy surpassing our technology. Evolution has shaped the breathtaking abilities of animals, leaving us the challenge of reconstructing their targets of control and mechanisms of dexterity. In this review we explore a corner of this fascinating world. We describe mathematical models for legged animal locomotion, focusing on rapidly running insects, and highlighting achievements and challenges that remain. Newtonian body-limb dynamics are most naturally formulated as piecewise-holonomic rigid body mechanical systems, whose constraints change as legs touch down or lift off. Central pattern generators and proprioceptive sensing require models of spiking neurons, and simplified phase oscillator descriptions of ensembles of them. A full neuro-mechanical model of a running animal requires integration of these elements, along with proprioceptive feedback and models of goal-oriented sensing, planning and learning. We outline relevant background material from neurobiology and biomechanics, explain key properties of the hybrid dynamical systems that

underlie legged locomotion models, and provide numerous examples of such models, from the simplest, completely soluble ‘peg-leg walker’ to complex neuro-muscular subsystems that are yet to be assembled into models of behaving animals.

1 Introduction

The question of how animals move may seem a simple one. They push against the world, with legs, fins, tails, wings or whole bodies, and the rest is Newton’s third and second laws. A little reflection reveals, however, that locomotion, like other animal behaviors, emerges from complex interactions among animals’ neural, sensory and motor systems, their muscle-body dynamics, and their environments [DFF⁺00]. This has led to three broad approaches to locomotion. Neurobiology emphasizes studies of central pattern generators (CPGs): networks of neurons in spinal cords of vertebrates and invertebrate thoracic ganglia, capable of generating muscular activity in the absence of sensory feedback (e.g. [Get88, CRE88, Pea00]). CPGs are typically studied in preparations isolated *in vitro*, with sensory inputs and higher brain ‘commands’ removed [CRE88, Gri99], and sometimes in neonatal animals. A related, reflex-driven approach concentrates on the role of proprioceptive¹ feedback in shaping locomotory patterns [Pea93]. Finally, biomechanical studies focus on body-limb-environment dynamics (e.g. [Ale03]) and usually ignore neural detail. No single approach can encompass the whole problem, although each has amassed vast amounts of data.

We believe that mathematical models, at various levels and complexities, can play a critical role in synthesizing parts of these data by developing unified *neuromechanical* descriptions of locomotive behavior, and that in this exercise they can guide the understanding of other biological systems, as well as bio-inspired robots. This review introduces the general problem, and, taking the specific case of rapidly running insects, describes models of varying complexity, outlines analyses of their behavior, compares their predictions with experimental data, and identifies a number of specific mathematical questions and challenges.

Guided by previous experience with both mathematical and physical (robot) models, we postulate that successful locomotion depends upon a hierarchical family of control loops. At the lowest end of the neuromechanical

¹Proprioceptive: activated by, related to, or being stimuli produced within the organism (as by movement or tension in its own tissues) [Gov85]; thus: sensing of the body, as opposed to exteroceptive (sensing of the external environment).

hierarchy, we hypothesize the primacy of mechanical feedback or *preflexes*²: neural clock-excited and tuned muscles acting through chosen skeletal postures. Here biomechanical models provide the basic description, and we are able to get quite far using simple models in which legs are represented as passively sprung, massless links. Acting above and in concert with this bottom layer, we hypothesize sensory, feedback-driven reflexes that further increase an animal’s stability and dexterity, by suitably adjusting the CPG and motoneuron outputs. Here modelling of neurons, neural circuitry and muscles is central. At the highest level, goal-oriented behaviors such as foraging or predator-avoidance employ environmental sensing and operate on a stride-to-stride timescale to ‘direct’ the animal’s path. More abstract notions of connectionist neural networks and information and learning theory are appropriate at this level, which is perhaps the least well-developed mathematically.

Some personal history may help to set the scene. This paper, and some of our recent work on which it draws, has its origins in a remarkable IMA workshop on gait patterns and symmetry held in June 1998, that brought together biologists, engineers and mathematicians. At that workshop, one of us (RJF) pointed out that insects can run stably over rough ground at speeds high enough to challenge the ability of proprioceptive sensing and neural reflexes to respond to perturbations ‘within a stride.’ Motivated by his group’s experiments on, and modeling of, the cockroach *Blaberus discoidalis* [FT90, FT91b, TBF94, KF99], and by the suggestion of Brown and Loeb that, in rapid movements, ‘detailed’ neural feedback (reflexes) might be partially or wholly replaced by largely mechanical feedback (preflexes) [BSL95, LBC99, BL00], we formulated simple mechanical models within which such hypotheses could be made precise and testable. Using these models, examples of which are described in §5 below, we confirmed the reflex hypothesis by showing that a simple, energetically-conservative model with passive elastic legs can produce asymptotically stable gaits [SH00b, SH00a, SGR⁺02]. This prompted ‘controlled impulse’ perturbation experiments on rapidly running cockroaches [JF02] that strongly support the reflex hypothesis in *Blaberus*, as well as our current development of more realistic models incorporating actuated muscles.

Workshop discussions in which we all took part also inspired the creation of RHex, a six-legged robot whose unprecedented mobility suggests that en-

²Brown and Loeb [BL00, Section 3] define a reflex as ‘the zero-delay, intrinsic response of a neuromusculoskeletal system to a perturbation’ and they note that they are programmable via preselection of muscle activation.

gineers can aspire to achieving the capabilities of such fabulous runners as the humble cockroach [SBK01]. In turn, since we know (more or less) their ingredients, such robots can help us better understand the animals that inspired them. Mathematical models allow us to translate between biology and engineering, and our ultimate goal is to produce a model of a ‘behaving insect’ that can also inform the design of novel legged machines. More specifically, we envisage a range of models, of varying complexity and analytical tractability, that will allow us to pose and probe, via simulation and physical machine and animal experimentation, the mechanisms of locomotive control.

Biology is a broad and rich science, collectively producing vast amounts of data that may seem overwhelming to the modeller. (In [Ree04], Michael Reed provides a beautifully clear perspective directed to mathematicians in general, sketching some of the difficulties and opportunities.) Our earlier work has nonetheless convinced us that simple models, which, in an exercise of creative neglect, ignore or simplify many of these data, can be invaluable in uncovering basic principles. We call such a model, containing the smallest number of variables and parameters that exhibits a behavior of interest, a *template* [FK99]. In robotics applications, we hypothesize the template as an attracting invariant submanifold on which the restricted dynamics takes a form prescribed to solve the specific task at hand (e.g. [BK90, RK94, NFK00, WGK03]). In both robots and animals, we imagine that templates are composed [KK02] to solve different tasks in various ways by a supervisory (CNS) controller. The spring-loaded inverted pendulum (SLIP), introduced in §2.2 and described in more detail in §4.4, is a classical locomotion template that represents the center of mass behavior of diverse legged animals [CHT77, BF93].

Most of the models developed below are templates, but we shall describe at least some of the ingredients of a more complete and biologically-realistic model: an *anchor* in the terminology of [FK99]. A model representing the neural circuitry of a CPG, motoneurons, muscles, individual limb segments and joints, and ground contact effects, would exemplify an anchor. In spite of such complexity, it is a fact that, under suitable conditions, animals with diverse morphologies and leg numbers, and many mechanical and yet more neural degrees of freedom, run as if their mass centers were following SLIP dynamics [CHT77, BF93, FF00]. Part of our challenge is to explain how their reflex and reflex control circuits make their complex anchors appear to behave like this simple template, and to understand why nature should exercise such a mathematically attractive reduction of complexity: a process sketched in Fig. 1. To whet the appetites of dynamical systems aficionados:

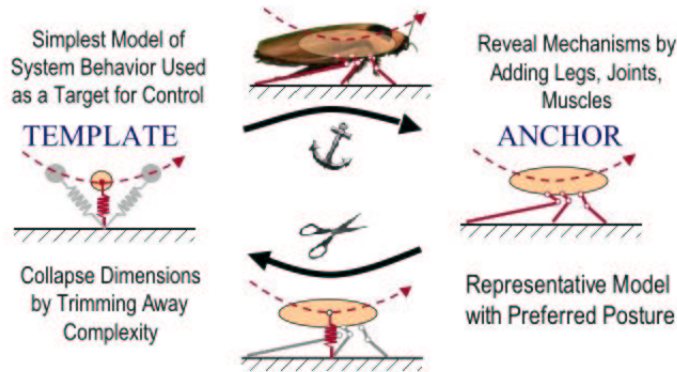


Figure 1: Templates and anchors. Schematic adapted from Full [?].

reduction to a center or inertial manifold does not alone explain this, but such ideas are central to the development of these ideas in robotics and also seem likely to play a helpful role in elucidating biological principles.

Legged locomotion appears to be more tractable than swimming or flying, especially at moderate or high Reynolds numbers, since discrete reaction forces from a (relatively) rigid substrate are involved, rather than fluid forces requiring integration of the unsteady Navier-Stokes equations (but see the comments on foot-contact forces in §2.3). Nonetheless, even at the simplest level, legged locomotion models have unusual features. Idealizing to a rigid body with massless elastic legs, or to a linkage of rigid elements with torsional springs at the joints, we produce a mechanical system, but these systems are not classical. As feet touch down and lift off, the constraints defining the Lagrangians change. The resulting ordinary differential equations of motion describe *piecewise-holonomic* mechanical systems, examples of more general *hybrid dynamical systems* [BGM93], in which evolution switches among a finite set of vector fields, driven by event-related rules determined by the location of solutions in phase space. We shall meet our first example in §2.1, and we discuss some properties of these systems in more detail in §§4-5.

This paper’s contents are as follows. §2 reviews earlier work on loco-

motion and movement modeling, introducing relevant mechanical, biomechanical, neurobiological, and robotics background, and §3 summarises key experimental work on walking and running animals that inspires and informs previous and current modeling efforts. In §4 we digress to describe an important class of hybrid dynamical systems that are central to locomotion models, and we describe some features of their analytical description, and numerical issues that arise in simulations, ending with a sketch of the classical SLIP model. §5 concentrates on models of horizontal plane dynamics of sprawled-posture animals, insects in particular. We start with a simple model of passive bipedal walking, special cases of which are (almost) soluble in closed form. We successively add more realistic features, culminating in our current hexapedal models that include CPG, motoneuron and muscle models, and demonstrating throughout that the basic features of stable periodic gaits, possessed by the simplest templates, persist. We summarise and outline some major challenges in §6.

We shall draw on a broad range of ‘whole animal’ integrative biology, biomechanics, and neurobiology, as well as control and dynamical systems theory, including perturbation methods. We introduce relevant ideas from these disparate fields as they are needed, mostly via simple explicit examples. Unlike genomics, locomotion studies are relatively mature: recent progress in neurophysiology, biomechanics, and nonlinear control and systems theory has poised us to unlock how complex, dynamical, musculoskeletal systems create effective behaviors, but a substantial task of synthesis remains. We believe that the language and methods of dynamical systems theory in particular, and mathematics in general, can assist that synthesis. Thus, our main goal is to introduce an emerging field in biology to applied mathematicians, drawing on relatively simple models both as examples of successful approaches and sources of interesting mathematical problems, some of which we highlight as **Questions**. Our presentation therefore differs from that of many Surveys and Reviews appearing in this journal in that we focus on modelling issues rather than mathematical methods per se. The models are, of course, formulated with the tools available for their analysis in mind, we sketch results that these tools afford, and we provide an extensive bibliography wherein mathematical results and details may be found.

We hope that this article will encourage the sort of multi-disciplinary collaboration that we – a biologist, two applied mathematicians, and an engineer – have enjoyed over the past five years, and that it will stimulate others to go beyond our own efforts.

2 Three traditions: biomechanics, neurobiology and robotics

In developing our initial locomotion models, we discovered some relevant parts of three vast literatures. The following selective survey may assist the reader who wishes to acquire working background knowledge.

2.1 Holonomic, nonholonomic, and piecewise-holonomic mechanics

Before introducing a key locomotion model in §2.2, the SLIP, we recall some basic facts concerning conservative mechanical and Hamiltonian systems. Holonomically constrained mechanical systems, such as linkages and rigid bodies, admit canonical Lagrangian and Hamiltonian descriptions [Gol80]. (Holonomic constraints are equalities expressed entirely in terms of configuration – position – variables; nonholonomic constraints involve velocities in an essential – ‘non-integrable’ – manner, or are expressed via inequalities). The symplectic phase spaces [Arn78] of holonomic systems strongly constrain the possible stability types of fixed points and periodic orbits: eigenvalues of the linearized ODEs occur in pairs or quartets [Arn78, AM85]: if λ is an eigenvalue, then so are $-\lambda$, $\bar{\lambda}$ and $-\bar{\lambda}$, where $\bar{\cdot}$ denotes complex conjugate. Thus, any ‘stable’ eigenvalue in the left-hand complex half-plane has an ‘unstable’ partner in the right-hand half-plane. Similar results hold for symplectic (Poincaré) mappings obtained by linearizing around closed orbits: an eigenvalue λ within the unit circle implies a partner $1/\lambda$ outside. Hence holonomic, conservative systems can at best exhibit neutral (Liapunov) stability.

2.1.1 Nonholonomic constraints and partial asymptotic stability

Nonholonomic constraints, in contrast, can lead to partial asymptotic stability. The Chaplygin sled [NF72] is an instructive example that also introduces other ideas that will recur. Consider an ‘ice-boarder’: a two-dimensional rigid body of mass m and moment of inertia I , free to move on a frictionless horizontal plane, equipped with a skate blade C , at a distance ℓ from the center of mass (COM) G , that exerts a force normal to the body axis: Fig. 2(a). The velocity vector at C is thereby constrained to lie along the body axis ($\mathbf{v}_C = v\hat{\mathbf{e}}_2$), although the body may turn about this point and v may take either sign (the skate can reverse direction). The angle θ specifies orientation in the inertial plane and the absolute velocity of G in terms of

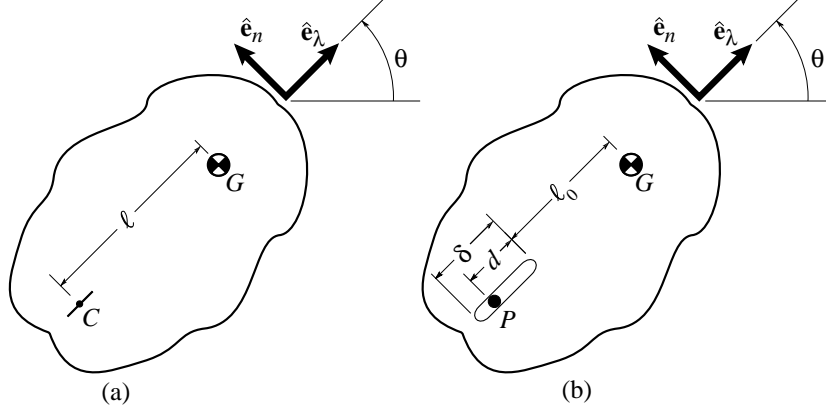


Figure 2: (a) The Chaplygin sled and (b) a piecewise-holonomic pegleg walker. Schematic adapted from Ruina [Rui98]. **Fig needs fixing, body coord basis vectors renaming, etc.!!!**

the body coordinate system is $\mathbf{v}_G = v \hat{e}_2 - l\dot{\theta} \hat{e}_1$.

Using the relations $\dot{\hat{e}}_1 = \dot{\theta} \hat{e}_2$, $\dot{\hat{e}}_2 = -\dot{\theta} \hat{e}_1$, we balance first linear momentum:

$$\mathbf{F} = F_c \hat{e}_1 = m(-\dot{\theta}v - l\ddot{\theta}) \hat{e}_1 + m(\dot{v} - l\dot{\theta}^2) \hat{e}_2; \quad (1)$$

and then angular momentum about C' , the non-accelerating point in an inertial frame instantaneously coincident with C :

$$0 = ml(v\dot{\theta} + l\ddot{\theta}) + I\ddot{\theta}. \quad (2)$$

These three (scalar) equations determine the constraint force and the equations of motion:

$$F_c = -m(\dot{\theta}v + l\ddot{\theta}), \quad (3a)$$

$$\dot{s} = v, \quad \dot{\theta} = \omega, \quad (3b)$$

$$\dot{v} = l\omega^2, \quad \dot{\omega} = \frac{-m\ell v\omega}{m\ell^2 + I}, \quad (3c)$$

where s denotes arclength (distance) travelled by the skate and ω is the body angular velocity. (Equations (3) can be derived in a Lagrangian framework [BKMR96], but the Newtonian force and moment balances given here appear simpler.)

Eqns. (3) have a three-parameter family of constant speed straight-line motion solutions: $\bar{\mathbf{q}} = \{\bar{s} + \bar{v}t, \bar{\theta}, \bar{v}, 0\}^T$. Linearizing (3) at $\bar{\mathbf{q}}$ yields eigenvalues $\lambda_{1-3} = 0$ and $\lambda_4 = -\left(\frac{m\ell\bar{v}}{m\ell^2 + I}\right)$. The first three correspond to a family

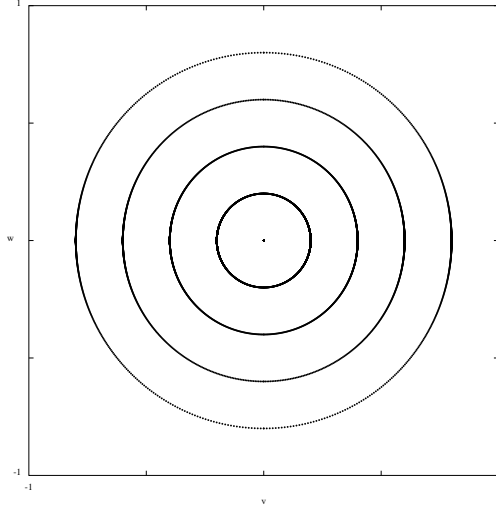


Figure 3: A phase portrait for the Chaplygin sled.

of solutions parameterized by starting point \bar{s} , velocity \bar{v} and heading $\bar{\theta}$; λ_4 indicates asymptotic stability for $\ell\bar{v} > 0$ and instability for $\ell\bar{v} < 0$: stable motions require that the mass center precede the skate.

The global behavior is perhaps best appreciated via a phase portrait in the *reduced* phase space (v, ω) of linear and angular velocity: Fig. 3. Noting that total kinetic energy,

$$T = \frac{mv^2}{2} + \frac{I\omega^2}{2}, \quad (4)$$

is conserved (since the constraint force $F_c \hat{e}_1$ is normal to \mathbf{v}_C and does no work), solutions of equations (3c) lie on the (elliptical) level sets of (4). The direction of the vector field, towards positive v , follows from the first of (3c). Explicit solutions as functions of time may be found in [CH99]. Taking $\ell > 0$ (skate behind COM), the line of fixed points $(\bar{v}, 0)$ with $\bar{v} < 0$ are unstable, while those with $\bar{v} > 0$ are stable. Typical solutions start with nonzero angular velocity, which may further grow, but which eventually decays exponentially as the solution approaches a fixed point on the positive v -axis. Angular momentum about the mass center G is *not* conserved since the constraint force exerts moments about G .

Fig. 3 also shows that the $\bar{v} > 0$ equilibria are only *partially* asymptotically stable; as noted above, they belong to a continuum of such equilibria and the eigenvalue with eigenvector in the \bar{v} direction is zero. Indeed,

the system is invariant under the group $SE(2)$ of planar translations and rotations, and COM position $\mathbf{x}_G = (x, y)$ and orientation θ are cyclic coordinates [Gol80]³. This accounts for the other two directions of neutral stability: \bar{s} and $\bar{\theta}$. Such translation and rotation invariance will be a recurring theme in our analyses of horizontal plane motions.

The full three-degree-of-freedom dynamics may be reconstructed from solutions $(v(t), \omega(t))$ of the reduced system (3c) by integration of (3b) to determine $(s(t), \theta(t))$, followed by integration of

$$\dot{x} = -v \sin \theta, \quad \dot{y} = -v \cos \theta \quad (5)$$

to determine the path in inertial space.

2.1.2 Piecewise-holonomic constraints: peg-leg walking

While the details of foot contact and joint kinematics, involving friction, deformation, and possible slipping, are extremely complex and poorly understood, one may idealize limb-body dynamics within a stance phase as a holonomically constrained system. As stance legs lift off and swing legs touch down the constraint geometry changes; hence, legged locomotion models are piecewise-holonomic mechanical systems. Here we describe perhaps the simplest example of such a system.

Ruina [Rui98] devised a discrete analog of Chaplygin’s sled, in which the skate is replaced by a peg, fixed in the inertial frame and moving along a slot of length d , whose front end lies a distance a behind the COM. When it reaches one end of the slot, it is removed and instantly replaced at the other. Fig. 2(b) shows the geometry: the coordinate system of 2(a) is retained. Ruina was primarily interested in the limit in which $d \rightarrow 0$ and the system approaches the continuous Chaplygin sled, but we noticed that the device constitutes a rudimentary and completely soluble, single-leg locomotion model: a peg-leg walker [CH99, SH00b]. The stance phase occurs while the peg is fixed, and (coincident) liftoff and touchdown correspond to peg removal and insertion. During stance the peg may slide freely, as in Ruina’s example [Rui98], move under prescribed forces or displacements $l(t)$, or move in response to an attached spring [SH00b]. Here we take the simplest case, supposing that $l(t)$ is prescribed and increases monotonically (the peg moves backward relative to the body, thrusting it forward). The models of §§4-5 will include passive springs and active muscle forces; also see [SH00b, §2].

³However, Noether’s theorem [Arn78] does *not* apply here: due to the constraint force neither linear nor angular momenta are conserved

Pivoting about the (fixed) peg, the body's kinetic energy may be written as

$$T = \frac{1}{2}m(\dot{l}^2 + l^2\dot{\theta}^2) + \frac{1}{2}I\dot{\theta}^2, \quad (6)$$

so the Lagrangian is simply $L = T$, and since $l(t)$ is prescribed, there is but one degree of freedom. Moreover, θ is a cyclic variable and Lagrange's equation simply states that

$$p_\theta = \frac{\partial L}{\partial \dot{\theta}} = (ml^2 + I)\dot{\theta} = \text{const.} : \quad (7)$$

angular momentum is conserved about P during each stride. However, at peg insertion, p_θ may suffer a jump due to the resulting angular impulse. Indeed, letting $\dot{\theta}(n^-)$ and $\dot{\theta}(n^+)$ denote angular velocities at the end of the $(n-1)$ 'st and beginning of the n 'th strides, and performing an angular momentum balance about the *new* peg position at which the impulsive force acts, we obtain the angular momentum in the n 'th stride as:

$$p_{\theta_n} = (ma^2 + I)\dot{\theta}(n^+) = ma(a+d)\dot{\theta}(n^-) + I\dot{\theta}(n^-).$$

Here the last expression includes the moment of linear momentum of the mass center at the end of the $(n-1)$ 'st stride, computed about the *new* peg position: $a \times m(a+d)\dot{\theta}(n^-)$. Replacing angular velocities by momenta via (7), this gives

$$p_{\theta_n} = \left[\frac{ma(a+d) + I}{m(a+d)^2 + I} \right] p_{\theta_{n-1}} \stackrel{\text{def}}{=} Ap_{\theta_{n-1}}. \quad (8)$$

Thus, angular momentum changes from stride to stride, unless $p_\theta = 0$, in which case the body is moving in a straight line along its axis. The change in body angle during the n 'th stride is obtained by integrating (7):

$$\theta((n+1)^-) = \theta(n^+) + p_{\theta_n} \int_0^\tau \frac{dt}{(ml^2(t) + I)} \stackrel{\text{def}}{=} \theta(n^+) + Bp_{\theta_n}, \quad (9)$$

where τ is the stride duration.

Equations (8-9) form the (linear) stride-to-stride Poincaré map:

$$\begin{pmatrix} \theta_{n+1} \\ p_{\theta_{n+1}} \end{pmatrix} = \begin{bmatrix} 1 & B \\ 0 & A \end{bmatrix} \begin{pmatrix} \theta_n \\ p_{\theta_n} \end{pmatrix}, \quad (10)$$

whose eigenvalues are simply the diagonal matrix elements. Echoing the ODE example of equations (3c) above, with its zero eigenvalue, one eigenvalue is unity, corresponding to rotational invariance, and asymptotic behavior is determined by the second eigenvalue A : if $|A| < 1$, $p_{\theta_n} \rightarrow 0$ as

$n \rightarrow \infty$ and θ approaches a constant value: the body tends towards motion in a straight line at average velocity $v = \frac{1}{\tau} \int_0^\tau \dot{l}(t) dt = d$, with final orientation θ determined by the initial data. From (8), $A < 1$ for all $I, m, d > 0$ and $a > -d$, and $A > -1$ provided that $I > md^2/16$; for $a < -d$, $A > 1$. Hence, if the back of the slot lies behind G and the body shape and mass distribution are ‘reasonable’, we have $|A| < 1$ (e.g., a uniform elliptical body with major and minor axes b, c , has $I = m(b^2 + c^2)/16$ and $b > d$ is necessary to accommodate the slot, implying that $I > md^2/16$).

Unlike the original Chaplygin sled, this discrete system is not conservative: energy is lost due to impacts at peg insertion (except in straight line motion), and energy may be added or removed by the prescribed displacement $l(t)$. However, regardless of this, the angular momentum changes induced by peg insertion determine stability with respect to angular velocity, and, if $|A| < 1$, the discrete sled asymptotically ‘runs straight.’ We shall see similar behavior in the energetically conservative models of §4.4 and §5.1. Also, here the stance dynamics is trivially summarized by conservation of angular momentum (7), and the stride-to-stride angular momentum mapping (8) determines stability. In more complex models, combinations of continuous dynamics within stance and touchdown/liftoff switching or impact maps are involved, resulting in higher-dimensional Poincaré maps, e.g. [McG90, GCRC98] and see §5.

2.2 Mechanical models and legged machines

As noted in the Introduction, diverse species that differ in leg number and posture, while running fast, exhibit center of mass (COM) motions approximating that of a spring-loaded inverted pendulum (SLIP) in the sagittal (vertical) plane [Bli89, MC90, BF93, FF00]. The same model also describes the gross dynamics of legged machines such as RHex [AMK⁺01, AKH04a], and as we shall show in §5, a second template model inspired by SLIP, the lateral leg spring (LLS) [SH00b, SGR⁺02] accounts equally well for horizontal plane dynamics. We shall briefly describe the SLIP and summarise some of the relevant mathematical work on it, returning to it in more detail in §4. Further details of the biological data summarised below can be found in §3.

At low speeds animals walk by vaulting over stiff legs acting like inverted pendula, exchanging potential and kinetic energy. At faster speeds, they bounce like pogo sticks, exchanging potential and kinetic energy with elastic strain energy. In running humans, dogs, lizards, cockroaches and even centipedes, the COM falls to its lowest position at midstance as if compressing a virtual or effective leg spring, and rebounds during the sec-

Fig. 3B

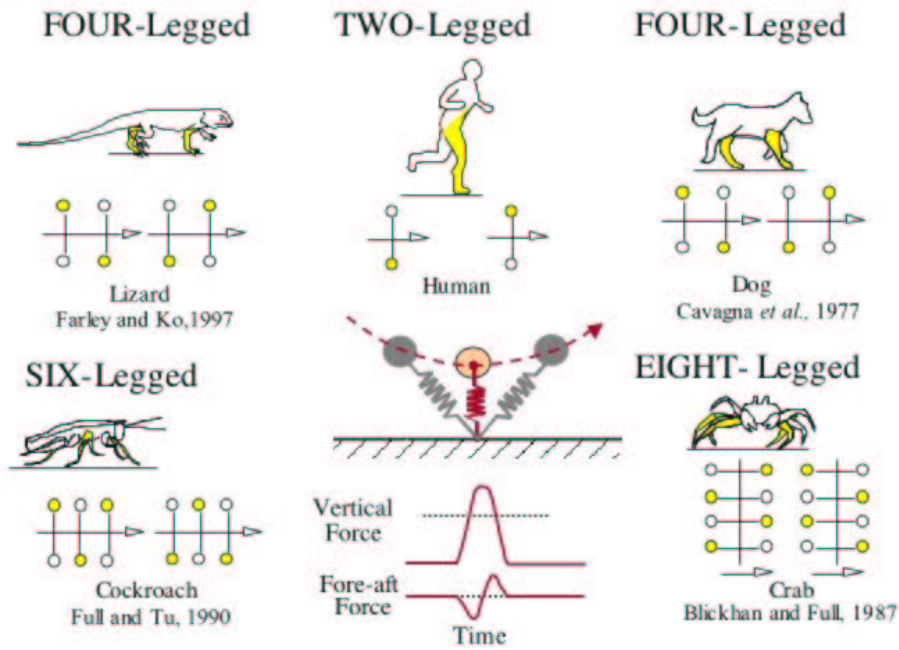


Figure 4: Center of mass dynamics for running animals with two to eight legs. Groups of legs act in concert so that the runner is an effective biped, and mass center falls to its lowest point at midstride. Stance legs shown shaded, with qualitative vertical and fore-aft force patterns at bottom center. The spring-loaded inverted pendulum (SLIP), which describes these dynamics, is shown in the center of the figure. Summarized and adapted from papers cited below each panel. **Remove 3B, Fix refs in standard form!**

ond half of the step as if recovering stored elastic energy. In species with more than a pair of legs, the virtual spring represents the set of legs on the ground in each stance phase: typically two in quadrupeds, three in hexapods such as insects, and four in octopods such as crabs [Ful89, FF00]: Fig 4. This prompts the idealized mechanical model for motion in the sagittal (fore-aft/vertical) plane shown in the center of Fig 4, consisting of a massive body contacting the ground during stance via a massless elastic spring-leg [Bli89, MC90] (a point mass is sometimes added at the foot). The SLIP generalizes an earlier, simpler model: a rigid inverted pendulum, the ‘compass-walker’ [MM80, MM81], cf. [McM84], which is more appropriate to low-speed walking. In running, a full stride divides into a stance phase, with one foot on the ground, and an entirely airborne flight phase. The model employs the same single leg to represent both left and right stance support legs.

Although the SLIP has appeared widely in the locomotion literature, we have found precise descriptions and mathematical analyses elusive. This prompted some of our own studies [SK97, Sch98, SK00], including a recent paper in which we proved that the ‘uncontrolled’ SLIP has stable gaits [GAHK03]. This fact was simultaneously, and independently, discovered via numerical simulation by Seyfarth et al. [SGGB02], who also matched SLIP parameters to human runners and proposed control algorithms [SG02, SGBH02, SGH03]. We shall therefore spend some time setting up this model and sketching its analysis in §4.4 both to exemplify issues involved in integrating hybrid dynamical systems, and to prepare for more detailed accounts of LLS models in §5. Here we informally review the main ideas.

In flight, the equations of ballistic motion are trivially integrated to yield the parabolic COM trajectory, assuming that resistance forces are negligible at the speeds of interest. Moreover, as we show in §4.4, if the spring force developed in the leg dominates gravitational forces during stance, we may neglect the latter and reduce the two-degree-of-freedom point mass SLIP to a single-degree-of-freedom system that may also be integrated in closed form. However, even in this approximation, the quadrature integrals typically yield special functions that are difficult to use, and asymptotic or numerical evaluations are required [SK00].

No matter how the stance phase trajectories are obtained, they must be matched to appropriate flight phase trajectories to generate a *full stride* Poincaré return map P . One then seeks fixed and periodic points of P which correspond to steady gaits, and investigates their bifurcations and stability. It is often possible to invoke bilateral (left-right) symmetry; for example in

seeking a symmetric period one gait of a biped modeled by a SLIP, it suffices to compute a fixed point of P , since although P includes only one stance phase, both right and left phases satisfy identical equations. However, there may be additional reflection- and time-shift-symmetric periodic orbits that would correspond to period two points of P .

More realistic models of legged locomotion, with extended body and limb components requiring rotational as well as translational degrees of freedom, generally demand entirely numerical solution, and even deriving their Lagrangians may be a complex procedure, requiring intensive computer algebra. Nonetheless, almost fifteen years ago McGeer [McG90] designed, built and (with numerical assistance) analysed passive walking machines with rigid links connected by knee joints, in which the dynamics was restricted to the sagittal plane. More recently, Ruina and his colleagues have carried out rather complete studies of simplified models of these machines [CCR97, GCRC98], as well as of a three-dimensional version, which they have shown is dynamically stable but statically unstable [CR98, CGMR01].

In the robotics literature there are very many numerical and a growing number of empirical studies of legged locomotion, incorporating varying degrees of actuation and sensory feedback to achieve increasingly useful gaits. Slow walking machines whose limited kinetic energies cannot undermine their quasi-static stability (i.e., with gaits designed to insure that the mass center always projects within the convex hull of a tripod of legs) have been successfully deployed in outdoor settings for years [WV84]. The first dynamically stable machines were SLIP devices built by Raibert two decades ago [Rai86], but their complexity limited initial stability analyses to single degree-of-freedom simplifications [KB91]. The more detailed analysis of SLIP stability that we will pursue in §4.1 is directly relevant to these machines. More recently, in laboratory settings, completely actuated and sensed mechanisms have realised dynamical gaits whose stability can be established and tuned analytically [WGK03], using inverse dynamics control⁴. However, such ideas are likely to have limited relevance to rapid running, since they require a very high degree of control authority. In contrast, our ‘low-affordance’ controlled robot RHex, introduced in §1, is the first autonomous, dynamically-stable, legged machine to successfully run over rugged and broken outdoor terrain [SBK01].

⁴Inverse dynamics employs high power joint actuators to inject torques computed as functions of the complete sensed state, together with an accurate kinematic and dynamical model and high speed computation to cancel the natural dynamics and replace them with more analytically-tractable terms designed to yield desired closed loop behavior.

Extensions of the analysis introduced in §4.2 are relevant to RHex’s behavior [AKH04b, AKH04a], but a gulf remains between the performance we can elicit empirically and what mathematical analyses or numerical simulations can explain. Modeling is still too crude to offer detailed design insights for dynamically stable autonomous machines in physically interesting settings. For example, in even the most anchored models, complicated natural foot-ground contacts are typically idealised as frictionless pin joints or smooth surfaces that roll without slipping. Similarly, in the models cited above and later in this paper, motion typically occurs over idealized horizontal or uniformly-sloping flat terrain.

Accounting for inevitable foot slippage and loss of contact on level ground is necessary for simulations relevant to tuning physical robot controls [SK03], but far from sufficient for gaining predictive insight into the likely behavior of real robots travelling on rough terrain. It is still not even clear which details of internal leg and actuator mechanics must be included in order to achieve predictive correspondence with the physical world. For example, numerical studies of more realistically underactuated and incompletely sensed autonomous runners, similar to RHex, fail to predict gait stability even in the laboratory, if motor torque and joint compliance models are omitted [PSB04]. Modeling foot contacts over more complex topography in a manner that is computationally-feasible and physically-revealing is an active area of mechanics research [Wri02] that does not yet seem ripe for exploitation in robot controller design, much less amenable to mathematical analysis. In any case, since the bulk of this paper is confined to template models such as the SLIP, we shall largely ignore these issues.

We regard the SLIP and similar templates as passive systems, since energy is neither supplied nor dissipated, although in practice some effort must be expended to reposit the leg during flight. In the case of McGeer’s and Ruina’s walkers, energy lost in foot impacts and friction is replaced by gravitational energy supplied as the machine moves down a slight incline. As noted above, more aggressively active hopping robots have been built by Raibert and colleagues [Rai86, KB91]. In that work, however, it was generally *assumed* that state variable feedback would be needed, not just to replace lost energy, but to achieve stable motions at all. The studies of [SGGB02] and [GAHK03], summarized above, and a recent numerical study of an actuated leg-body linkage [MLBS02], suggest that this is not necessary.

The nature of directly sensed information required for stabilization – the so-called ‘static output feedback stabilization’ problem – is a traditional question of acknowledged importance in control theory that is in general

algorithmically intractable even for linear, time-invariant dynamical systems [BT97]. In the very low dimensional setting of present interest, where algorithmic issues hold less sway, two complications still impede the corresponding local analysis. First, the representation of physical sensors in abstracted SLIP models does not seem to admit an obvious form, so that alternative ‘output maps’ relative to which stabilizability might nominally be assessed are missing. Second, neither the hybrid Poincaré map nor even its Jacobian matrix (respecting which the local stabilizability properties are computed) can be derived in closed form. We have recently been able to show [AKH04b] that deadbeat stabilization is impossible in the absence of an inertial frame sensor, but the question of sensory burden required for SLIP stabilization remains open.

Nonetheless, the SLIP is a useful model on which to build, and so we close this section by summarizing the common ground among animals, legged machines, and SLIP in Fig. 5, which also introduces the symbols for neural and mechanical oscillators that we shall use again below. While the sources and mechanisms of leg movements range from CPG circuits, motoneurons and muscles to rotary motors synchronised by proportional derivative controllers, the net behavior of the body and coordinated groups of legs in both animals and legged machines approximates a mass bouncing on a passive spring.

2.3 Neural circuitry and central pattern generators

Animal locomotion is not, of course, a passive mechanical activity. Muscles supply energy lost to dissipation and foot impacts; they may also remove energy: retarding and managing inertial motions (e.g. in downhill walking), or in agonist-antagonist phasic relationships, e.g. [FSAJ98]. The timing of muscular contractions, driven by a central pattern generator, shapes overall motions [ADO97, Pea00, Mar00a], but in both vertebrates [CRE88, Swi02] and invertebrates [ABGB01], motor patterns arise through coordinated interaction of distributed, reconfigurable [Mar00b] neural processing units incorporating proprioceptive and environmental feedback and goal-oriented ‘commands.’

Whereas classical physics can guide us through the landscape of mechanical locomotion models as reviewed in §2.1-2.2, there is no obvious recourse to first principles in the thicket of neural modeling. Rather, one must choose an appropriate descriptive level and adopt a suitable formal representation, often phenomenological in nature. In this section we introduce models at two different levels that address the rhythm generation, coordination and control behaviors to be reviewed in §2.4 and taken up again in technical

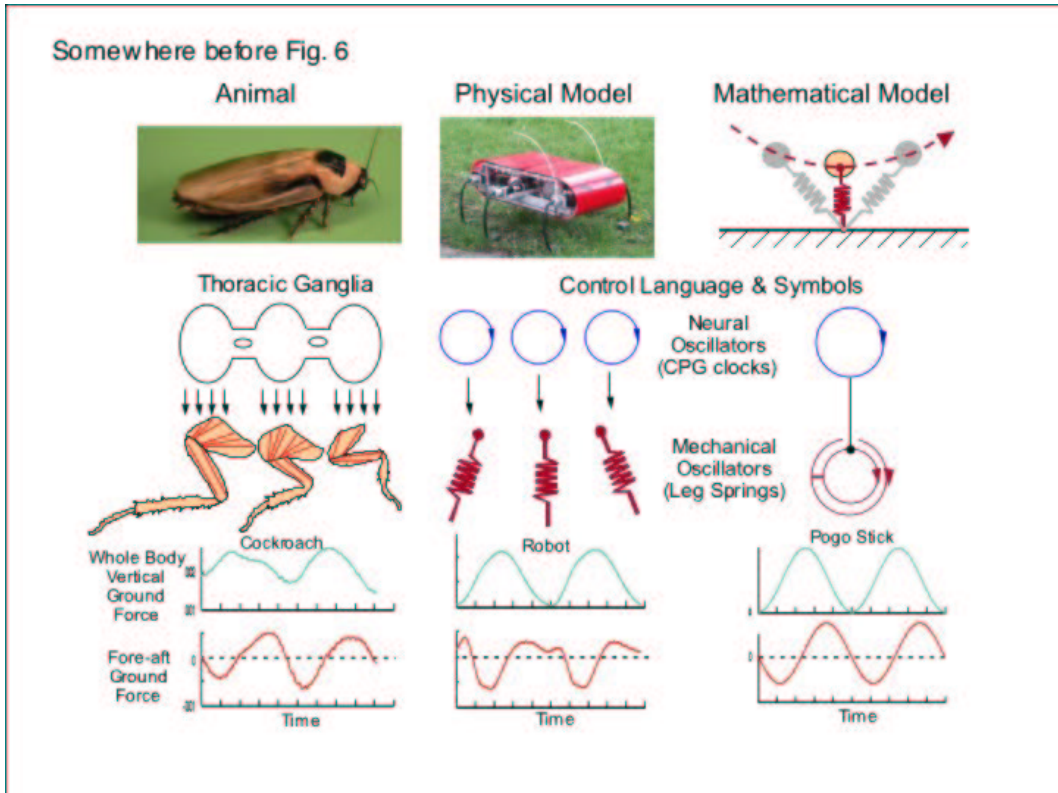


Figure 5: The spring-loaded inverted pendulum (SLIP) as a model for the center of mass dynamics of animals and legged machines. Left panel shows the cockroach *Blaberus discoidalis* with schematic diagrams of thoracic ganglia, containing the central pattern generator (CPG), legs and muscles. Central panel shows the robot RHex, with motor driven springy legs, and right panel shows SLIP. Single circles denote neural oscillators or ‘clocks,’ double circles denote mechanical oscillators. Lower panels show typical vertical and fore-aft forces experienced during rapid running. **Remove ‘Somewhere ...’!**

detail in §5.

2.3.1 Single neuron models and phase reduction

Neurons are electrically active cells that maintain a potential difference across their membranes, modulated by the transport of charged ions through gated channels in the membrane. They fire action potentials (spikes), both spontaneously and in response to external inputs, and they communicate via chemical synapses and direct electrical contact. Neurons admit descriptions at multiple levels. They are spatially complex, with extensive dendritic trees and axonal processes. Synaptic transmission involves release of neurotransmitter molecules from the presynaptic cell, their diffusion across distributed synaptic clefts, and complex receptor biochemistry within the postsynaptic cell. Texts such as [JW95, DA01] provide extensive backgrounds on experimental and theoretical neuroscience.

These complexities pose wonderful mathematical challenges, but here they will be subsumed into the single compartment ODE description pioneered by Hodgkin and Huxley [HH52]. This assumes spatial homogeneity of membrane voltage within the cell, and treats the distributed membrane transport processes collectively as ionic currents, determined via gating variables that describe the fraction of open channels. See [Abb94, KS98] for good introductions to such models, which take the form:

$$C\dot{v} = -I_{\text{ion}}(v, w_1, \dots, w_n, c) + I_{\text{ext}}(t) \quad (11a)$$

$$\dot{w}_i = \frac{\gamma_i}{\tau_i(v)} (w_{i\infty}(v) - w_i); \quad i = 1, \dots, N. \quad (11b)$$

Equation (11a) describes the voltage dynamics, with C denoting the cell membrane capacitance, I_{ion} the multiple ionic currents, and $I_{\text{ext}}(t)$ synaptic and external inputs. Equations (11b) describe the dynamics of the gating variables w_i , each of which represents the fraction of open channels of type i , and γ_i is a positive temperature-like parameter. At steady state, gating variables approach voltage-dependent limits $w_{i\infty}(v)$, usually described by sigmoidal functions:

$$w_{i\infty}(v; k_{i_0}, v_{i_{th}}) = \frac{1}{1 + e^{-k_{i_0}(v - v_{i_{th}})}}, \quad (12)$$

where k_{i_0} determines the steepness of the transition occurring at a threshold potential $v_{i_{th}}$. Gating variables can be either *activating* ($k_{i_0} > 0$), with $w_{i\infty} \approx 1$ for depolarized voltages $v > v_{i_{th}}$ and $w_{i\infty} \approx 0$ for hyperpolarized levels $v < v_{i_{th}}$, or *inactivating* ($k_{i_0} < 0$), with $w_{i\infty} \approx 1$ when hyperpolarised

and $w_{i\infty} \approx 0$ when depolarised. The time scale τ_i is generally described by a voltage-dependent function of the form:

$$\tau_i(v; k_{i0}, v_{ith}) = \text{sech}(k_{i0}(v - v_{ith})) . \quad (13)$$

The term I_{ion} in (11a) is the sum of individual ionic currents I_α , each of which takes the form

$$I_\alpha(v, \mathbf{w}) = \bar{g}_\alpha w_i^a w_j^b (v - E_\alpha) , \quad (14)$$

where E_α is a (Nernstian) reversal potential, \bar{g}_α is the maximal conductance for all channels open, and the exponents a, b can be thought of as representing the number of subunits within a single channel necessary to open it. Hodgkin and Huxley's model [HH52, KS98] of the giant axon of squid included a sodium current with both activating and inactivating gating variables (m, h) and a potassium current with an activating variable alone (n), and they fitted sigmoids of the form (12) to space-clamped experimental data. Many other currents, including calcium, chloride, calcium-activated potassium, etc. have since been identified and fitted, and a linear leakage current $I_L = \bar{g}_L (v - E_L)$ is usually also included.

The presence of several currents, each necessitating one or two gating variables, makes models of the form (11) analytically intractable. However, often several of the gating variables have fast dynamics, i.e. $\gamma_i/\tau_i(v)$ is relatively large in the voltage range of interest: such variables can then be set at their equilibrium values $w_j = w_{j\infty}(v)$ and their dynamical equations dropped. Likewise, functionally related variables with similar time scales may be lumped together [RE99]. This reduction process, pioneered in FitzHugh's polynomial reduction of the Hodgkin-Huxley model [Fit60, Fit61], cf. [HR84, RH89, KS98], may be justified via geometric singular perturbation theory [Jon94]. We shall appeal to it in deriving a three-dimensional model for bursting neurons in §5.4.

A deeper geometrical fact underlies this procedure and allows us to go further. Spontaneously spiking neuron models typically possess hyperbolic (exponentially) attracting limit cycles [GH90]. Near such a cycle, Γ_0 , of period T_0 , the $(N + 1)$ -dimensional state space of (11) locally splits into a phase variable ϕ along Γ_0 , and a foliation of transverse *isochrons*: N -dimensional manifolds M_ϕ with the property that any two solutions starting on the same leaf M_{ϕ_0} are mapped by the flow to another leaf M_{ϕ_1} and approach Γ_0 with the same asymptotic phase [Guc75]. Writing (11) in the form

$$\dot{\mathbf{x}} = \mathbf{f}(\mathbf{x}) + \epsilon \mathbf{g}(\mathbf{x}, \dots) \quad (15)$$

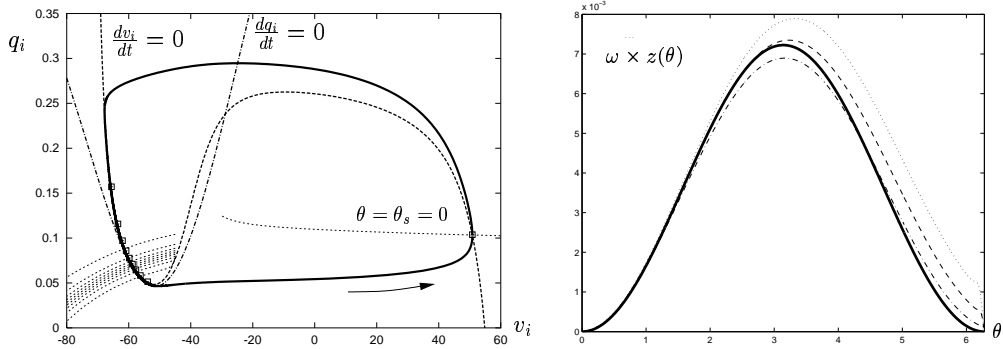


Figure 6: (a) Phase space structure for a repetitively spiking Rose-Hindmarsh model, showing attracting limit cycle and isochrons. The thick dashed and dash-dotted lines are nullclines for $\dot{v} = 0$ and $\dot{w} = 0$, respectively, and squares show points on the perturbed limit cycle, equally spaced in time, under a small constant input current I_{ext} . (b) PRCs for the Rose-Hindmarsh model; the asymptotic form $z(\phi) \sim [1 - \cos \phi]$ is shown solid, and numerical computations near the saddle node bifurcation on the limit cycle yield the dashed result. For details see [BMH⁺03], from which these figures are taken. **Need to redo variables v, w ! Remove dots and dot-dash!**

where $\mathbf{g}(\mathbf{x}, \dots)$ represents external (synaptic) inputs, choosing the phase coordinate such that $\dot{\phi} = \omega_0 = 2\pi/T_0$ and employing the chain rule, we obtain the scalar oscillator equation:

$$\dot{\phi} = \omega_0 + \epsilon \frac{\partial \phi}{\partial \mathbf{x}} \cdot \mathbf{g}(\mathbf{x}(\phi), \dots) |_{\Gamma_0(\phi)} . \quad (16)$$

Here we implicitly assume that coupling and external influences are weak ($\epsilon \ll 1$), and that Γ_0 perturbs to a nearby hyperbolic limit cycle Γ_ϵ , allowing us to compute the scalar phase equation by evaluating along Γ_0 . For neural models in which inputs and coupling enter only via the first equation (11a), the vector $\frac{\partial \phi}{\partial \mathbf{x}}$ contains only a single nonzero component $\frac{\partial \phi}{\partial v} \stackrel{\text{def}}{=} z(\phi)$. This *phase response curve* (PRC) describes the sensitivity of the system to inputs as a function of phase on the cycle. It may be computed asymptotically, using normal forms, near local and global bifurcations at which periodic spiking begins: see [Erm96, BMH04].

Figure 6 shows an example of isochrons and PRCs computed for a two-dimensional reduction due to Rose and Hindmarsh [RH89] of a multi-channel

model. Here the gating variables have been collapsed to a single scalar w , and so isochrons are one-dimensional arcs. Note that these arcs, equally-spaced in time, are bunched in the refractory region in which the nullclines almost coincide and flow is very slow.

The phase reduction method was originally developed by Malkin [Mal49, Mal56], and independently, with biological applications in mind, by Winfree [Win01]; also see [Erm96]. It has recently been applied to study the response of populations of neurons to stimuli [BMH04, BMH⁺03]. We shall use it below, followed by the averaging theorem [GH90, EK86, Kop88, HI97], to simplify the CPG model of §5.4.

2.3.2 Integrate-and-fire oscillators

We shall shortly return to phase descriptions, but first we mention another common simplification. Since action potentials are typically brief (~ 1 msec) and stereotyped, the major effect of inputs is in modulating their timing, and this occurs during the refractory period as the membrane potential v recovers from post-spike hyperpolarization. Integrate-and fire models [Abb94, DA01] neglect the details of channel dynamics and consider the membrane potential alone, subject to the leakage current and inputs:

$$\dot{v} = \bar{g}_L(v_\infty - v) + \sum_{i,j} A(t - t_{i,j}). \quad (17)$$

Thus, v increases towards a limit v_∞ and when (and if) it crosses a preset threshold v_{Thres} it is reset to 0 (another example of a hybrid system). In this model postsynaptic (external) influences on the cell are characterised by a function $A(t)$ (often of the type $t^k \exp(-k_j t)$), summed over input cells j and the times $t_{i,j}$ at which they spike.

2.3.3 Networks of phase oscillators

Phase oscillators have the advantage of mathematical tractability – along with integrate and fire models they are perhaps the prime templates of mathematical neuroscience – but they have rarely been anchored in biophysically-based models such as those of §2.3.1. Indeed, in many cases the precise neural circuitry remains unknown, although there are exceptions (e.g. [CBD⁺97]), and in §5.4 we shall summarise current work [GH04] in which phase reductions and averaging are used to derive oscillator networks from (relatively) detailed Hodgkin-Huxley type models. Nonetheless, phase descriptions are

useful as phenomenological models of CPGs even when little or incomplete information on neuron types, numbers, or connectivity is available.

In such models, each phase variable may represent the state of one cell or, more typically, a *group* of cells, including interneurons and motoneurons, constituting a quasi-independent, internally synchronous subunit of the CPG. This was the approach adopted in early work on the lamprey notocord [CHR82, CRH88], in which each oscillator describes the output of a spinal cord segment, or a pair of oscillators, mutually inhibiting and thus in antiphase, describe the left and right halves of a segment. In reality, there are probably $\mathcal{O}(100)$ active neurons per segment, and the architectures of individual ‘oscillators’ can extend over as many as four segments [CW80, CHR82]. Murray’s book [Mur01] introduces and summarises some of this work.

Since we will return to them in §5.4, it is worth describing phase models for networks of oscillators in more detail. They take the general form:

$$\dot{\phi}_i = f_i(\phi_1, \phi_2, \dots, \phi_N); \quad i = 1, \dots, N, \quad (18)$$

where the f_i are periodic in each variable; such a system defines a flow on an N -dimensional torus. In many cases a special form is assumed in which each uncoupled unit rotates at constant speed and coupling enters only in terms of phase differences $\phi_j - \phi_k$. As noted in §2.3.1 and outlined for an insect CPG example of §5.4, this form may be justified by assuming that each underlying ‘biophysical’ unit has a normally hyperbolic attracting limit cycle [GH90], that coupling is sufficiently weak, and by appeal to the averaging theorem: see [HI97, EK86, EK91] for more details.

In the simplest possible case of two oscillators, symmetrically coupled, we obtain ODEs whose right hand sides contain only the phase difference $\phi_1 - \phi_2$:

$$\dot{\phi}_1 = \omega_1 + f(\phi_1 - \phi_2), \quad \dot{\phi}_2 = \omega_2 + f(\phi_2 - \phi_1); \quad (19)$$

note that we allow the uncoupled frequencies ω_j to differ, but here the functions $f_i = f$ are supposed identical. Letting $\theta = \phi_1 - \phi_2$ and subtracting Eqns (19), we obtain the scalar equation

$$\dot{\theta} = (\omega_1 - \omega_2) + f(\theta) - f(-\theta). \quad (20)$$

A fixed point $\bar{\theta}$ of (20) corresponds to a *phase locked* solution of (19) with frequency

$$\bar{\omega} = \omega_1 + f(\bar{\theta}) = \omega_2 + f(-\bar{\theta}),$$

as may be seen by considering the differential equation for the phase sum $\phi_1 + \phi_2$. In the special case that f is an odd function and $f(-\theta) = -f(\theta)$,

the resulting frequency is the average $(\omega_1 + \omega_2)/2$ of the uncoupled frequencies. For smooth functions, stability is determined by the derivative $f'(\theta) - f'(-\theta)|_{\theta=\bar{\theta}}$ – negative (resp. positive) for stability (resp. instability) – and stability types alternate around the phase difference circle. Fixed points appear and disappear in saddle-node bifurcations [GH90], which occur when the value of a local maximum or minimum of $f(\theta) - f(-\theta)$ coincides with $\omega_1 - \omega_2$. The number of possible fixed points is bounded above by the number of local maxima and minima of this function, but hyperbolic fixed points must always occur in stable and unstable pairs, since they lie at neighboring simple zeros of $f(\theta) - f(-\theta)$.

Coupling typically imposes a relation between the oscillator phases, determined by inverting the fixed point relation

$$f(\theta) - f(-\theta) = \omega_2 - \omega_1, \quad (21)$$

and vector equations analogous to (21) emerge in the case of a chain of N oscillators with nearest-neighbor coupling [CHR82]. The original lamprey model of [CHR82] took the simplest possible odd function $f(\theta) = -\alpha \sin(\theta)$ (the negative sign being chosen so that ‘excitatory’ coupling would have a positive coefficient). In this case, a stable solution with a nonzero phase lag, corresponding to the traveling wave propagating from head to tail responsible for swimming, requires a nonzero frequency difference $\omega_i - \omega_{i+1} > 0$ from segment to segment. At the time of the original study [CHR82], evidence from isolated sections taken from different parts of spinal cords suggested that there was indeed a frequency gradient, with rostral (head) segments oscillating faster in isolation than caudal (tail) segments. Subsequent experiments showed this not to be the case: a significant fraction of animals was found to have caudal frequencies exceeding rostral ones, and to account for this Kopell and Ermentrout [EK86, Kop88] introduced non-odd, ‘synaptic,’ coupling functions with a ‘built-in’ phase lag. Indeed, as they pointed out, although electrotonic (gap junction) coupling leads to functions that vanish when membrane voltages are equal, the biophysics of synaptic transmission implies that nonzero phase differences typically emerge even if the cells fire simultaneously.

Regardless of oscillator details, rather powerful general conclusions may be drawn regarding possible periodic solutions of symmetric networks of oscillators using the group-theoretic methods of bifurcation with symmetry [GS85, GSS88]. Golubitsky, Collins and their colleagues have applied these ideas to CPG models, thereby finding network architectures that support numerous gait types, especially those of quadrupeds [GSBC98,

GSBC99], although Collins and Stewart also have a paper specifically on insect gaits [CS93]. Here the symmetries are discrete, primarily the left-right bilateral body symmetry, and (approximate) front-hind leg symmetries. In §§2.1-2.2 and §§4-5, the continuous symmetry of planar translations and rotations with respect to the environment plays a different role in biomechanical models.

2.4 On control and coordination

We have seen that CPGs, including the motoneurons that generate their outputs, acting in a feedforward manner through muscles, limbs and body, can produce motor segments that might constitute a ‘vocabulary’ from which goal-oriented locomotory behaviors are built. As we argue in §5.4-5.5, integrated, neuromechanical CPG-muscle-limb-body models are still largely lacking, but the analysis of simple neural and mechanical oscillators, such as the phase and SLIP models introduced above, can elucidate animal behavior [KKK01] as well as suggesting coordination strategies for robots [KK02]. However, assembling these motor segments, and adapting them to environmental demands, requires both reflexive feedback and supervisory control. We therefore end this section with a discussion of control issues, focusing on two specific questions.

How are the distributed neural processing units, referred to at the start of §2.3, coordinated? What roles do they play in the selection, control or modulation of the distributed excitable musculoskeletal mechanisms? Little enough is presently known about these questions that motor science may perhaps best be advanced by developing prescriptive, refutable hypotheses. Here ‘prescriptive’ loosely denotes a control procedure that can be shown mathematically (or perhaps empirically, in a robot) to be in a logical relationship of necessity or sufficiency with respect to a specific behavior. Refutable implies that the behavior admits biological testing. Before sketching our working version of such hypotheses for insect locomotion in §3 we review parts of a vast relevant literature.

2.4.1 Mechanical organization: Collapse of dimension and posture principles

Empirical laws describing movement trajectories both in the inertial (world) frame and within the body-limb frame have been formulated and their neural correlates sought. For example, a power law inversely relating speed to path curvature, originally derived from observations of voluntary reaching

movements [LTV83], has been proposed to describe diverse mammalian motor patterns, including walking [IGML02]. Moreover, primate motor cortex recordings of voluntary arm movements [SM99] reveal a neural velocity ‘reference signal’ that precedes and predicts observed mechanical trajectories, prescribing via variable time delay the power law of [LTV83]. This suggests partition of a reference trajectory into modular constituents of a putative motor vocabulary, and meshes with yet more prescriptive notions of optimal trajectory generation whose cost functionals can be shown to generate signals that respect such power laws [TJ98, RF02].

However, interpreting such descriptive patterns is challenging. Trajectories generated by mere low frequency harmonic oscillations fit to motion-capture data in joint space also respect a power law as an accidental artifact of nonlinear kinematics [SS01]. Moreover, when these fitted oscillations grow large enough in amplitude to violate the pure power law, they do so in a punctuated manner, again apparently accidentally evoking a composed motor vocabulary. Moreover, in a critique of proposals addressing the role of neural precursors to voluntary arm motion, Todorov [Tod00] has pointed out that motor cortex signals have been correlated in various papers with almost all possible physical task space signals: an array of correspondences that could not be simultaneously realised. In sum, power law and other empirical descriptions do not seem central to our aims. **OK DAN?? I thought we needed to ‘summarise’ this discussion.**

The mechanical patterns of central concern in this review arise from a *collapse of dimension*: the emergence of a low-dimensional attractive invariant submanifold in a much larger state space. Apparently associated with this dynamical collapse is a *posture principle*: the restriction of motion to a low dimensional subspace within a high dimensional jointspace. A kinematic posture principle has been discovered in mammalian walking [LGZ99], as demonstrated by planar covariation of limb elevation angles which persists in the face of large variations in steady state loading conditions [IGML02]. More directly relevant to the models to be developed in this paper, a preliminary study of kinematic posture in a running cockroaches using principal components analysis [KFK03] also reveals very low-dimensional linear covariation in joint space (cf. [BBL96]). Such biomechanical discovery of dimension collapse and posture principles complements increasing evidence in both vertebrate [Bur99, GTM02, SWDA⁺01, Bur02] and invertebrate [Pea93] neuroscience that neural activation results in precise, kinematically selective synergies of muscle activation. Posture principles have also proved useful in designing controllers for legged robots [SSK98, SK03]. In §§5.3-5.4 we will address the collapse of more complex models to the

templates introduced earlier in §2.3 and to be described in §§5.1-5.2.

The question arises how to render such descriptive observations more prescriptive by finding refutable hypotheses connected with them. The selection of a motor control policy may be governed by energy costs, muscle or bone stress or strain levels, stability criteria, or speed and dexterity requirements. Gait changes in quadrupeds, especially horses, have been shown to correlate with reductions in energy consumption as speeds increase [Mar76, HT81, WHCM03]. Muscle and bone strain criteria have also been suggested [FT91a, BT86]. With regard to stability, our own recent work using the LLS model of §5 suggests that animal design and speed selection might place gaits close to stability optima [SGR⁺02, FKS⁺02]. However, we are wary of the optimality framework, commonly employed in engineering [BH75], as a foundation for the prescription of natural or synthetic motion control, in part because it transfers the locus of parameter tuning from plant loop parameters to the cost function, which largely determines the quality of the resulting solution. Similarly, in biology, cost function details can significantly modify the resulting solutions, potentially shifting the phenomenology of describing the task to that of choosing the right cost function⁵.

Instead, we prefer to examine and model locomotion dynamics in regimes in which the laws of Newtonian mechanics dominate, and hence constrain possible control mechanisms. Specifically, at high speeds, inertial effects render passive mechanics an essential part of the overall dynamics, and there are severe time constraints on reflex control pathways. Recent impulsive perturbation experiments on running cockroaches in [JF02] reveal, for example, that corrective motions are initiated within 10-15 msec, while corrective neural and muscle activity is estimated to require 25-50 msec. We shall therefore focus on regimes in which, even if control target trajectories are being selected by higher centers, they must conform to mechanical constraints.

2.4.2 Neuromechanical coupling: Centralized and decentralized coordination; feedforward and feedback control

However they are formed, mechanical synergies such as templates and posture principles offer the nervous system attractive points of influence over the musculo-skeletal system's interaction with its environment. Recent work on the cellular and molecular basis of sensory-motor control [BM98], and the

⁵Optimization ideas can, of course, be useful in fitting model parameters if they cannot be directly measured or estimated, e.g. [CBMWC98].

use of non-invasive imaging to reveal specific brain regions active in learning and the planning and execution of movements [Pea00, Kaw99, LPSB01], corroborate a growing consensus within the animal neuromotor community that control is organized in a distributed modular hierarchy [MI99]. In this view, complex motor functions are governed by afferent-mediated [Pea95] networks of variably-coupled [Bur99], feedforward, pattern-generating units [Gri85] located remotely [BTSD00] from higher (brain) centers of function, and which supply ‘motor program segments’ that may be combined in various ways at cortical command. It is tempting to think of these segments as solutions of coupled CPG-muscle-body-limb-environment dynamical systems, excited by appropriately-shaped motoneuronal outputs and amplified by appropriately-tuned muscles. Indeed, as we shall argue, cortical stimulation of such dynamical models can parsimoniously account for many of the observed correlations, and we offer the beginnings of a prescriptive interpretation in §3.3.

In reading the motor coordination literature as well as in formulating the hypotheses of §3.3 we have found it helpful to refer to the architectural ‘design space’ depicted in Fig. 7 as a two-dimensional coordination-control plane whose axes represent the degree of centralization and the influence of feedback. Adopting this view, we may divide the studies of motor rhythms within distributed networks into three subgroups.

The first employs networks of biophysically-based, ion channel neuron models of Hodgkin-Huxley [HH52] type, or reductions thereof [Fit61, HR84, KS98], patterned closely upon the specific physiology of isolated tissues such as lamprey notocord [GWBL91] or the arthropod stomato-gastric ganglion [SER⁺98, GGMA01]. These models, summarised in §2.3.1 above, and the experiments on which they are based, typically isolate the CPG by removing signals from sensory neurons, and lesioning ‘control’ inputs from higher brain centers [Del80, CRE88, Gri99]. Fairly detailed neural architectures and details of individual neuron types are required for their formulation; hence they are most appropriate for ‘small’ systems. In this work the spontaneous generation and stability of rhythms are studied, perhaps in the presence of tonic excitation, but not their volitional control or translation into physical motion.

The second group focuses on modeling the internal generation of rhythmic CPG patterns in the vertebrate spinal and supraspinal nervous systems by networks of coupled phase oscillators of the type introduced in §2.3.3. Here the neurobiology is more complex and often less well-characterised, so phenomenological models are more appropriate. The work on lamprey CPG cited there [CHR82, CRH88], and substantial extensions and general-

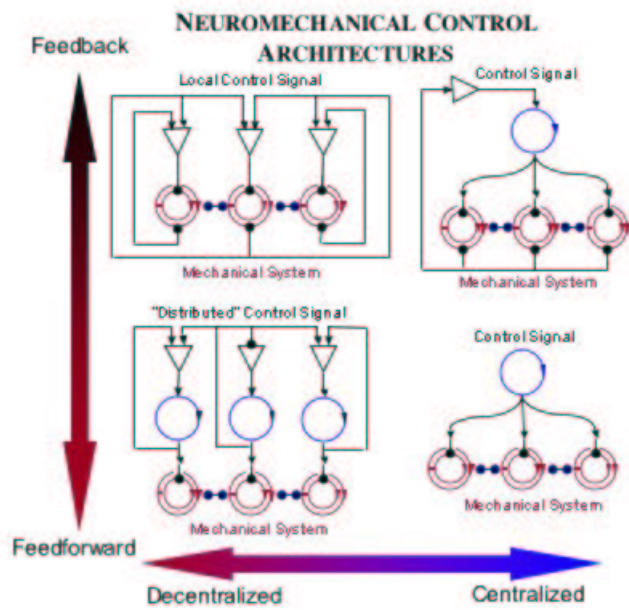


Figure 7: The schematic two-dimensional space of control architectures. Single circles represent CPG oscillators, double circles represent mechanical oscillators such as limb components, and triangles represent neural control elements (analogous to operational amplifiers).

izations of it by Kopell, Ermentrout and others (e.g. [EK86, Kop88, EK90, KE90, KEW91, CK93, KL94, JKC96]), provide examples of this approach. As noted in §2.3.3, in going directly to phase oscillators representing pools of neurons or local circuits containing several neuron types, one frequently abstracts away from specific physiological identification, although important information on coupling strengths along the cord can be derived by fitting parameters in such models [KC98]. These models also typically exclude muscles and mechanical aspects of the motor system and interactions with its environment, although in [KEW91], for example, the effect of mechanical forcing of a fish’s tail is modeled.

Their focus on the emergence of synchrony in distributed networks and their necessary presumption of the primacy of neural excitation in eliciting motor activity places these two classes of models on the feedforward level of Fig. 7, at various points along the centralized-decentralized axis. Moreover, in both of these approaches, the generation and stability of rhythms are studied, but not their translation into physical motion. Indeed, in the absence of a mechanical model, the relative influence of mechanical feedback cannot be addressed.

Integrative neuromuscular models are beginning to appear. Simple coupled models of the nervous system and its mechanical environment have been developed by a third ‘ecological’ school [KFDC01, BPD02], following the lead of the Haken-Kelso-Bunz (HKB) model of coordinated finger-tapping [HHB85]. In these systems, (neural) phase oscillators are coupled to phenomenological (generic mechanical) oscillators representing simplified muscle-limb dynamics that may be interpreted as phase coordinate representations of the hybrid templates introduced in §2.1-2.2. There appear to be few comprehensive studies of specific locomotory systems, however, with the exception of lamprey (anguilliform = eel-like) swimming, which has been modelled by Ekeberg and Grillner [Eke93, EG99] and Bowtell, Carling and Williams [BW91, BW94, CWB98]. In the former papers, bodies composed of rigid links actuated by simplified spring/damper muscle models are used and the fluid environment is represented by empirical drag and lift forces applied along the body; a recent paper on salamander locomotion considers both aquatic and terrestrial gaits [Ijs01] from a similar viewpoint. In [BW91, BW94, CWB98], continuum body models coupled with the Navier-Stokes equations of incompressible hydrodynamics are solved numerically with a prescribed moving boundary representing the lamprey’s body. Models of even the former (finite-dimensional) type are too complex to permit substantial analysis, although studies of linearized systems can be helpful, even for continuum models [BW94], so this work relies heavily on numerical

simulations. Analytical treatment of explicitly coupled neuro-mechanical oscillators seems heretofore limited to very simple one degree of freedom dynamical manipulation such as juggling [SSA96, SBK95].

As Fig. 7 illustrates, control architectures may also be described in terms of their reliance on sensory feedback from body mechanics and the environment. For example, proprioceptive sensing of leg forces and joint angles may directly influence CPG and motoneurons to maintain phase relationships in a decentralized, peripheral manner [Pea72, PI72, BB98, RFRZ98], while visual and tactile sensing, or odor tracking, may require central processing before appropriate feedback can be applied to adjust gaits or change direction [Gil97]. Alternatively, cockroach antennal sensing can induce turning at high speeds with very short delays [CJ99], suggesting that fast direct pathways to the CPG may exist. In turn CPG activity and central commands can modulate and even reverse the negative feedback typically exerted by proprioceptive sensors such as the stretch reflex [CCR00].

More prescriptive versions of the power laws reviewed above emphasize optimal feedforward trajectory generation, although feedback is known to play an important role in both vertebrate [ZS99] and invertebrate [DCC00] locomotion, and the importance of feedforward reference signals is by no means generally accepted [Cru02]. The observation that certain degrees of freedom exhibit significantly higher variability than others can be interpreted in the framework of stochastic optimal feedback control as a hedge against noise [TJ02]. Depending on environmental demands, the full range from pure feedback to pure feedforward control policies is probably employed in animal motion. Indeed, the suggestion, based on linear systems theory, that feedback should be preferred when internal models are uncertain or unavailable, while feedforward strategies should be more appropriate in the presence of significant sensor noise [Kuo02], seems very reasonable. The extremes of this continuum are exemplified respectively by ‘mirror laws’ developed for juggling machines [BK90] and legged robots [SSK98, SK03], and passive stabilization based on reflexes, as exhibited by the SLIP and LLS models described in this paper. Overall, since centralised feedback circuits imply greater time delays, as running speeds increase, we expect control to emphasise decentralized modes, and increasingly rely on feedforward strategies.

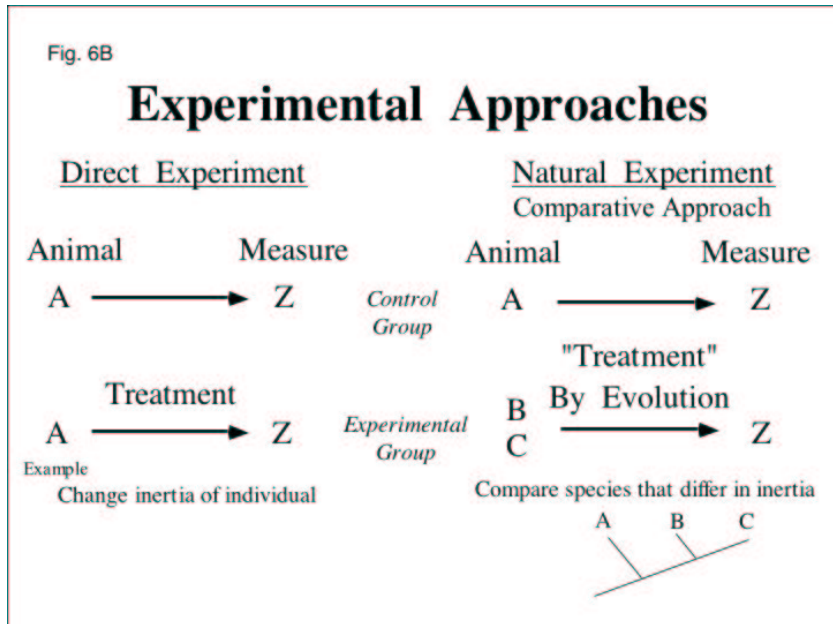


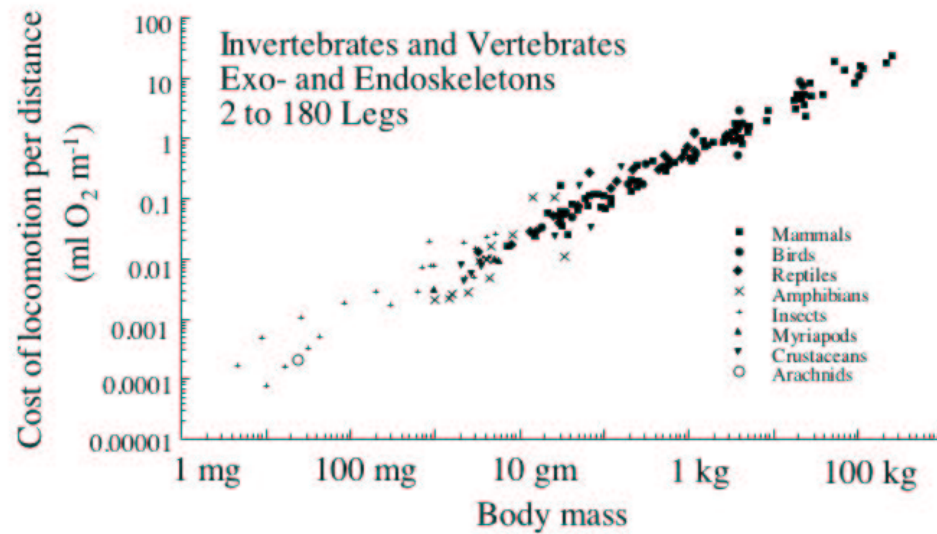
Figure 8: A schematic illustration of the direct and comparative experimental approaches, with an example of investigation of the effects of moment of inertia.

3 Experimental evidence: Comparative studies

Simple models of legged locomotion, such as the SLIP of §2.2, have emerged from data collected using a powerful approach: the comparative method [Wake, 19; Full and Farley, 1993?]. Direct experiments on individual animals in which a single variable is manipulated are often effective in establishing cause and effect relationships, but large parameter ranges can rarely be probed without disrupting function elsewhere in a finely integrated system. There are limits, for example, to how much an animal's mass or moments of inertia can be changed by the addition of weights, in studying their influence on its dynamics.

The comparative approach takes advantage of nature's diversity to enable the discovery of general principles as well as remarkable exceptions to the rules. We can infer function by comparing among species that differ widely in a variable of interest, rather than by direct experimental manipulation of a single species. Effectively, we observe experiments performed by nature, in which the 'treatment' has been evolution, and naturally-occurring

Fig. 6C



Full, 1997

Figure 9: Metabolic cost of locomotion vs. body mass for a broad range of animals, showing an approximate power law relationship: $\text{cost} \propto m^?$. From [Ful97]. **BOB: Insert exponent!**

variations in dependent variables permit investigation and isolation of mechanisms of interest in nearly-ideal settings of exceptional function. Fig. 8 illustrates the direct and comparative methods.

The largest variations are found in comparing animals that differ greatly in size [Schmidt-Nielsen; Calder]. Fortunately, variation in dependent variables as a result of size often shows remarkably general correlations that can be used to infer function and predict performance. For example, while the metabolic cost of legged locomotion typically varies less than ten-fold when speed, stride frequency, inclines or added loads are altered in individuals, it naturally differs by over five orders of magnitude, while exhibiting a single relationship, when all legged animals are compared: see Fig 9.

Equally important are those animals that demonstrate spectacular performance and deviate from the general pattern. Large, measurable differ-

ences have evolved over millions of years in diverse species with different lifestyles or operating in extreme environments. Characterization of these specialized systems can allow extrapolation to others in which the properties of interest are not as extreme, but for which the principles of function are the same. For example, hopping red kangaroos can increase speed without increasing metabolic energy cost [Dawson and Taylor, 1973], and measurements of ground reaction and muscle forces reveal substantial elastic strain energy storage in the tendons of kangaroos and wallabies [Alexander and Vernon, 1975, Alexander 1988; Biewener and Baudinette, 1995]. It is therefore reasonable to conclude, at least in large vertebrates such as humans, that tendons serve a similar role, albeit to a lesser extent than in specialized, bipedal hoppers.

Natural experiments are imperfect because they lack an appropriate control: Fig. 8. Seldom do even closely-related species under comparison differ *only* in the variable of interest. However, the comparative method is strengthened by knowledge of evolutionary history or phylogeny [Huey, 1987; Garland and Adolph, 1994; Lauder, 2001]. Techniques in phylogenetic analysis [Felsenstein, 1985; Garland et al., 1992] can remove the effects of history or use them to hint at present function. If the process of interest has severe functional or structural constraints or nearly complete adaptation has taken place, then the potentially confounding effects of historical differences may be of little consequence. If, however, constraint and adaptation have been less than completely dominant, then the most parsimonious assumption is that the process operates as it did in the ancestor. An evolutionary, comparative approach can aid in answering mechanistic questions, but only if each species is studied in sufficient depth to elucidate the mechanism and a satisfactory phylogeny exists [Autumn et al 2002; Mangum and Hochachka, 19??]. Unfortunately, agreed-upon phylogenies are rare and in-depth studies of many species can take years.

BOB: Sounds like you are criticising Comp method above, then immediately going on to praise it again. Needs better connective tissue between paras, or some textual tuning at end of previous and beginning of next??

In-depth studies are often made possible by nature's diversity. As August Krogh remarked at the 13th International Congress of Physiology in Boston in 1929: 'For many problems there is an animal on which it can be most conveniently studied' [Krebs, 1975]. The selection of 'choice' or model species is based on their amenability to particular experimental procedures. The giant squid axon and the gastrocnemius muscle of frogs are notable, relevant examples, although results from model species that are

easy to study are not necessarily generalizable. Chances **BOB: Do you mean ChanGes??** are often greater at the lowest levels of organization such as cell and molecular structures and genetic and biochemical networks. In this regard, *E. coli*, nematodes and fruit flies have proved invaluable model organisms. At the level of organs and organisms, careful selection using existing phylogeny of more basal species will more likely lead to general discoveries. The nervous system of the lamprey has been argued to be such an example [CRE88] [Grillner]; hence its use as a model to probe vertebrate CPG architectures, as noted in §2.3.3. Alternatively, direct measurements of performance for a wide range of species that differ in size can be invaluable for identifying possible generality. For example, the metabolic cost of legged locomotion appears to be independent of leg number, leg design, type of skeleton used and whether the animal is warm or cold-blooded (Fig. 9). Phylogenetic effects that may limit the generality of conclusions are absent from relationships such as these. It is therefore reasonable to assume that discoveries in insects, as discussed here, will lead to general principles for all legged locomotors.

3.1 Mass center mechanics of legged locomotion

Cavagna et al. [1964] provided early experimental evidence for the spring-mass model of legged locomotion introduced in §2.2. The metabolic energy cost of human running was determined by measuring oxygen consumption, and mechanical energy estimated from the fluctuations in kinetic and potential energy calculated from ground reaction forces measured with a force platform. Efficiencies, much higher than estimated for muscle, supported the use of leg springs. Similarly, using movie film and force platforms to study jumping dogs and hopping kangaroos, Alexander [1974, 1975] calculated a substantial degree of elastic recoil in ankle extensor tendons. More recently, Biewener et al. [1998] directly measured tendon force and muscle length change in hopping wallabies and found that elastic strain energy storage in ankle extensor tendons reduces total work by 45% during hopping at the fastest speeds. **BOB: I ran last 2 sentences together. OK? Was this 45% the finding of Biewener et al.??**

Alexander and Jayes [AJ83] proposed that dynamically similar legged locomotors should exhibit equal ratios of inertial to gravitation forces (Froude number, v/\sqrt{gl}) for equivalent gaits. This is based on the idea that the centrifugal force acting on the body as it rotates over a (rigid) supporting limb of length l must balance the ground reaction force on the limb. Animals as diverse as dogs and camels all follow a single function when data on rela-

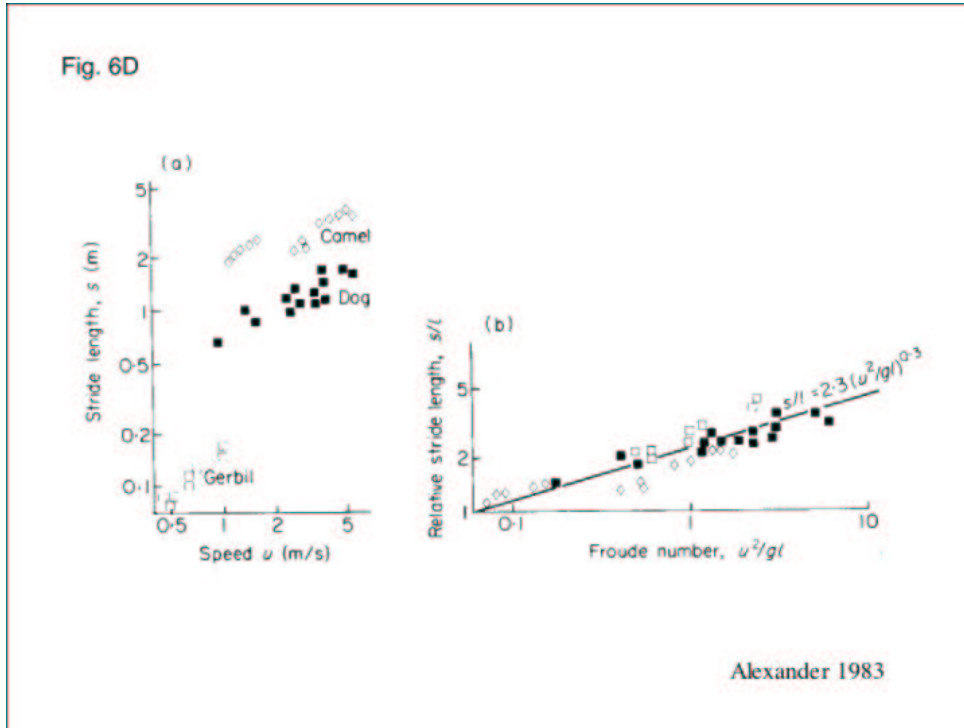


Figure 10: Stride length s vs. speed and relative stride length s/l vs. Froude number for various animals. From [AJ83]. **BOB: Horiz axis is actually Froude²! (conventional Froude No in fluid mech is v/\sqrt{gl}). How best to fix this?**

tive stride length is plotted as a function of Froude number: Fig 10. Froude number is essentially the (square root of the) ratio of kinetic to potential energy and is often viewed as a dimensionless speed; it will play an important role in nondimensionalizing the models of §5. Moreover, and remarkably, mammals with different evolutionary histories change gait from a walk to a trot at Froude numbers of 0.3 to 0.5, and from a trot to a gallop between 2 and 3.

BOB: Their argument seems to assume rigid leg - like compass walker - see my insert 'a (rigid) supporting limb'. Does this require a comment to relate to our springy leg models, in wch we also have ELASTIC energy storage. cf. my nondiml param $\tilde{k} = mv^2/kl^2$, also a Froude², for LLS??

3.1.1 Walking and running data viewed in the sagittal plane

In 1977 Cavagna et al. [CHT77] collected ground reaction force data on two and four-legged mammals in an effort to explain the general energetic relationship of Fig. 9. Their data supported two basic mechanisms for minimizing energy: an inverted pendulum, and a mass atop a spring. Walking was proposed to be an energy-conserving mechanism analogous to an inverted pendulum, much like an egg rolling end over end [CTZ76, CHT77] [Heglund et al. 1982] (cf. the compass walker described by McMahon [McM84]). Kinetic energy and gravitational potential energy fluctuate in anti-phase in such a mechanism, allowing exchange of energy as the animal's center of mass rises and falls during each step. Vaulting over a stiffened leg in humans was once argued to conserve up to 70% of the energy that must otherwise be provided by muscles and tendons [CTZ76], but recent models including a double support phase and collision losses question the extent of exchange [Donelan et al., 2002].

At faster speeds, animals behaved more like a mass atop a springy leg [CHT77], in which kinetic and gravitational energy remain in phase, but fluctuate in antiphase with the elastic energy stored in the spring. Cavagna et al. [1997] hypothesized that kinetic and gravitational potential energy lost during the first half of the stance phase were stored as elastic strain energy at midstance and then returned as the animal's center of mass rose and accelerated forward. As noted in §2.2, the inverted pendulum and spring-mass mechanisms have been combined into a single model: the spring-loaded inverted pendulum (SLIP) [Sch98], which limits on the inverted pendulum or compass walker as stiffness increases.

3.1.2 Evidence for a general spring-loaded inverted pendulum (SLIP) model

Blickhan and Full [BF87] discovered that SLIP behavior was far more general than imagined and not restricted to upright-posture birds and mammals. Force platform data showed that 8-legged sideways-moving crabs can use a pendulum-like mechanism during walking, recovering as much as 55% of the energy otherwise supplied by muscles. At faster speeds, ghost crabs change gait from a walk to a bouncing trot. Full and Tu [FT90, FT91b] used a miniature force platform to show that the most prevalent taxon on earth, *Insecta*, bounce dynamically as they run over a wide range of speeds. Indeed, the SLIP describes the center of mass dynamics during locomotion in animals ranging in body size from a cockroach (0.001 kg) to a horse (135

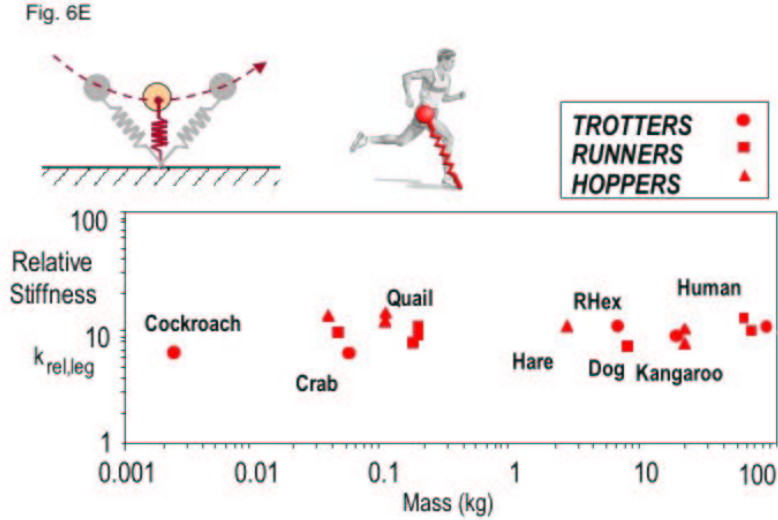


Figure 11: Relative individual leg stiffness vs. body mass for various animals and for the hexapedal robot RHex. From [BF93]. **BOB: Is this the correct citation?**

kg), a five decade range: Fig. 11.

The effective spring stiffness can be estimated as the ratio of the peak ground reaction force to maximal leg compression at midstance. If F_{vert} denotes the vertical whole-body ground reaction force and Δl the compression of the whole body leg spring, then the absolute SLIP spring stiffness (k) is:

$$k = \frac{F_{vert}}{\Delta l}. \quad (22)$$

Force platform data on mammals from Farley et al., [1993] show that larger animals have stiffer SLIPs: a trotting horse has a SLIP stiffness 100-fold greater than a rat. Comparison of mammals over a thousandfold range of body mass m shows that the SLIP stiffness increases as $m^{\frac{2}{3}}$.

To compare leg stiffnesses of diverse animals, allowances for both size and leg number must be made [BF93]. A dimensionless stiffness relative to size is required to correct for body weight and length differences. Such a relative SLIP stiffness k_{rel} can be calculated by dividing the peak whole body ground reaction force at midstance, normalized for body weight, mg ,

by the compression normalized by hip height, l :

$$k_{\text{rel}} = \frac{F_{\text{vert}}/mg}{\Delta l/l}. \quad (23)$$

The number of legs supporting the body during stance that sum to produce SLIP behavior varies from one in running bipeds to four in trotting crabs (see Fig. 4 above). For example, insects trotting in a double tripod gait compress their SLIPs by one third relative to bipedal runners. Because the relative force is the same as in bipedal runners, the SLIP stiffness of the insect is three-fold greater than for bipeds. Since the SLIP stiffness is determined by the number of legs supporting body weight, a relative individual-leg stiffness $k_{\text{rel,ind}}$ can be estimated by dividing the relative SLIP stiffness by this number (e.g. for an insect $k_{\text{rel,ind}} = k_{\text{rel}}/3$, and for a trotting quadruped or a hopper such as the kangaroo $k_{\text{rel,ind}} = k_{\text{rel}}/2$). Relative individual-leg stiffness is surprisingly similar in trotters, runners and hoppers using from one to four legs in stance: the data summarised in Fig 11 indicates $k_{\text{rel,ind}} \approx 10$. Thus, relative individual-leg force is about ten-fold greater than relative compression in six-legged trotters (cockroaches), four-legged trotters (dogs, horses), 2-legged runners (humans, birds) and two-legged hoppers (kangaroos).

3.2 Dynamics of sprawled postures and many legs: Running insects

Insects have become model organisms for the study of locomotion, as evidenced by advances in areas such as neurobiology [PI70, PI71, Pea72, PI72, Del80, Del85, Del91, Cru02, Bur80, BS83, TR00a, TR00b] [Cruse, Pearson, Dickinson, Burrows, Laurent, Delcomyn, Ritzmann], muscle function [FSAJ98, WR98a, WR98b] [Josephson; Full] and biomechanics [FT90, FT91b]. Insects can exhibit extraordinary locomotor performance, are inexpensive, hearty and abundant, have experimentally-tractable neuro-muscular systems, and often follow remarkably general relationships, encompassing both invertebrates and vertebrates (cf. Figs 9 and 11).

BOB: Based on the names you cited I picked out some refs from my bibliog database. Pls check and add/subtract. We probably only need a representative sampling here.

3.2.1 Evidence for equivalent gaits

Cockroaches exhibit bouncing gaits over 85% of their speed range Even at lower speeds they do not walk like inverted pendula [FT90, FT91b], and

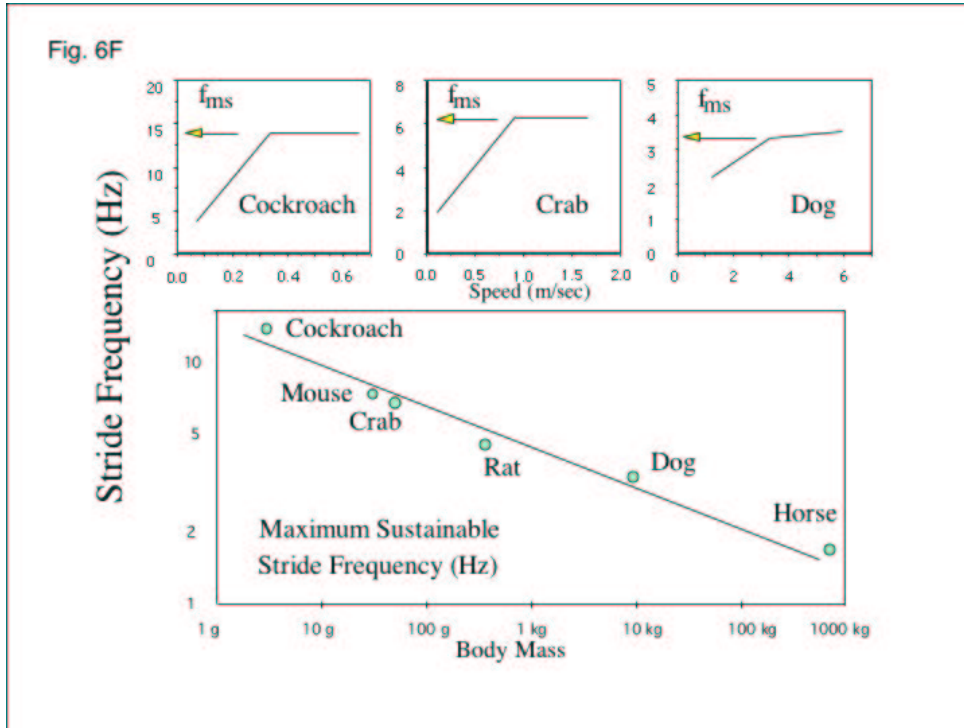


Figure 12: Stride frequency vs. speed for cockroaches, crabs and dogs, and stride frequency vs mass for a range of animals. From [?]. **BOB: Pls provide citations!**

although their energy recovery averages only 6-15%, their dynamics suggest that arthropods with exoskeletons can use springs and bounce during running much like mammals. Equivalent gaits may exist among legged runners that differ greatly in morphology. Further evidence of this equivalence comes from examining relationships between stride frequency and running speed, examples of which are shown in Fig. 12.

In quadrupedal mammals, stride frequency increases linearly with speed during trotting [?, HT88] [Heglund et al. 1974; Heglund and Taylor, 1988], but becomes nearly independent of speed as mammals switch to a gallop, higher speeds being obtained by increasing stride length. Similar relationships have been found in cockroaches and ghost crabs [FT90, BF87]: as speed increases stride frequency attains a maximum. Comparison of maximum sustainable stride frequency and the speed at which it is attained in crabs and cockroaches with data from mammals [?, HT88] suggests the possibility

of equivalent gait transitions in two-, four- six- and eight-legged animals. Surprisingly, when the size effect is removed, legged animals attain a similar maximum sustainable stride frequency at a similar speed [Ful89, Ful91] [Full, 1989, 1991]. For example, a crab and a mouse of the same mass change gait at the same stride frequency (9 Hz) and speed (0.9 m sec^{-1}) [BF87]. Proposed causes for the trot to gallop transition include a decrease in metabolic energy cost [HT81] and a reduction in musculo-skeletal strain [FT91a]. Blickhan et al. [?] [1993] placed strain gauges on ghost crab legs and found an abrupt change at the trot-gallop transition, but strain *increased* five-fold rather than decreased. Until the recent modeling efforts reported in §5.3 (see Fig. 32 below), no explanation was available for the proposed gait change in cockroaches.

3.2.2 Individual leg function

Trotting quadrupedal mammals, such as dogs, produce nearly the same ground reaction force pattern with each leg [CHT77, AJ78] [Jayes and Alexander, 1978] **BOB: Alexander-Jayes 1978 OK?**, much like SLIP ground reaction forces. In fact successful trotting quadrupedal robots have been designed that produce similar forces on each leg, differing only in relative phase [Rai86] [Raibert et al. 1986]. However, individual leg ground reaction forces, measured using a miniature force platform [FBT91] and photo-elastic gelatin [FYJ95] show that hexapedal runners do *not* behave like quadrupeds with an added set of legs. At constant average running speed, each contralateral leg pair of the cockroach is characterized by a unique ground reaction force pattern, as indicated in the left column of Fig. 13. The front leg decelerates the center of mass in the fore-aft direction throughout a step, the hind leg accelerates it, and the middle leg does both, initial deceleration being followed by acceleration, much like legs of bipedal runners and quadrupedal trotters. Peak vertical ground reaction forces for each leg are equal in magnitude, and significant lateral ground reaction forces are directed toward the body. Nonetheless, differing individual leg forces in insects combine to produce net forces on the body COM in the sagittal plane similar to those of the single leg of a bipedal runner.

One important consequence of the large lateral and opposing leg ground reaction forces involves muscle force production. In the cockroach, peak ground reaction forces are oriented toward the coxal joints (analogous to bipedal hips) that articulate with the body. This tends to minimize joint moments and muscle forces [FBT91]. Legs of animals do not generate vertically directed ground reaction forces that result in large torques about the

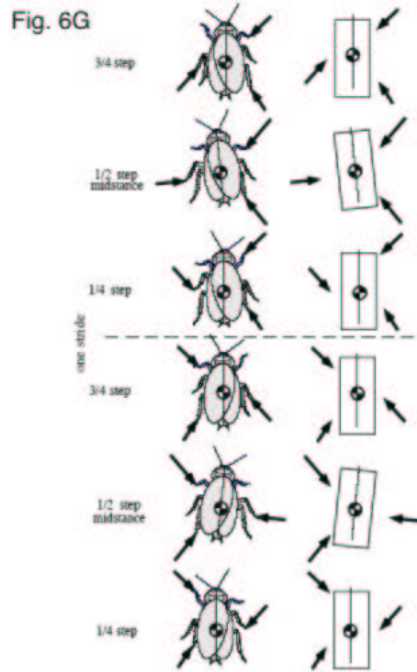


Figure 13: Left column: the double tripod gait of insects, showing typical individual foot force vectors near beginning, at middle, and near end of each stance phase. Right column: the rigid body prescribed force model of Kubow and Full [KF99]. From [KF99].

‘hip’ as do some legged robots, nor do they operate under the horizontal, zero-foot force criterion used in some robot designs [Wal86]. Insect legs push against one another, but force vectors are aligned approximately along the legs, and directed largely toward joint centers of rotation, much as in upright-posture birds and mammals. Hence, sprawled posture locomotion of arthropods, amphibians and reptiles does not necessarily result in large joint moments or muscle forces. This appears consistent with data showing that the minimum metabolic costs of locomotion in species that differ in posture can be similar [Ful91] [Full, 1991], cf. Fig 9.

To discover if individual insect legs can function as springs, Dudek and Full [67] oscillated legs dynamically with a computer-controlled lever. Cockroach legs, in particular, have the potential to function as passive exoskeletal springs in the sagittal plane because of their more vertically oriented joint

axes. Stiffness, damping, and resilience were measured during vertical oscillations orthogonal to the plane of joint rotations [68, 69]. Leg resilience was high, ranging from 65-85%, and was independent of oscillation frequency. Dudek and Full [68] estimated a damping ratio using the stiffness and damping coefficients from a Voigt model, assuming the body rests on a support tripod of legs during stance phases in running. Values predict that the tripod of legs used by running cockroaches is under-damped, thus permitting some energy storage and recovery.

BOB: What is (leg) ‘resilience’? Stiffness? Inverse of stiffness? stiffness divided by damping?? Also I need the refs that you give only as numbers [67,68,69] and more appearing below!

3.2.3 Static and dynamic stability

The springy legs of insects radiating from their mass centers almost certainly provide performance advantages beyond energy storage and return. A sprawled-posture bestows a wide base of support and low center of mass, both of which reduce overturning moments. Additionally, most insects use an alternating tripod gait over a broad range of speeds (Fig. 13); indeed, Hughes [1952] stated that the six-legged condition is the ‘end-product of evolution,’ because the animal can always be statically stable.

However, while Ting et al. [TBF94] found that running death’s head cockroaches *Blaberus discoidalis* do keep their centers of mass within a tripod of support over a wide range of speeds, these insects are *statically unstable* at their fastest speeds. Their percent stability margin (the shortest distance from COM to the boundaries of support normalized by the maximum possible stability margin) was found to decrease with increasing speed from 60% at 10 cm s^{-1} to negative values (implying static instability) at speeds faster than 50 cm s^{-1} . Certainly, the fastest gait of the American cockroach *Periplaneta americana* cannot be statically stable, for at 1.5 m sec^{-1} – nearly 50 body lengths per second – this species runs bipedally [FT91b]. In both animals, dynamic stability is maintained throughout.

Discoveries of spring-mass behavior, static instability in a fast tripod gait, and dynamically stable bipedal running such as those summarised above suggest that energy use in insects might not be minimized, but rather *managed*, to ensure dynamic stability. Moreover, preliminary studies on cockroaches also show that preferred speed is maintained during rapid running over rough terrain [59]. A fractal arrangement of blocks reaching up to three times higher than the COM offers little resistance: animals do not step carefully over it or adopt a follow-the-leader gait like those of some legged

robots, but continue to use the same alternating tripod gait observed on flat terrain. Simple feedforward motor output appears to be effective in the negotiation of such rough terrains when used in concert with a mechanical system that may be tuned to stabilize passively.

Overall, these data lead to the hypothesis that dynamic stability and a conservative motor program allow many-legged, sprawled posture animals to miss-step and collide with obstacles, but suffer little loss in performance. Rapid disturbance rejection appears to be an emergent property of the musculoskeletal mechanical system.

3.2.4 Self-stabilization in the horizontal plane

To develop a more precise hypothesis on the mechanical system's role in stabilizing running, Kubow and Full [KF99] created a feed-forward, three-degree-of-freedom dynamic model of a hexapod, representing a sprawled-posture insect in the horizontal plane: see the righthand column of Fig. 13. Vertical motions and gravity were excluded, yaw and translation instabilities being assumed to be more critical than the insect flipping over or falling and striking its abdomen. The model, a rigid body with six massless legs, was formulated with direct biomechanical data taken from death-head cockroaches, including body mass and inertia, individual leg ground reaction forces, and foot positions relative to the body [FT90, FBT91, BF93, TBF94, FYJ95, KWF97, 01]. Stereotyped periodic force inputs were prescribed at foot positions fixed in inertial space throughout each step, but force vector directions were allowed to rotate with the body. The model was driven by a this feed-forward signal with no equivalent of neural feedback among any of the components.

Bob: You had: 'Forces stayed fixed relative to the ground for the duration of a step. Leg forces were generated relative to the body using the same pattern during every step.' These two sentence seem contradictory. I thought you allowed the stereotyped force patterns to rotate with the body. Is my rewrite above correct?

The model's forward, lateral and rotational velocities were similar to those measured in the animal at its preferred velocity. More surprisingly, the model self-stabilized on a biologically-relevant time scale following instantaneous velocity perturbations acting on its center of mass. The rate of recovery depended on the orientation of the perturbation. Recovery from lateral perturbations took multiple strides, whereas recovery from rotational velocity perturbations occurred within one step. Recovery to 63% from fore-aft velocity perturbations was very slow, taking almost 50 strides. Heading

(i.e. the compass direction of COM) never recovered from lateral velocity perturbations. Recovery was dynamically coupled such that perturbations in one velocity component necessarily changed the others. Perturbed COM positions and body angles relative to the fixed feet provided ‘mechanical feedback’ by altering leg moment arms. This ‘anchored’ model inspired the LLS templates that we discuss in §5, and both it and they motivated the following experiments.

Jindrich and Full [JF02] perturbed rapidly running insects to experimentally test the self-stabilization hypothesis. An apparatus was mounted onto the thorax of a cockroach and positioned to propel a projectile laterally, delivering a specific impulse in linear momentum near the the animal’s COM. The apparatus used chemical propellants to accelerate a small metal ball, producing impulsive reaction forces less than 10 ms in duration, but yielding an almost ten-fold increase in lateral velocity relative to maxima observed during unperturbed locomotion. Lateral velocity began to recover within 13 ms after initiation of the perturbation. This recovery duration is comparable to all but the fastest reflex responses measured in insects [72] and is likely shorter than a neurally-mediated correction when the delays of the musculo-skeletal system response are considered. Cockroaches recovered completely in 27 ms and did not require step transitions to recover from imposed lateral perturbations. The animal’s center of mass response exhibited viscoelastic behavior in the lateral direction with leg spring stiffnesses similar to those estimated for unperturbed running. This rapid onset of recovery from lateral perturbations supports the hypothesis that mechanical reflexes augment or even dominate neural stabilization by reflexes during high-speed running.

3.3 Towards a theory of locomotion: templates, anchors, and some hypotheses

* Describe the four hypotheses H1-4 from NISFFIBR Propl.

* Could be some repetition of ideas introduced in §§ 1- 2.

** DAN will supply. How do we prevent this form being redundant with sections one and two?

4 Hybrid dynamical systems

The models of legged locomotion considered in this paper are more complicated than classical (smooth) mechanical systems. Due to impacts, ground

reaction forces, and changing stance patterns, the governing equations define *hybrid* systems in which the continuous-time vector fields describing evolution change at discrete times or *events*. Indeed, since the constraints that define these vector fields depend on the number and identity of legs in contact with the ground, even the dimension of the governing vector field may change at an event, and different coordinate systems may be called for. While various definitions have been proposed for hybrid systems, we shall follow one similar to that introduced by Back, Guckenheimer and Myers [BGM93]. Their approach is predicated upon four requirements: (1) existence of solutions in a general setting, (2) straightforward implementation of simulations, (3) inclusion of systems drawn from a wide range of applications and (4) amenability to analysis using tools from singularity theory and the theory of smooth dynamical systems. From a computational perspective, however, there are some differences between the present situation and that of [BGM93] in that, due to the piecewise-holonomic constraints noted in §2.1, the equations of motion are typically *differential-algebraic equations* (DAEs) rather than purely differential equations.

4.1 Introductory examples

There are several mathematical and computational obstacles to formulating a fully satisfactory definition of hybrid systems. The basic idea of following a vector field until an event occurs, then ‘jumping’ to a new initial condition for a new vector field and continuing to flow from there is clear, but it seems impossible to fully maintain the basic properties of existence and continuous dependence of solutions of ordinary differential equations on initial data. We illustrate this with a pair of two-dimensional examples.

Consider first a piecewise constant vector field \mathbf{f} defined by $\mathbf{f}(x, y) = (1, -1)$ if $y \geq 0$ and $\mathbf{f}(x, y) = (1, 1)$ if $y \leq 0$, assigning different discrete states to the upper and lower half planes. When a trajectory arrives at the x -axis, the event changes its discrete state but leaves its location unchanged. It is evident that there is no solution of the system with initial condition on the x -axis. Trajectories in the upper half plane point into the lower half plane and those in the lower half plane point into the upper half plane. The state is stuck on the attracting line $y = 0$, on which the vector field is multi-valued, perhaps ‘wanting’ to switch back and forth between the two discrete states infinitely often. This *chattering* conundrum is well known in engineering, and two strategies have been developed to address it. The ‘thermostat’ strategy derives from the desire to turn heat on when temperature is below a set point T_0 and off when it exceeds T_0 . Indeterminacy at T_0 is overcome

by overlapping the regions in which the heat is on and off. An offset δ is defined and switches from on to off are made at $T_0 + \delta$ and from off to on at $T_0 - \delta$, producing hysteretic cycling, whose rate can be adjusted by changing δ .⁶

The second strategy for dealing with chattering is to try to constrain the system to lie along the boundary between the two states. This is not feasible for the thermostat, but in mechanical devices we often wish to maintain such a constraint. The theory of *sliding modes*, based upon differential inequalities, achieves this [Utk77]. In the context of motor control, imagine a situation in which two muscles with nearby insertion points can be contracted to achieve motion of a limb. Since forces from the two muscles add, a suitable linear combination of contraction can be applied to enforce the desired constraint. Both of these strategies are clearly relevant and appropriate to biomechanical systems. In terms of hybrid systems theory, we regard sliding modes as distinct discrete states in their own right, with differential-algebraic equations defining the vector field which maintains a constraint.

A second example shows that conflicting choices between ‘target’ states seems unavoidable in hybrid systems. Consider a two-dimensional vector field describing discrete state 1 of a system. When a trajectory in the first quadrant reaches the x -axis, we assume that there is a transition to discrete state 2, and when a trajectory reaches the y -axis, there is a transition to a distinct discrete state 3. When a trajectory reaches the origin, a decision must be made between transitions to states 2 and 3 or the origin must be regarded as a further discrete state. Whichever choice is made, we lose continuous dependence of solutions on initial data. Whether this is reasonable in the example depends on the underlying ‘physics.’ The situation is reminiscent of what happens in a locomotion model when two feet make simultaneous ground contact. In the analogous problem of *triple* collisions in the three body problem [McG75], it is known that no ‘regularization’ is possible and that solutions do not depend continuously on initial conditions (in contrast, double collisions are regularizable).

Issues such as these leave us in a quandary regarding formal definitions of hybrid systems. More restrictive definitions yield stronger results on existence, uniqueness and continuous dependence on initial data, while less

⁶A second approach to the thermostat problem is to define a minimum time that the heat remains off or on. Theoretically, we regard this approach as undesirable for two reasons: it introduces ‘delays’ into the system that complicate the theory, and the choice of off/on state at temperature T_0 is not really resolved: two different trajectories are allowed from the same initial point.

restrictive ones encompass a larger set of examples. We adopt the principle that computational simulation of models is a priority: without simulation, it is difficult to extract useful information about model behaviors. Consequently, we choose definitions that ease the implementation of simulations. With this in mind, we turn to the definition proposed by Back et al. [BGM93].

4.2 Formal definitions

The state space of a hybrid system is a union

$$V = \bigcup_{\alpha \in I} V_\alpha,$$

where I is a finite index set and each V_α is a connected open set in R^{n_α} . The V_α are called *charts*. Note that the dimension of the charts may depend upon α . A state of the system consists of an index α together with a point in the chart V_α . We assume that a continuous time dynamical system is defined on each chart. If these systems are defined by DAEs rather than ODEs, we regard the chart as the set of points satisfying the algebraic constraints and suppose that the system is (uniquely) solvable at each point of the chart. Inside each chart V_α , we assume that there is a *patch* U_α , an open set whose closure $\bar{U}_\alpha \subset V_\alpha$ lies in the chart. We assume that the boundary of the patch is a finite union of level sets of smooth *boundary functions* $h_{\alpha,i} : V_\alpha \rightarrow R$. We further assume that there are *transition maps* $T_\alpha : \partial U_\alpha \rightarrow V \times I$ that apply a change of states to points of the patch boundaries. Depending upon context, we may want to leave the transition maps undefined on (small) subsets of the patch boundaries where the evolution of the system is not determined by underlying physics. We assume that the images of the transition maps lie at states that are initial points for a continuous time trajectory inside the closure of a patch. Intersection of a continuous time trajectory with a patch boundary is called an *event*.

Global evolution of the system consists of concatenation of flows along continuous time trajectories to events, followed by applications of the transition map at the event point. More precisely, a *trajectory* defined on the time interval $[t_0, t_n]$ with events at times $t_1 < \dots < t_{n-1}$ consists of discrete states $\alpha_0, \dots, \alpha_{n-1}$ and smooth curves $\gamma_i : [t_i, t_{i+1}] \rightarrow V_{\alpha_i}$ with the properties that

- γ_i is a trajectory of the continuous time dynamical system on V_{α_i} , and
- $T_{\alpha_i}(\gamma_i(t_{i+1})) = \gamma_{i+1}(t_{i+1})$.

We call the time intervals $[t_i, t_{i+1}]$ *epochs*.

Steady gaits in locomotion are represented by periodic orbits in models. This prompts us to examine carefully the stability properties of periodic orbits in hybrid systems. For generic systems and periodic orbits, a Jacobian for the Poincaré return map can be constructed as the composition of derivatives of the flow maps during each epoch, interleaved with derivatives of the transition maps between the epochs. The fact that flow maps along the epochs lead to variable event times, determined by when trajectories hit patch boundaries, makes this computation somewhat subtle. The derivative of the map along the flow to the event surface is not simply the derivative of the flow map at a prespecified time, but must be computed as follows.

Let $\dot{\mathbf{x}} = \mathbf{f}(\mathbf{x}, t)$ be an n -dimensional vector field with flow $\Phi(\mathbf{x}, t) : R^n \times R \rightarrow R^n$, and let $g : R^n \rightarrow R$ be a smooth function whose level set $g = c$ defines the patch boundary hit by trajectories with initial conditions near \mathbf{x}_0 . We assume that the level set of g is transverse to the vector field: $\mathbf{D}g \cdot \mathbf{f} \neq 0$, at the point where the event occurs. We denote the time of an event along the trajectory with initial condition \mathbf{x} by $\tau(\mathbf{x})$, a function determined implicitly by $g(\Phi(\mathbf{x}, \tau(\mathbf{x}))) = c$. We define $\Psi : R^n \rightarrow R^n$ to be the map that sends \mathbf{x} to the intersection of its trajectory with the surface $g = c$; i.e., $\Psi(\mathbf{x}) = \Phi(\mathbf{x}, \tau(\mathbf{x}))$. Thus $g \circ \Psi$ is constant, Ψ is singular and

$$\mathbf{D}\Psi(\mathbf{x}) = \mathbf{D}_x\Phi + D_t\Phi\mathbf{D}_x\tau. \quad (24)$$

Differentiating the equation $g(\Phi(\mathbf{x}, \tau(\mathbf{x}))) = c$ gives

$$\mathbf{D}_xg \cdot (\mathbf{D}_x\Phi + D_t\Phi \cdot \mathbf{D}_x\tau) = 0. \quad (25)$$

Now $D_t\Phi = (\mathbf{x}, \tau)$ by the flow property and $\mathbf{D}_xg \cdot \mathbf{f} \neq 0$, so (25) implies that $\mathbf{D}_x\tau = -(\mathbf{D}_xg \cdot \mathbf{f})^{-1} \cdot \mathbf{D}_xg \cdot \mathbf{D}_x\Phi$. Using this, we compute from (24):

$$\mathbf{D}_x\Psi = \mathbf{D}_x\Phi - (\mathbf{D}_xg \cdot \mathbf{f})^{-1} \cdot \mathbf{f} \cdot \mathbf{D}_xg \cdot \mathbf{D}_x\Phi. \quad (26)$$

These formulae are used in the numerical computations of periodic orbits and their eigenvalues, to be described next.

4.3 Numerical Methods

Models of legged locomotion are hybrid dynamical systems in which the continuous-time vector fields are constrained Lagrangian mechanical systems. These differ from generic ODEs in two substantive ways, both of which must be addressed to achieve accurate simulation.

- Events encountered by trajectories must be detected and computed accurately.
- The differential-algebraic equations have index 3.

With regard to the second point, a DAE has differential index k if k differentiations of the original system are required to obtain a system of *ordinary* differential equations whose trajectories coincide with solutions of the DAE [HW91]. Mechanical systems with holonomic constraints can be written in the form

$$\begin{aligned}\dot{\mathbf{q}} &= \mathbf{u}, \\ \mathbf{M}(\mathbf{q})\dot{\mathbf{u}} &= \mathbf{f}(\mathbf{q}, \mathbf{u}) - \mathbf{G}^T(\mathbf{q})\lambda, \\ \mathbf{0} &= \mathbf{g}(\mathbf{q}),\end{aligned}$$

where \mathbf{M} is a positive ‘mass matrix,’ \mathbf{g} specifies the constraint functions, $\mathbf{G}(\mathbf{q}) = \mathbf{D}_q\mathbf{g}$ and λ is a vector of Lagrange multipliers. To obtain a system of ordinary differential equations from this DAE, it is necessary to differentiate the third equation three times.

Before addressing numerical issues *per se*, one must first express the equations of motion in consistent forms amenable to the solution methods to be used. For multibody mechanical systems, doing this by hand is tedious and error-prone. In this section, we describe new methods from E. Phipps’ thesis [Phi03] that have the potential to significantly outperform existing methods in accuracy and ease of problem formulation.

Newton’s laws of motion for a constrained multibody system state that the time-derivatives of its linear and angular momenta are given by the forces and moments acting on the bodies. Application of these laws requires a minimal set of coordinates that specify the state of the system. As even the simpler examples of §5 below indicate, expressions for velocities and accelerations in these coordinates can be lengthy, making it cumbersome to derive Newton’s equations in this ‘direct’ manner. While automated systems have been developed to aid in these derivations, Lagrangian formulations give a more concise approach, their main advantage being that the system’s kinetic and potential energies can be described in terms of redundant coordinates so long as these are subjected to the relevant constraints. The price paid for doing this is that the resulting Euler-Lagrange equations of motion are DAEs rather than ODEs. Moreover, even in the Lagrangian formulation, the differentiations that produce the Euler-Lagrange differential equations yield lengthy expressions for systems of modest size. It is therefore desirable to simulate a system automatically from inputs that consist *only* of the

Lagrangian and the constraints. Phipps [Phi03] designed and implemented codes to do just this.

Phipps computes Taylor series expansions of trajectories, as functions of time, directly from the Lagrangian and the constraints. He allows constraint functions that are smooth in positions and linear in velocities. In principle, this is a straightforward process involving substitution of expansions with undetermined coefficients into the Euler-Lagrange and constraint equations and solving for the coefficients. In practice, one needs methods that handle data structures for the Taylor series expansions and the lengthy algebra involved in solving the equations. Such methods have been developed as part of a collection of techniques known as *automatic differentiation* or *computational differentiation* [Gri00, GJM⁺96]. A code that evaluates a function expressed in terms of elementary functions contains the information needed to compute its derivatives. Automatic differentiation codes carry out the process by applying differentiation rules for elementary functions and binary operations in a step-by-step fashion. Many intermediate results are generated in automatic differentiation; these need not be explicitly displayed, but the methods are memory intensive. Indeed, the Euler-Lagrange equations themselves can be hidden from the user. One of the advantages of automatic differentiation over approximation of derivatives by finite differences is that there are no truncation errors: accuracy is limited only by round-off errors in applying differentiation rules.⁷

The result of applying automatic differentiation to a Lagrangian with constraints is a large system of equations for the coefficients of the degree- d Taylor polynomial of a trajectory. Here d is an algorithmic parameter that determines the asymptotic order of accuracy of the algorithm. In the case of ODEs, the system of equations is triangular and readily solved. Equations derived from DAEs are not triangular, so it is necessary to address their regularity and efficient methods for their solution. Phipps states hypotheses that the constraints must satisfy for regularity to hold, implying that the DAE reduces to an ODE on a submanifold of the state space. (These are satisfied for many locomotion models; indeed, a minimal set of generalized coordinates explicitly defines the vector field on such a submanifold.) He then gives procedures for evaluating this vector field and computing its Taylor series expansion.

⁷Since the Euler-Lagrange equations contain derivatives of the Lagrangian, automatic differentiation codes must be capable of recursive application: if F is defined by applying automatic differentiation to a function f , then we want to be able to apply automatic differentiation to the function F . Making extensive use of C++ templates, Phipps developed an automatic differentiation code with this capability.

The problem of computing events accurately is easy to solve with Taylor series methods. The representation of trajectories as a concatenation of segments defined by Taylor polynomials is *dense*: its order of accuracy is maintained at all points of the segment. Therefore, intersections of the curves defined by the Taylor polynomials with patch boundaries locate the events to the same order of accuracy employed in the numerical integration. This property is manifestly *not* true for many numerical integration methods in which the order of accuracy is attained only at the endpoints of an integration step. Here, the computation of events reduces to a one dimensional root finding problem along the curves defined by the Taylor polynomials.

Steady gaits are represented by periodic orbits of locomotion models. The simplest method for seeking periodic orbits is to follow trajectories for a long time, hoping that they converge to the desired periodic orbit. This strategy works best when the periodic orbit is asymptotically stable with return map having eigenvalues well inside the unit circle. In these circumstances, the orbit has a neighborhood that is attracted to it at an exponential rate determined by the eigenvalues. However, as the examples of §2.1 and those to come indicate, the periodic orbits of interest here come in continuous families and there are directions which may be unstable or only weakly stable. Thus, algorithms that compute periodic orbits directly are a valuable tool for the analysis of locomotion models. We briefly describe methods that can be built ‘on top’ of the Taylor series integrator described above.

Direct computation of a periodic orbit is a boundary value problem. If Φ is the flow of an n -dimensional dynamical system, we seek solutions of the equation $\Phi(\mathbf{x}, t) = \mathbf{x}$. Boundary value methods solve discretized versions of this equation. The most widely used method for computing periodic orbits directly is a *collocation* method implemented in the program AUTO [DCF⁺97], but this has not yet been adapted to hybrid systems. In contrast, *shooting* algorithms assume that Φ and its Jacobian can be computed via a numerical integration method and used directly to solve the equation. In *simple shooting*, one tries to solve the equation $\Phi(\mathbf{x}, t) = \mathbf{x}$. One technical problem that must be addressed is that the system is underdetermined: there are n equations but $n + 1$ variables (\mathbf{x}, t) . To obtain a unique solution, one adds another equation (called a *phase condition*), that is satisfied by isolated points of the periodic orbit. Simple shooting algorithms are indeed simple to implement; the Jacobian of Φ is easy to obtain automatically with the Taylor series methods described above. If return map has no unit eigenvalues and the phase condition defines a surface transverse to the periodic orbit, then the Jacobian of the augmented

simple shooting system of equations will be regular and Newton’s method will converge quadratically to the solution from nearby starting values.

Simple shooting methods are hopelessly ill-conditioned on many problems. Multiple shooting methods alleviate this difficulty by breaking up the periodic orbit into segments, solving a system of equations $\Phi(\mathbf{x}_i, t_i) = \mathbf{x}_{i+1}$ for points $\mathbf{x}_0, \mathbf{x}_1, \dots, \mathbf{x}_N$ and times t_0, \dots, t_N with $\mathbf{x}_{N+1} = \mathbf{x}_0$. This seems to complicate the problem, creating a larger system of equations to solve and making the system even more underdetermined. The payoff is that a much broader class of problems can be solved, and extension to hybrid systems is straightforward. Specifically, transition maps are included in the discretization (\mathbf{x}_i, t_i) of the periodic orbit by regarding the boundary functions defining events as phase conditions for the boundary value solver. The transition maps are applied at events and their Jacobians are inserted in the computation of Jacobians for the periodic orbit. Guckenheimer and Meloon [GM00] describe implementations of multiple shooting methods using the Taylor series integration described above. Phipps [Phi03] extends these multiple shooting methods to hybrid systems.

4.4 A piecewise holonomic example: the SLIP

The discrete Chaplygin sled of §2.1.2 shows that (partial) asymptotic stability is possible in some hybrid system, even if the continuous-time vector fields defining each epoch are Hamiltonian. We now return to a more complex and realistic locomotion model that also exhibits asymptotic stability, the SLIP. However, before describing it we note that other hybrid systems have return maps whose natural canonical structures preclude asymptotic stability. One set of such examples are ‘billiards’ problems involving rigid bodies bouncing elastically at collisions with each other or with prescribed boundaries [Bir27, Sin91]. A particularly simple case – a single elastic ball bouncing on a sinusoidally-vibrating table – may be simplified as the area-preserving standard map [GH90, §2.4].

In order to relate to horizontal plane (LLS) models in which yawing motions play an essential role, we describe a generalized SLIP, endowed with rotational inertia: Fig. 14, cf. Fig. 4, although we subsequently restrict to the non-rotating or point mass case. A massless, axially-sprung leg is attached to an extended body of mass m and moment of inertia I at a hip joint, H, a distance d from the COM, G. The system’s configuration is determined by the pitch angle θ and COM position (x_G, y_G) referred to an inertial frame, although during stance, it is convenient to replace the Cartesian coordinates (x_G, y_G) by polar coordinates: the angle ψ between the line joining foothold

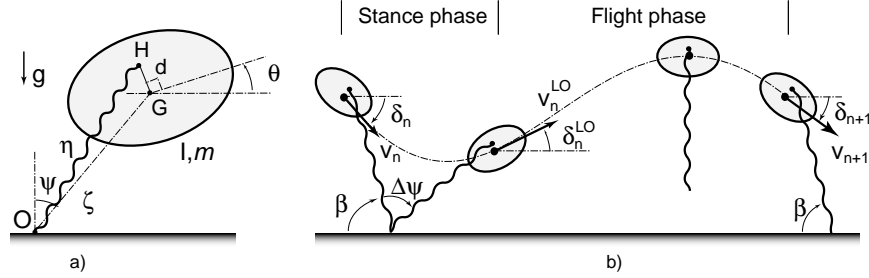


Figure 14: The spring-loaded inverted pendulum (SLIP) including pitching. (a) The stance coordinate system; (b) the stance and flight phases comprising a full stride. Adapted from [GAHK03].

O to G and the vertical (gravity) axis, and the distance ζ from foothold to COM: Fig. 14(a). (Note that ψ increases clockwise, while θ increases counterclockwise.) The (compressed) spring length is

$$\eta = \sqrt{d^2 + \zeta^2 + 2d\zeta \cos(\psi + \theta)}. \quad (27)$$

For simplicity, we take frictionless joints at O and H. Cartesian coordinates provide the simplest description during flight. The body is assumed to remain in the sagittal plane throughout.

A full stride divides into a stance state with foothold O fixed, the leg under compression, and the body swinging forwards (ψ increasing); and a flight state in which the body describes a ballistic trajectory under the sole influence of gravity. Stance ends when the spring unloads at leg length l and the foot reaction force drops to zero; flight then begins, continuing until touchdown, which occurs when the landing leg, uncompressed and set at a predetermined angle β relative to horizontal, contacts the ground: Fig. 14(b). Control is applied only to reorient the leg during flight, prior to touchdown. The touchdown and liftoff events are respectively determined by COM height y_G first reaching $l \sin \beta - d \cos \theta$ from above and leg length η first reaching l from below, and COM positions and velocities are unchanged by either event. Thus, relative to the stance phase coordinate origin O of Fig. 14, at liftoff $(x_G^{LO}, y_G^{LO}) = (\zeta^{LO} \sin \psi^{LO}, \zeta^{LO} \cos \psi^{LO})$. A similar transition map from Cartesian to polar coordinates applies at touchdown.

Using the coordinate system of Fig. 14, the kinetic and potential energies of the body may be written as

$$T = \frac{1}{2}m \left(\dot{\zeta}^2 + \zeta^2 \dot{\psi}^2 \right) + \frac{1}{2}I\dot{\theta}^2, \quad (28)$$

$$V_{tot} = mg\zeta \cos \psi + V(\eta(\zeta, \psi, \theta)), \quad (29)$$

where V denotes the spring potential. Forming the Lagrangian $L = T - V_{tot}$ and writing $\partial V/\partial\eta = V_\eta$, we obtain the equations of motion for the stance phase:

$$\ddot{\zeta} = \zeta\dot{\psi}^2 - g \cos \psi - \frac{V_\eta(\eta)}{m\eta} (\zeta + d \cos(\psi + \theta)) , \quad (30a)$$

$$\zeta\ddot{\psi} = -2\dot{\zeta}\dot{\psi} + g \sin \psi + d \frac{V_\eta(\eta)}{m\eta} (\sin(\psi + \theta)) , \quad (30b)$$

$$\ddot{\theta} = d\dot{\zeta} \frac{V_\eta(\eta)}{I\eta} \sin(\psi + \theta) . \quad (30c)$$

The flight phase dynamics are determined by the ballistic COM translation and torque-free rotation equations, which may be integrated in Cartesian coordinates to yield:

$$x_G(t) = x_G^{LO} + \dot{x}_G^{LO}t , \quad y_G(t) = y_G^{LO} + \dot{y}_G^{LO}t - \frac{1}{2}gt^2 , \quad \theta(t) = \theta^{LO} + \dot{\theta}^{LO}t , \quad (31)$$

where the superscripts LO refer to the system state at liftoff.

Eqns. (30) are in general non-integrable [Arn78, GH90, Hol90] and the stance trajectory must be obtained numerically, even in the special case $d = 0$ in which the rotation (θ) variable decouples and the system reduces to the two-degrees-of-freedom point mass SLIP of [Bli89, BF93]. However, if we additionally assume that the spring is sufficiently strong, elastic energy dominates the gravitational potential during most of the stance phase and we may neglect the gravitational force and moment entering Eqns. (30a) and (30b), in which case the moment of linear momentum of the COM about the foot, $m\dot{\psi}\zeta^2$, is also conserved and (30a) may be integrated precisely as in the $d = 0$ and truly gravity-free LLS analyzed in §5.1.1. (This approximation is assessed and discussed in detail in [SK00], cf. [GAHK03]). Composition of the resulting stance and flight phase dynamics results in the approximate touchdown-to-touchdown Poincaré map:

$$P : \begin{bmatrix} v_{n+1} \\ \cos(\delta_{n+1}) \end{bmatrix} = \begin{bmatrix} v_n \\ \sqrt{1 - \frac{2gl}{v_n^2} (\sin(\beta + \Delta\psi) - \sin\beta)} \cos(\delta_n + \pi - \Delta\psi - 2\beta) \end{bmatrix} , \quad (32)$$

in which the system's state at the n 'th touchdown is described by the COM velocity magnitude v_n and direction δ_n with respect to a horizontal datum (Fig. 14(b)). In (32) the angle $\Delta\psi$ swept by the leg is given by the quadrature

$$\Delta\psi(v_n, \delta_n) = 2 \int_{\zeta_b}^{\zeta} \frac{d\zeta}{\zeta \sqrt{\frac{[mv_n^2 - 2V(\zeta)]\zeta^2}{mv_n^2 l^2 \sin^2(\beta - \delta_n)} - 1}} , \quad (33)$$

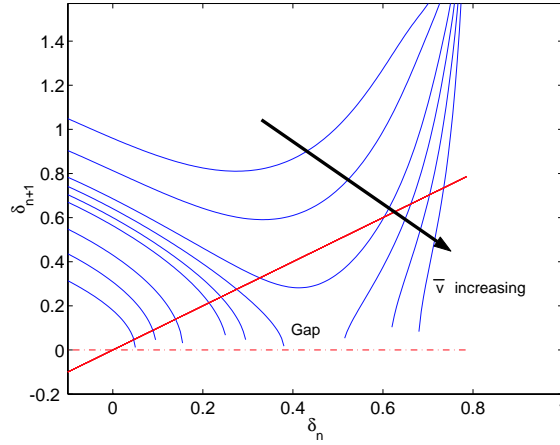


Figure 15: A family of approximate one-dimensional Poincaré maps for a linear spring SLIP with $k = 10$, $m = 1$, $l = 1.5$, $\beta = \pi/4$ and speeds \bar{v} ranging from 3.2 to 8. The fixed points appear in a saddle-node bifurcation, and a gap then opens as \bar{v} increases. When a pair of fixed points exists, that at larger δ is unstable; the lower δ one may be stable or unstable, and for very high speeds only the latter exists. From [GAHK03].

where ζ_b is the leg length at midstride. In reducing this two-degree-of-freedom system to a two-, rather than three-dimensional return map, we are using the fact that the prescribed leg touchdown angle fixes the COM position relative to the stance coordinate origin: $(x_G^{TD}, y_G^{TD}) = (-l \cos \beta, l \sin \beta)$. If pitching motions were allowed, two further state variables, θ_n and $\dot{\theta}_n$, would be required, and the map would be four-dimensional, as for the LLS and other models of §5.

Note that, due to energy conservation and the ‘constant height’ touchdown protocol for $d = 0$, the COM speed v_n is the same at each touchdown: this is true even when gravity is included during stance. The dynamics is therefore captured by the one-dimensional map formed from the second component of (32) with speed $v_n = \bar{v}$ viewed as a parameter. Fig. 15 shows an example for a linear spring $V = k(\eta - l)^2/2$. The gap in the domain of definition for higher speeds is caused by liftoff conditions for which the COM fails to reach the necessary touchdown height during flight and ‘stumbling’ ensues [GAHK03]. The maps shown here indicate that, for speeds \bar{v} above a critical lower limit \bar{v}_{SN} at which a saddle-node bifurcation [GH90] occurs, a stable fixed point exists, although its domain of attraction shrinks dramatically as \bar{v} increases. For other parameter choices and spring laws,

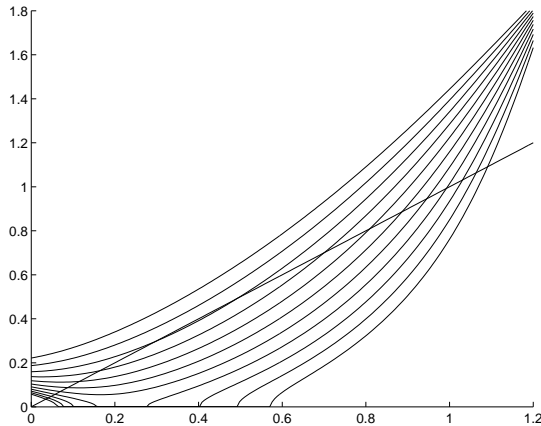


Figure 16: A family of one-dimensional Poincaré maps computed by Phipps’ method. Gravity was included during stance. Fixed parameters are $m = 1$ and $l = 1.5$ with the gravitational constant normalized to be 1. The touchdown speed \bar{v} is varied from 3.2 to 8 in steps of 0.48, to match the speeds used for Fig. 15. Newton’s method was used to precisely compute the stable periodic orbit with $\bar{v} = 5.12$. The non-trivial eigenvalue of its monodromy map is -0.146 .

period-doubling and even chaos may occur [GAHK03]. For $\bar{v} < \bar{v}_{SN}$, the forward velocity at touchdown is too low to overcome the potential energy barrier due to the forward-oriented spring leg, and the mass (eventually) bounces backward: no periodic gaits exist.

Although the quadrature of (33) can be evaluated, in the case of a quadratic potential, in terms of Jacobian elliptic functions [SH00b], the expressions are difficult to use and the return maps of Fig. 15 were computed by direct (fourth order Runge-Kutta) integration of (30a-30b) for $d = g = 0$.

We have computed analogous maps including gravitational effects (but still for $d = 0$) using Phipps’ Taylor series methods described in § 4.3. Rather than reducing to a two- or one-dimensional map, here one finds polynomial approximations to trajectories of this two-degree-of freedom hybrid system in the full four-dimensional phase space. Applying Newton’s method to the resulting return map and computing its Jacobian, we find for example that the stable fixed point has eigenvalues $0, 1, 1$ and approximately -0.146 at $\bar{v} = 5.12$. The (generalized) eigenspace of 1 is tangent to the plane spanned by the vector field (i.e., the direction along the orbit) and the family of periodic orbits obtained by varying \bar{v} , and the zero eigenvalue is due to the

singularity of the transition map at touchdown. The final eigenvalue is that of the reduced one-dimensional map. Fig. 16 shows results for a range of speeds (total energies); this Figure should be compared with Fig. 15.

The partial asymptotic stability of the SLIP, and of the LLS models to be studied in §5, prompts the following

Question: What are the characteristics of the events and transition maps needed to obtain asymptotically stable periodic orbits in a (conservative) piecewise holonomic system? In systems with symmetries, what is needed to obtain partially asymptotically stable periodic orbits? See Altendorfer, Koditschek and Holmes [AKH02] for a relevant, albeit far from complete, discussion.

At this point it is worth noting an important distinction between *inertial* and *body frame* coordinate systems. Newton’s laws must be formulated in an inertial (non-accelerating) frame [Gol80], while limb positions and forces generated in muscles or collectively by limbs, are usually most conveniently represented in body coordinates. Proprioceptive sensing and reflex or reflex control also take place in the body frame. In formulating Eqns. (30-31) we use only inertial frames, but in the models of §5 we pass back and forth between inertial and body frames using rotation matrices.

The point mass SLIP with the fixed touchdown protocol described above is simple enough to be amenable to (almost) complete analysis, although little is known about coupled pitching motions (in case $d \neq 0$), or other touchdown protocols. Here we have assumed the simplest such, requiring a minimum of feedback: mere knowledge of the inertial horizontal datum during flight; given this, leg placement is effected by feedforward control. More complex procedures have been proposed, including ones in which the leg is retracted so that it either begins its back swing prior to touchdown [SG02, SGBH02, SGH03, AKH02], or, as in the hexapedal robot RHex [SBK01, SK03], after liftoff it continues to rotate in the same direction, passing ‘over the shoulder.’ These effectively enlarge the domain of attraction of stable gaits, partly by allowing the SLIP to recover from stumbling.

5 Mathematical models for horizontal plane dynamics

As we have described, legged dynamics in the sagittal plane is often modelled by an inverted elastic pendulum or SLIP (e.g., [CHT77, McM84, Bli89,

MC90, BF93]). Since the typical splayed insect leg posture implies sagittal static stability for the majority of stance positions [TBF94], in [SH00b, SH00a] we introduced a similar model (without gravity) to explore motions in the horizontal plane: the lateral leg spring (LLS) system. Our hope is that, at least in near-steady gaits, sagittal and horizontal plane dynamics might be only weakly coupled, so that independent analyses will help us build towards an understanding of the full six degree-of-freedom body motions. Moreover, since in many insects leg masses are a small fraction of body mass, we neglected limb masses. (In *Blaberus*, for example, if we include the coxa joint, which does not move appreciably, with the body, total leg mass is $\approx 5\%$ of body mass [KWF97, Table 1].) For additional simplicity, and to capitalize on conservation of angular momentum in central force problems, we at first restricted our analysis to bipedal models with a 50% duty cycle, so that precisely one ‘effective foot’, representing three legs of a tripod acting as one, is in ground contact at any time. If foot contact is assumed torque-free, for such models angular momentum is conserved about the stance foot, as it is about the peg in the model of §2.1.2.

We shall give a fairly detailed description of the simplest model, to make the main ideas clear, and successively curtail our accounts as we move to more complex models, referring the reader to relevant literature.

5.1 The simplest passive model

The basic LLS model is shown in Fig. 17(a). A rigid body of mass m and moment of inertia I moves freely in the plane under forces generated by two massless, laterally rigid, axially-elastic legs, pivoted at a point P (generally displaced forward or backward a distance d from the COM G), and intermittently contacting the ground at feet F, F' with a 50% duty cycle. F, F' and P are pin joints (no torques). In considering multilegged animals, we appeal to the stereotyped use of a double-tripod gait in hexapods [FT91b] and a double quadruped gait in crabs [BF87], and represent each support set in stance by a single effective or *virtual leg*. Errors induced by collapsing leg groups linked in such stance phases to a single virtual leg are discussed below. We shall describe a hexapedal model in §5.3.

A full stride begins at left touchdown at time $t = t_n$ with the left leg spring relaxed at angle $+\beta$ relative to body orientation; the left stance phase ends at t_{n+1} when the spring is again relaxed, the body having ‘run past its foot.’ The left leg then begins its swing phase and the right leg simultaneously touches down at angle $-\beta$; its stance phase, and the stride, ends with spring relaxation at right liftoff/left touchdown t_{n+2} . We use the conven-

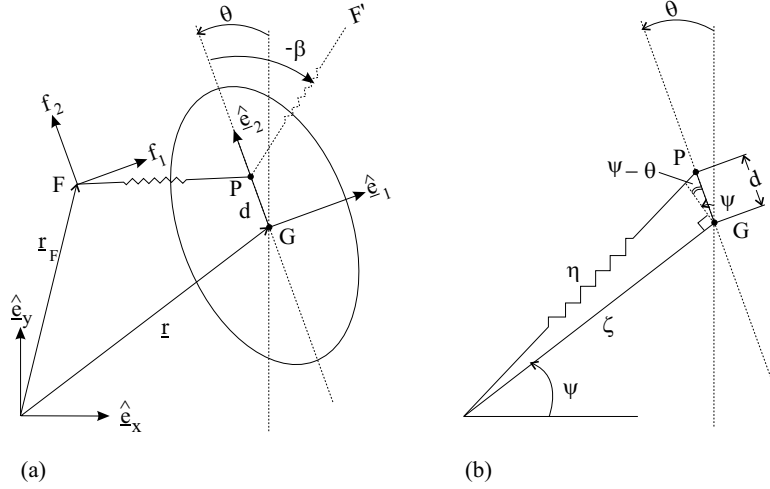


Figure 17: The LLS model: (a) The general set-up; (b) The (ζ, ψ, θ) polar coordinate system used during left stance phase. Here leg length is η and $\pm\beta$ denote leg touchdown angles. From [SH00b].

tion that n even (resp. odd) refers to left (resp. right) stance. Balance of linear and angular momentum results in three equations of motion for COM translation $\mathbf{r}(t) = (x(t), y(t))$ and body orientation $\theta(t)$ during stance:

$$m\ddot{\mathbf{r}} = \mathbf{R}(\theta(t)) \mathbf{f}, \quad I\ddot{\theta} = (\mathbf{r}_F(t_n) - \mathbf{r}) \times \mathbf{R}(\theta(t)) \mathbf{f}, \quad (34)$$

where $\mathbf{R}(\theta)$ is the rotation matrix, needed to transform leg forces \mathbf{f} , usually specified relative to the body, to the inertial frame; $\mathbf{r}_F(t_n)$ denotes touchdown foot position, expressed via d, l, β and body angle $\theta(t_n)$ at touchdown, and \times denotes the vector cross-product. The ‘hip-pivot’ P may be fixed, or may move in a prescribed manner (perhaps dependent on leg angle ϕ relative to body); the specific (linear) rule

$$d = d_0 + d_1(\psi - \theta) \quad (35)$$

exemplifies both cases ($d_1 = 0$: fixed; $d_1 \neq 0$: moving). We shall initially suppose that d is fixed.

Global conservation of total energy, and conservation of angular momentum $L_F = I\dot{\theta} + (\mathbf{r} - \mathbf{r}_F) \times m\dot{\mathbf{r}}$ about the foot in each stance phase, assist in integration of (34), which is most easily done in a polar coordinate system centered on the foot: Fig. 17(b). We summarise the results, a complete account of which appears in [SH00b]. In terms of the polar coordinates (ζ, ψ)

and θ , the kinetic and potential energies and the total angular momentum about the (left) stance foot take the forms:

$$T = \frac{1}{2}m(\dot{\zeta}^2 + \zeta^2\dot{\psi}^2) + \frac{1}{2}I\dot{\theta}^2, \quad (36)$$

$$V = V(\eta) \quad \text{with} \quad \eta = \sqrt{\zeta^2 + d^2 + 2\zeta d \sin(\psi - \theta)}, \quad (37)$$

$$L_F = m\zeta^2\dot{\psi} + I\dot{\theta} \stackrel{\text{def}}{=} p_\psi + p_\theta (= \text{const.}), \quad (38)$$

and Lagrange's equations are:

$$m\ddot{\zeta} = m\zeta\dot{\psi}^2 - \frac{V_\eta}{\eta}[\zeta + d \sin(\psi - \theta)], \quad (39a)$$

$$m(2\zeta\dot{\zeta}\dot{\psi} + \zeta^2\ddot{\psi}) = -d\frac{V_\eta}{\eta}\zeta \cos(\psi - \theta), \quad (39b)$$

$$I\ddot{\theta} = d\frac{V_\eta}{\eta}\zeta \cos(\psi - \theta). \quad (39c)$$

Reflecting about $\theta = 0$, which takes $\theta \mapsto -\theta$, we obtain an analogous description for right foot stance; thus, appeal to our n even-left odd-right convention and replacement of θ by $(-1)^n\theta$ in (39) supplies the two vector fields that, alternately applied, define a hybrid dynamical system. This formulation allows a general spring potential V , but the explicit examples that follow assume a linear spring $V = \frac{k}{2}(\eta - l)^2$. Note that (39) is a gravity-free version of the full SLIP model (30) (with a different definition of leg angle ψ).

Assuming that one stiffness parameter suffices to describe the spring, as in the linear case, the entire model is characterised by six physical parameters: leg stiffness, k , relaxed length, l , and pivot position relative to COM, d , along with m, I and β . Normalizing lengths with respect to l and nondimensionalizing time \tilde{t} , these may be reduced to four nondimensional groups:

$$\tilde{k} = \frac{kl^2}{mv^2}, \quad \tilde{I} = \frac{I}{ml^2}, \quad \tilde{d} = \frac{d}{l}, \quad \text{and} \quad \beta; \quad \text{with} \quad \tilde{t} = \frac{vt}{l}. \quad (40)$$

Here v is a representative speed (e.g. COM velocity magnitude at touch-down, or average forward speed $\langle v \rangle$) and $\sqrt{\tilde{k}}$ is a Strouhal number characterising the ratio of storable potential to kinetic energy. For fixed $\tilde{k}, \tilde{I}, \tilde{d}$ and β , solutions of (34) describe *identical* paths in (\mathbf{r}, θ) -space, scaled by l , at rates determined by \tilde{t} . This formulation is useful for parameter studies [SH01], but here we shall retain dimensional quantities to permit direct

$\mathbf{r}_F(t_n)$) and body angle θ relative to inertial frame appear in the governing equations. We find it convenient to define a reduced set of four variables that describe the body’s ‘internal dynamics’ at touchdown: as in the SLIP of Fig. 14 these are the COM velocity magnitude $v(t_n) = |\dot{\mathbf{r}}_n(t)|$, COM velocity direction or ‘heading’ $\delta(t_n)$ relative to body axis, along with body orientation $\theta(t_n)$ relative to the inertial reference frame, and body angular velocity $\omega(t_n) = \dot{\theta}(t_n)$: see Fig. 18(a). Here we retain the ‘mechanical’ terminology of [SH00b, SH00a]. In traditional biological usage, heading denotes the COM velocity with respect to compass direction, *i.e.* the quantity $\delta + \theta$, and body orientation denotes the angle the body makes with the velocity vector (δ). Note that δ is positive *towards* the leg that is touching down, and $\delta \in [\beta - \pi/2, \beta]$.

Given the total (kinetic) energy at touchdown:

$$E = T_0 = \frac{p_\zeta^2}{2m} + \frac{p_\psi^2}{2m\zeta_0^2} + \frac{p_\theta^2}{2I}, \quad (41)$$

where

$$\zeta_0 = \frac{l \sin(\pi - \beta)}{\sin \alpha} \quad \text{and} \quad d \sin \alpha = l \sin(\beta - \alpha) \quad (42)$$

are determined by touchdown geometry, and noting that

$$\dot{\zeta} = v \cos(\beta - \delta) \quad \text{and} \quad \dot{\psi} = \frac{v}{\zeta_0} \sin(\beta - \delta) \quad (43)$$

at touchdown, all six initial values necessary for integration of (39) may be found from $(v, \delta, \theta, \omega)$ and the touchdown parameters l, β . Integration yields left and right *single stance maps* \mathbf{F}_L and \mathbf{F}_R specifying these variables at each touchdown instant t_{n+1} in terms of their values at the preceding touchdown t_n , and composition yields the ‘full L-R stride’ Poincaré map $\mathbf{P} = \mathbf{F}_R \circ \mathbf{F}_L$:

$$(v_{n+2}, \delta_{n+2}, \theta_{n+2}, \omega_{n+2}) = \mathbf{P}(v_n, \delta_n, \theta_n, \omega_n), \quad (44)$$

where $v_n = v(t_n)$, *etc.*. Note that the ‘full stride’ includes left and right stance phases, unlike the stance-flight SLIP map of §2.2, and might more properly be called ‘double stride.’

Four-dimensional Poincaré maps of the form (44) suffice to describe *all* the models treated in this section. No matter how many or complex their legs, muscles or neural architectures, the feet in stance ultimately supply forces and moments to the body via equations of the general form (34), leading to incrementation of the dynamical variables $(v, \delta, \theta, \omega)$ from stride

to stride. Thus, the locomotive behaviors of both the LLS template, and the more complex and anchored hexapedal and neuromechanical models of §§5.3-5.4, are summarised by the four-dimensional maps. Of course, this does not mean that the maps are simple to compute in *any* of the examples, but solutions of some special cases may be found in closed form or approximated perturbatively. To these we now turn.

5.1.1 An integrable limit: $d = 0$

Using (38), Eqns. (39) can be reduced to two degrees of freedom, but in general no further constant of motion, excepting the total energy, exists. However, if the legs are attached at the COM ($d \equiv 0$), the rotation degree of freedom θ trivially uncouples and each component p_ψ and p_θ of L_F is individually conserved (cf. (39b,c): both ψ and θ are cyclic coordinates). The system is therefore completely integrable and may be reduced to a quadrature using conservation of energy [Gol80, Arn78]:

$$E = \frac{m\dot{\zeta}^2}{2} + \frac{p_\psi^2}{2m\zeta_0^2} + \frac{p_\theta^2}{2I} + V(\zeta) = E_0. \quad (45)$$

Specifically, since $\zeta \equiv \eta$, symmetry of the phase portraits about mid-stance implies that the angle $(\beta - \delta)$ between the mass center velocity direction and the leg is equal at lift-off to its value at touchdown. As may be seen from Fig. 17(b), this implies that the angle δ_{n+1} at right touchdown may be computed from v_n, δ_n at left touchdown as

$$\delta_{n+1} = \delta_n + \pi - (\Delta\psi_n + 2\beta) + (\theta_{n+1} - \theta_n), \quad (46)$$

where $\Delta\psi_n = \Delta\psi(v_n, \delta_n)$ is the net angle the leg turns through during the stance phase. This leads to the single stance maps (n even-left, odd-right):

$$\begin{aligned} v_{n+1} &= v_n \\ \delta_{n+1} &= \delta_n + \pi - (\Delta\psi(v_n, \delta_n) + 2\beta) + (-1)^n \omega \tau(v_n, \delta_n) \\ \theta_{n+1} &= \theta_n + \omega_n \tau(v_n, \delta_n) \\ \omega_{n+1} &= \omega_n \end{aligned} \quad (47)$$

where $\tau(v_n, \delta_n)$ denotes the stance phase duration.

Using (43) with $\zeta_0 = l$ and the conserved mass center kinetic plus po-

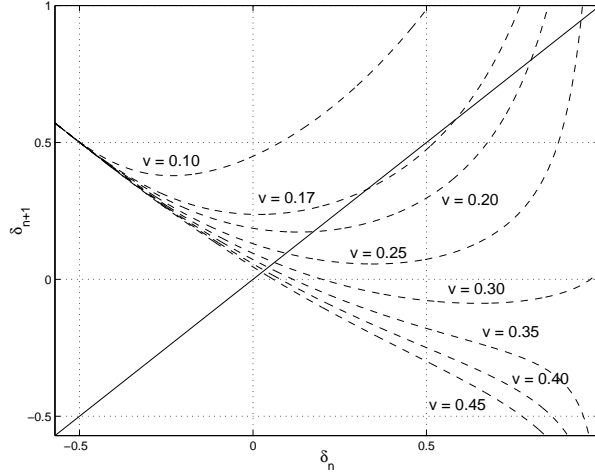


Figure 19: The single-stance return map for mass center touchdown velocities $\bar{v} = 0.1 - 0.45 \text{msec}^{-1}$ in the case of a linear spring with $m = .0025$, $l = .01$, $k = 2.25$ and $\beta = 1$. From [SH01].

tential energy, from (39) with $d = 0$ we compute the quadratures:

$$\tau(v, \delta) = 2 \int_{\zeta_b}^l \frac{\sqrt{m} \zeta d\zeta}{\sqrt{[mv^2 - 2V(\zeta)]\zeta^2 - mv^2 l^2 \sin^2(\beta - \delta)}}, \quad (48)$$

$$\Delta\psi(v, \delta) = 2 \int_{\zeta_b}^l \frac{d\zeta}{\zeta \sqrt{\frac{[mv^2 - 2V(\zeta)]\zeta^2}{mv^2 l^2 \sin^2(\beta - \delta)} - 1}}, \quad (49)$$

where ζ_b is the (minimal) spring length at mid-stride ($\dot{\zeta} = 0$: Fig. 18(b)), given by:

$$[mv^2 - 2V(\zeta_b)]\zeta_b^2 = mv^2 l^2 \sin^2(\beta - \delta). \quad (50)$$

Explicit formulae for the cases of quadratic and inverse square potentials, corresponding to a linear spring and a model for an ‘air spring’ [Rai86], are given in [SH00b], but the former are in terms of Jacobi elliptic functions and awkward to use. Schwind and Koditschek [SK00] provide useful approximations in terms of elementary functions. An upper bound for $\Delta\psi$ is easily found by considering the limit $\bar{v} \rightarrow \infty$, in which potential energy may be neglected and the COM travels in a straight line [SH00b]:

$$\Delta\psi(v, \delta) \leq \pi - 2(\beta - \delta). \quad (51)$$

Fig. 19 shows graphs of the resulting one-dimensional single stance return map (the second row of (47)) for a linear spring and parameters characteristic of *Blaberus discoidalis* over a range of touchdown velocities. When $\Delta\psi$ has a unique maximum and its slope is always less than 2 (for which (51) is necessary but not sufficient, but which holds for linear and air springs [SH00b, SH01]) then this map is unimodal [GH90] and has at most one stable fixed point, an unstable fixed point, and no other invariant sets. Moreover, there is no gap in its domain of definition. (Compare Fig. 19 with the SLIP Poincaré maps shown in Figs. 15-16 of §4.4.)

Question: An open question which may appeal to analysts is to classify those potential energy functions $V(\eta - l)$ that, via (49-50), yield return maps possessing at most a unique stable fixed point, or, more generally, a single attractor. The latter would follow if it could be proved that $\delta - \Delta\psi$ has negative Schwarzian derivative [Sin78, GH90]. Direct computation of derivatives of $\Delta\psi$ yield indeterminate forms that appear difficult to deal with, and the Schwarzian involves derivatives up to order three.

Fixed points of (47) correspond to symmetric gaits in which left and right stance phases are mutual reflections, and the COM oscillates about a straight path: $(\bar{v}, \bar{\delta}, \bar{\theta}, 0)$, with $\bar{\delta}$ implicitly determined in terms of \bar{v} by

$$\Delta\psi(\bar{v}, \bar{\delta}) = \pi - 2\beta. \quad (52)$$

The eigenvalues of the linearized map $\mathbf{DP}(\bar{v}, \bar{\delta}, \bar{\theta}, 0)$ are $\lambda_{1-3} = 1$, with eigenvectors $(0, 0, 1, 0)^T$, $(\partial\Delta\psi/\partial\delta, -\partial\Delta\psi/\partial v, 0, 0)^T$ and a generalized eigenvector; and $\lambda_4 = 1 - \partial\Delta\psi/\partial\delta|_{(\bar{v}, \bar{\delta})}$, with eigenvector $(0, 1, 0, 0)^T$. The first of these is associated with rotational invariance and the second with conservation of energy; the third is special to this uncoupled case; as we shall see, for $d \neq 0$ it perturbs away from 1. Note that, as \bar{v} increases, fixed points appear at a critical speed \bar{v}_c in a saddle-node bifurcation when (52) is satisfied and simultaneously $\partial\Delta\psi(\bar{v}, \bar{\delta})/\partial\delta = 1$. For $\bar{v} < \bar{v}_c$ kinetic energy at touchdown is insufficient to overcome the spring potential and the body bounces back. Bifurcation diagrams illustrating branches of steady gaits arising in a similar saddle-node are shown below for $d \neq 0$.

5.1.2 Fixed COP: $d \neq 0$

For $d \neq 0$ (39) is not longer integrable, so we resort to numerical solutions to construct the full stride map \mathbf{P} . Details of the methods adopted, including finite difference methods to approximate the Jacobian \mathbf{DP} , are given

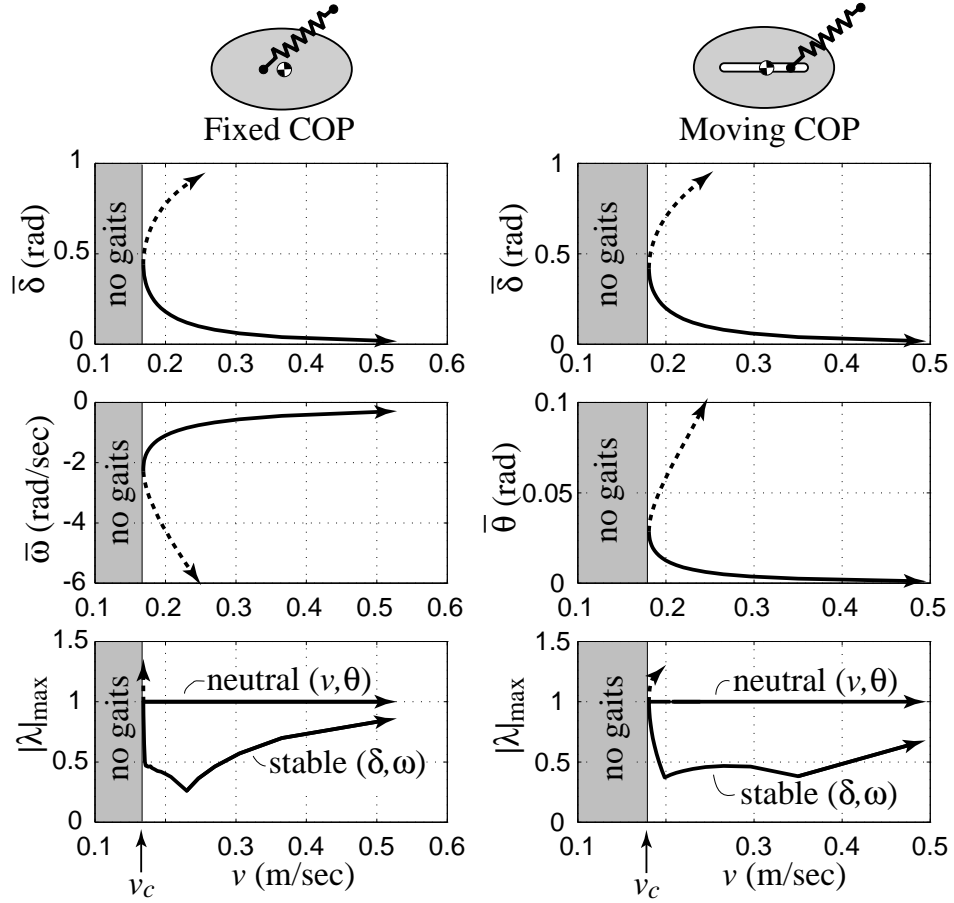


Figure 20: Families of periodic gaits for the fixed and moving COP models with ‘standard’ parameters characteristic of *Blaberus discoidalis*. From top to bottom the panels show COM velocity vector direction $\bar{\delta}$, body angular velocity $\bar{\omega} \equiv \dot{\theta}$ or body orientation $\bar{\theta}$ at touchdown, and eigenvalue magnitudes $|\lambda|$. (For fixed COP $\theta = \text{const.}$ at touchdown; for moving COP $\omega = 0$ at touchdown: hence our display of ω and θ respectively.) Stable branches shown solid, unstable branches dashed (only the neutral and least stable eigenvalues are shown here). Note the saddle-node bifurcations at \bar{v}_c , below which gaits do not occur. From [SGR⁺02].

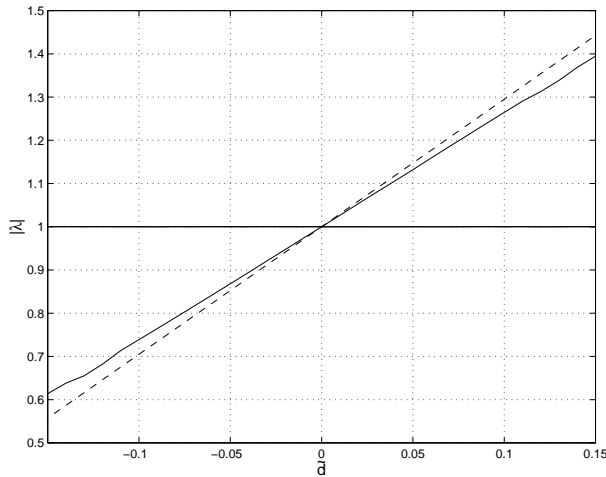


Figure 21: Numerically (solid) and analytically (dashed) computed eigenvalues versus nondimensional hip offset $\tilde{d} = d/l$ for the standard (*Blaberus*) parameter set. From [SH01].

in [SH00b]. For small d a perturbative calculation, using power series approximations for the state variables (η, ψ, θ) , confirms these results [SH01]. We find that the branches of fixed points persist, as shown in Fig. 20(left), and that one of the multiple eigenvalues breaks away from 1, moving inside the unit circle for $d < 0$ and outside for $d > 0$: Fig. 21. Thus, for hip behind COM, rotational coupling leads to bounded yawing oscillations and the body still moves along a straight path. Fig. 22 illustrates the effect of an impulsive body angle perturbation applied at touchdown on the third stance phase. After 1-2 steps, the body recovers a straight path, having suffered a net heading change due to the angular impulse. The manner in which the touchdown states recover is also shown. Further examples are given in [SH00a].

The fixed COP model, with appropriate geometry, exhibits partially asymptotically stable motions; indeed, since it is a conservative, rotationally-invariant system, two of the four eigenvalues strictly less than one in magnitude are the best we can do. But how well does the gait dynamics compare with experimental data? Fig. 23 shows forces, moments and velocities during a full left-right stride. Comparing forward and lateral velocities during the stride to those reported in [FT90, KWF97] and reproduced in the model of [KF99], reveals that they match reasonably closely those observed for the cockroach. Forces generated at the foot (or equivalently, at P) also compare

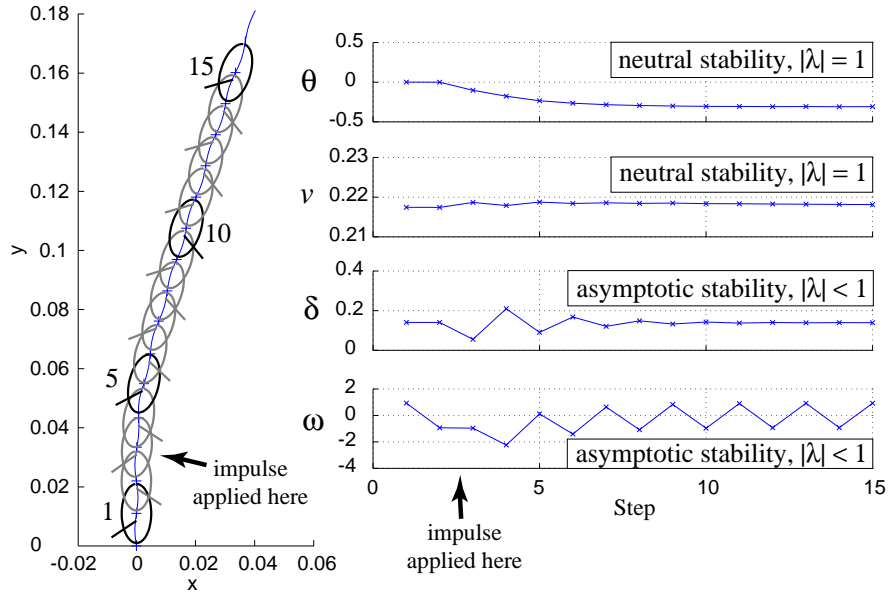


Figure 22: Response to perturbations and stability explanation. The fixed COP model with standard parameter values recovers from an impulsive angular perturbation (arrow in (a)). Evolution of variables at touchdown is shown in (b). The model is neutrally stable in θ and v (corresponding eigenvalues $|\lambda_{1,2}|$ of unit magnitude) and asymptotically stable in ω ($\equiv \theta$) and δ . From [SGR⁺02].

fairly well to net leg tripod forces both in orders of magnitude and time histories, although the peak fore-aft forces ($\pm 0.0014 N$) and lateral forces ($\pm 0.0041 N$) have magnitudes ‘reversed’ from $\pm 0.004 N$ and $\pm 0.0032 N$ taken to represent typical data in [KF99]. However, the yawing θ variation for the model differs markedly from observations: it approximates a negative *sinusoid* (central bottom panel of Fig. 23(b)). This is due to the torque, which is positive during L-stance and negative during R-stance, since $d < 0$ (third panel of Fig. 23(c)). Experimental studies ([KWF97], and see Fig. 25 below) reveal that θ behaves more like a positive *cosinusoid*, with $\dot{\theta} \approx 0$ at touchdown and liftoff.

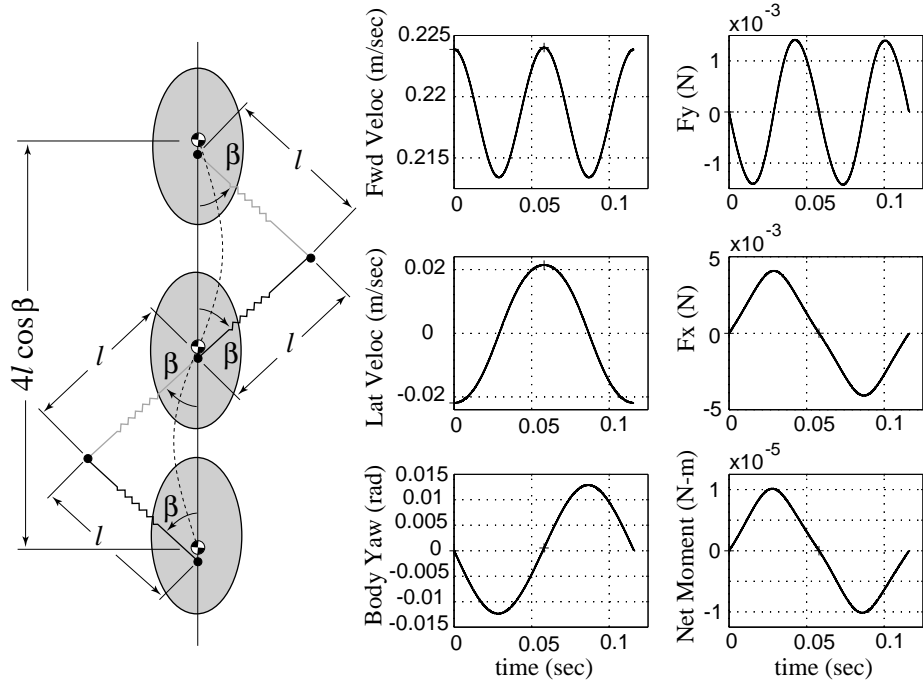


Figure 23: COM path, velocity, yaw, and leg force and body moment variations for steady gait of the fixed COP model with standard parameters running at preferred speed 0.22 m s^{-1} . From [SGR⁺02].

Question: While explicit quadratures can be evaluated for specific spring laws [SH00b], the resulting expressions are often difficult to use. Taylor series approximations of orbit segments about mid-stance were developed in [SH01, SH03], but these are lengthy. Can more elegant approximations be found?

5.1.3 Moving COP

We have noted that the fixed COP model (Fig. 23) produces yaw oscillations of sinusoidal rather than the observed cosinusoidal form, due to body torques incurred by the fixed ‘hip’ P . This may be remedied by allowing a moving COP, as in Fig. 24, for which d was specified by Eqn. (35) with $d_0 = 0$ and $d_1 = -0.0035 \text{ m}$, resulting in variation of $d = \pm 0.002 \text{ m}$, with $d \approx 0$ at mid stance: compare the bottom panels of Figs. 23 and 24. For these computations, we took $l = 0.008 \text{ m}$ and $k = 3.52 \text{ N m}^{-1}$; again l and β are

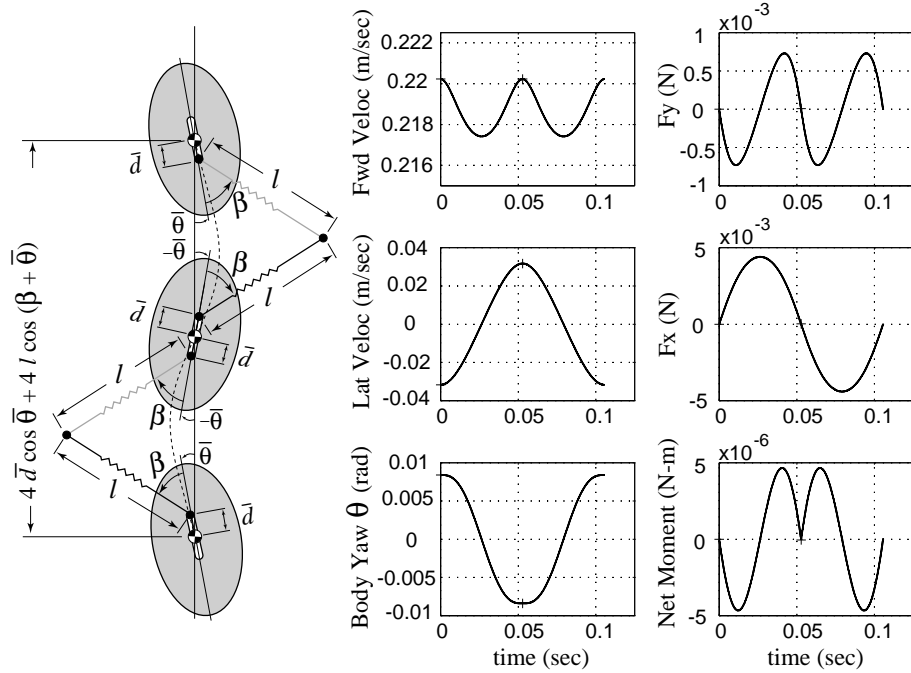


Figure 24: COM path, velocity, yaw, and leg force and body moment variations for steady gait of the moving COP model with standard parameters running at preferred speed 0.22 m s^{-1} . The strideleness formula assumes that $d(t)$ varies symmetrically between \bar{d} and $-\bar{d}$ respectively; $\bar{\theta}$ is the value of θ at leg touchdown. From [SGR⁺02].

constrained by the stride geometry: see Fig. 24. Branches of gaits exist for speeds above critical much as in the fixed COP case: Fig. 20(right).

Quantitative comparisons of lateral force and velocity magnitudes remain good, model values being $\approx 30\%$ higher than experimental values. However, fore-aft magnitudes differ more appreciably, being lower than in the fixed COP model, and lower than experimental values by factors of 2-10 when compared over a large data set [FT90, FBT91, KWF97]. (There is significant variation among trials of individual animals, and among animals, even after scaling to the mass value ($m = 0.0025\text{kg}$) used in the model.) The data shown as solid curves in Fig. 25 were reconstructed for a typical run of one animal as in unpublished work of Garcia, Full, Kram and Wong (2000), from trials of [FBT91] and [KWF97]. These data were selected for their clean phase relationships, although the fore-aft values are unusually high, and we include fore-aft data (dashed) from [FT90] for a second animal, closer

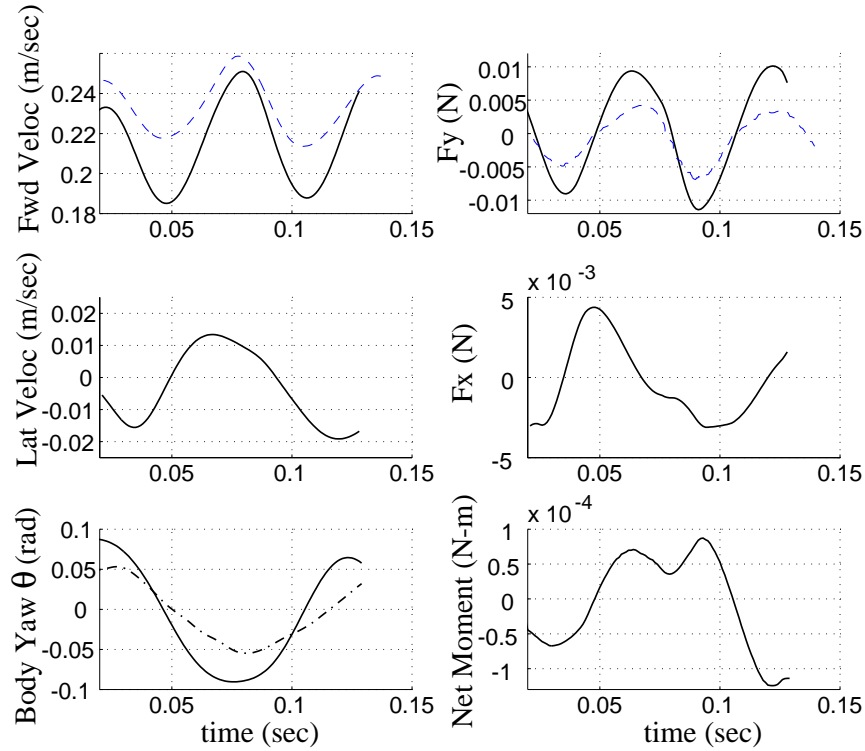


Figure 25: Velocity, yaw, leg force and moment variations over about one stride for *Blaberus discoidalis* moving at 0.22 m s^{-1} . The sign convention is the same as for the models. Data for all components from a single trial [FBT91, KWF97] are shown solid, with yaw angle computed from net moments; the direct kinematic yaw measurement is chain-dotted. The top panels also show as dashed curves fore-aft force and velocity data from a different trial [FT90], to illustrate variation in magnitudes and average speed (stride durations are adjusted to match). Since lateral forces were not simultaneously measured in [FT90], moments could not be computed, but they exhibit less variability. From [SGR⁺02].

to the mean values adopted in [KF99], to illustrate the variability.

We also note that the LLS model describes only horizontal plane dynamics, while Fig. 25 is derived from three-dimensional motions. This may partially account for the underestimate of fore-aft forces and velocity variations by our models. More strikingly, moments and yaw angles are significantly lower than observed (by factors of 10-20); we ascribe this primarily to the collapse of the leg support tripod to a single virtual leg; for further details see [SGR⁺02]. In §5.3 we show that a hexapedal model can rectify these quantitative mismatches.

5.1.4 On scaling and similarity

The LLS model was developed with insects, cockroaches in particular, in mind. However, it may have relevance for other sprawled posture animals, of differing sizes, through similarity relations. For geometrically-similar animals, $m \propto l^3$ and $I \sim ml^2 \propto m^{5/3}$. Stiffnesses are usually assumed to scale according to elastic similarity: $k \propto m^{2/3}$ [MB83], and animals are most often compared at equal Froude numbers, $Fr = v/\sqrt{gl}$, as in the SLIP model [Bli89]. The relaxed leg length l defined for the LLS model is the horizontal projection of a full leg length, and thus we may still appeal to Froude number similarity, leading to the relation $v \propto l^{1/2} \propto m^{1/6}$. Substituting these similarity relations into the nondimensional parameters of (40) reveals that \tilde{k} , \tilde{I} and \tilde{d} all remain constant for geometrically similar animals. Thus, the model predicts that geometrically similar animals should possess the same gait characteristics and stabilities, merely scaled in size and time (frequency).

For non-geometrically similar species, scaling relationships developed in [SH01] permit prediction of gait families from a single, ‘standard’ parameter set.

5.2 Muscles as activated springs

In [SH03] we augmented the passive bipedal LLS models by adding rudimentary models of muscles in the form of actuated linear springs, whose unstressed (zero force generating) lengths change according to fixed or feedback protocols. Specifically, the second class of models adopted in that paper assume the form illustrated in Fig. 26. An actuated (variable length) spring pushes or pulls on an extension of the effective leg beyond the pivot, producing forces and moments similar to those of the musculo-apodeme complexes of [FA95]. For simplicity, we assume that the single effective leg is pivoted at

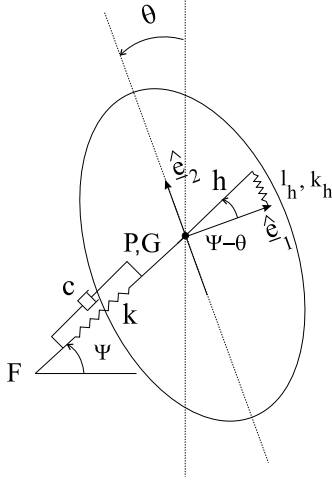


Figure 26: A compliant leg bipedal model with actuated linear hip spring, $k_h, l_h(t)$. From [SH03].

the COM and, in place of the elastic knee and two-element limb of [FA95], we retain the passive axial leg spring of § 5.1 [SH00b, SH01], adding a linear viscous damper to represent losses due to muscles and flexure of the exoskeleton [GKP⁺00].

The nominal actuated hip spring length l_h may be determined either as a function of time alone, or may depend on time and the configuration variables, e.g.: $l_h(\psi, \theta, t)$, the explicit time dependence representing stereotyped CPG (motoneuron) outputs. The kinetic and potential energies of the LLS with passive linear leg and active hip springs are then:

$$\begin{aligned}
 T &= \frac{m(\dot{\zeta}^2 + \zeta^2\dot{\psi}^2)}{2} + \frac{I\dot{\theta}^2}{2} \\
 V &= \frac{k_h}{2}(-h \sin(\psi - (-1)^n\theta) - l_h(\psi, \theta, t))^2 + \frac{k}{2}(\zeta - l)^2, \quad (53)
 \end{aligned}$$

In this formulation, it is assumed that the hip spring is always aligned parallel to the body centerline, so that its actual length, measured from stance center where the leg is at 90° to the body axis, is $-h \sin(\psi - (-1)^n\theta)$.

The functional form for the actuated spring length is chosen to produce a qualitatively correct moment history: for the left (resp. right) stance phase: i.e. negative (resp. positive) moment about the COM during the first half of each stance phase, followed by a positive (resp. negative) moment during the second half (cf. Fig. 25, lower right panel). This requires that l_h be

approximately odd in θ about midstride and approximately equal to its actual length at both the start and end of stride. We therefore suppose that l_h depends on leg angle as well as time, specifically setting:

$$l_h(\psi, \theta, t) = -h \sin(\psi - (-1)^n \theta) \left(\frac{2t}{t_s} - 1 \right)^2, \quad (54)$$

where t_s is the desired stance period duration. This guarantees that l_h is approximately odd about midstride, as evidenced by its dependence on the leg angle relative to the body, and zero at the start of the stride and approximately zero near the end, provided the actual stance duration is close to t_s : the stance duration ‘programmed’ by the CPG.

The formulation (54) implies a feedback law in which the current leg angle $\psi - (-1)^n \theta$ is sensed and the CPG’s ‘autonomous’ signals to the muscles are modulated thereby. The resulting Lagrangian computed from (53), with generalized damping in the first variable, yields the following equations of motion:

$$\begin{aligned} m\ddot{\zeta} &= m\zeta\dot{\psi}^2 - k(\zeta - l) - c\dot{\zeta} \\ m(2\zeta\dot{\zeta}\dot{\psi} + \zeta^2\ddot{\psi}) &= -\frac{1}{2}k_h h^2 \sin(2(\psi - (-1)^n \theta)) \left(1 - \left(\frac{2t}{t_s} - 1\right)^2\right)^2 \\ I\ddot{\theta} &= \frac{(-1)^n}{2} k_h h^2 \sin(2(\psi - (-1)^n \theta)) \left(1 - \left(\frac{2t}{t_s} - 1\right)^2\right)^2. \end{aligned} \quad (55)$$

A typical stride, with a relatively strong muscle spring constant k_h and dissipation c included, is illustrated in Figure 27. The hip torques produced by the actuated spring now match experimental moments about the COM reasonably well (compare the bottom panels of Fig. 27 with those of Fig. 25), but the reaction forces induced at the foot have *reversed* the phasing of the fore-aft force patterns, so that forces are positive in the first half of stance and negative in the second, *opposite* to those observed: compare the top panels of Fig. 27 with those of Fig. 25. Weaker muscle spring constants retain the appropriate fore-aft force patterns, but suffer the same low magnitudes as the passive LLS model (cf. [SH03, Fig. 10]). Similar behavior occurs in a simpler model, also treated in [SH03], in which hip torques are directly imposed. The lateral forces and velocity variations remain approximately correct.

The observation that higher torques imposed by actuation can correct yawing motions at the expense of producing incorrect fore-aft translational dynamics underlines the need for a hexapedal model, in which additional actuation degrees of freedom are available due to the multiple legs active in stance.

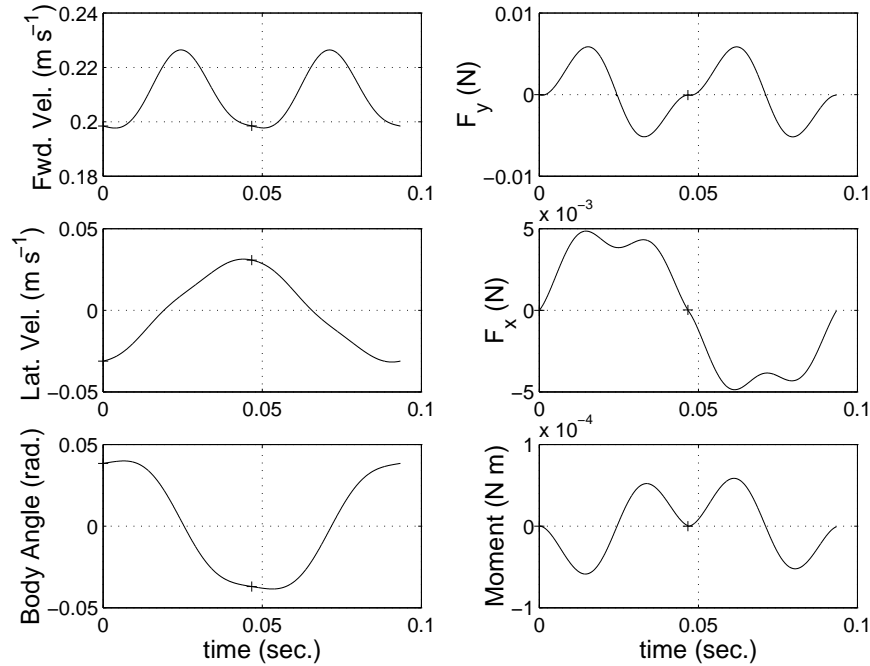


Figure 27: Characteristics of a typical periodic stride for the compliant leg model with a ‘strong’ actuated linear hip spring and dissipation in the passive leg spring: $c = 0.01$, $k_h = 300$, $h = 0.001$, $t_s = 0.0475$. Other parameters were set to values typical of the cockroach *Blaberus discoidalis*, as described in §5.1. From [SH03].

As in the passive models of Section 5.1, a family of gaits may be produced by varying the desired stance period, t_s . A typical example is illustrated in Figure 28. The energy balance induced by the actuated spring now brings a third eigenvalue, corresponding to COM speed variations, into the unit circle, leaving only the single (rotational) eigenvalue at 1. This behavior is not dependent upon the presence of dissipation; even if $c = 0$, the stride duration imposed by t_s and the balance of positive and negative work done by the actuated spring suffices to determine a stable speed.

It is not immediately obvious that actuation or prescription of leg forces should preserve the inherent stability of the passive LLS models. Kubow and Full [KF99] showed, via numerical simulations of equations of the form (34) with alternating tripods summing to produce forces $\mathbf{f}(t)$ given as sinusoidal functions of time in the body frame, that purely prescribed forces could

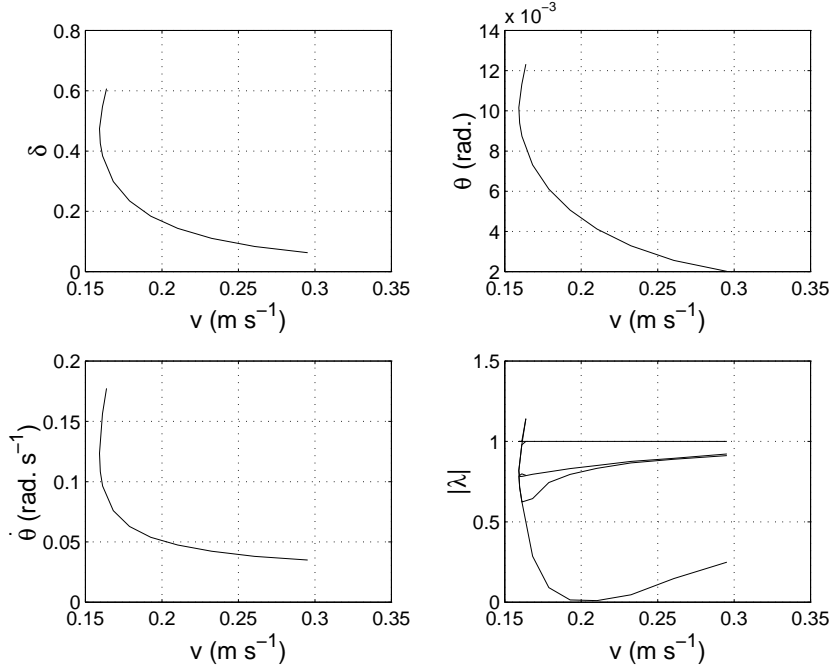


Figure 28: Periodic gait family for the compliant leg system with an actuated hip spring. Gait family was computed by varying t_s between 0.035 – 0.078, with $k_h = 30$, $h = .1l$, and $c = .001$. Other values were held constant at values typical of the cockroach *Blaberus discoidalis*, as described in §5.1. From [SH03].

produce stable motions and select a preferred speed. In contrast, in [SH01] it was shown analytically (and hence proved) that bipedal LLS models with prescribed sinusoidal forces that do *not* rotate with the body (essentially, setting $\mathbf{R}(\theta(t)) \equiv \mathbf{Id}$ in (34)) are *always* unstable; their (unique) periodic gaits have at least one eigenvalue outside the unit circle. These observations, and the model described above, suggest that a subtle combination of actuation and mechanical feedback, involving either (or both) rotation coupling and passive springs, may be required for stability. Our next model incorporates these effects.

5.3 A hexapedal model

We describe a simple hexapedal model that was proposed, and is described in greater detail, in [SHF04]. The basis of the model is the actuated spring

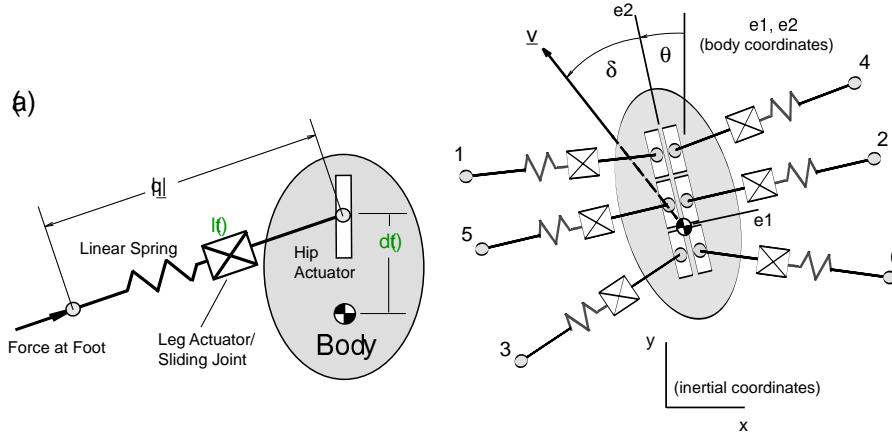


Figure 29: Mechanical model for a single leg (a), and the hexapedal coordinate systems and leg numbering scheme (b). Legs 1, 2 and 3 form the left tripod, and 4, 5, and 6 the right tripod. From [SHF04].

leg illustrated in Fig. 29(a), in which a rudimentary analog of neurally-activated muscle complexes is provided by the ‘programmable’ length $l(t)$, and hip position $d(t)$. Each of these *inputs* may be independently prescribed, endowing the leg with two control variables, and permitting one to match the horizontal plane components of observed single leg forces. However, unlike the purely prescribed model of [KF99], $l(t)$ sets only the relaxed (force-free) length; actual leg forces depend upon relative foot-hip displacements, and thus forces can respond to perturbations in a more natural manner. Six such units are assembled as indicated in Fig. 29(b), although for simplicity we assume that the hips all move on the body centerline.

We derive the six inputs $l_j(t), d_j(t)$ for each leg tripod by requiring that the forces generated at the feet match those of the idealized model of [KF99], F_{jx}, F_{jy} , which were, in turn, derived from single leg force measurements in [FBT91]. These forces are sinusoids of the forms:

$$F_{jx} = A_{jx} \sin \Omega t \quad (\text{lateral forces, all feet}) ; \quad (56a)$$

$$F_{jy} = A_{jy} \sin \Omega t, j = 1, 3 \quad (\text{fore-aft forces, front and hind feet}) ; \quad (56b)$$

$$F_{2y} = A_{2y} \sin 2\Omega t \quad (\text{fore-aft forces, middle foot}) . \quad (56c)$$

Parameter values are given in [SHF04].

We compute the COM path through a half stride: only one tripod need be considered, the left here, since bilateral symmetry supplies the inputs for the other stance phase. Neglecting body rotation, this follows simply

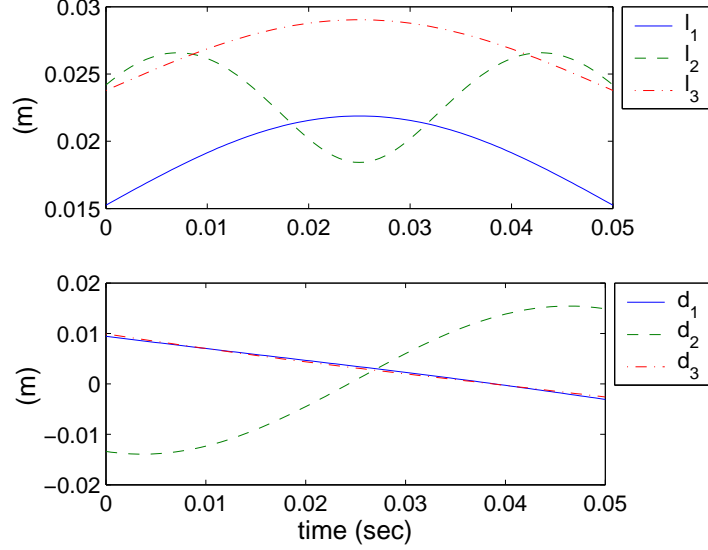


Figure 30: The prescribed inputs, $d_i(t)$ and $l_i(t)$, for $i = 1, 2, 3$; $V_{des} = 0.25$ m s⁻¹, $\Omega = 20\pi$ rad s⁻¹ and $k = 1$ N m. From [SHF04].

from integration of the first equation of (34) with $\mathbf{R}(t) = \mathbf{I}d$, using the net idealized forces $\sum_{j=1}^3 F_{jx}$, $\sum_{j=1}^3 F_{jy}$:

$$(x(t), y(t)) = (-A_{3x}(m\Omega^2)^{-1} \sin \Omega t, -A_{2y}(4m\Omega^2)^{-1} \sin 2\Omega t + V_{des}t), \quad (57)$$

where we use the fact that certain force components cancel ($A_{2x} = -A_{1x}$; $A_{3y} = -A_{1y}$). The average forward speed, denoted by V_{des} , is a constant of integration that may be adjusted, but initially we set it at the preferred speed 0.25 m s⁻¹ and leg cycle frequency $f = \Omega/2\pi = 10$ Hz for which the idealized leg forces and touchdown foot positions were derived. These and other physical parameters are given in [KF99] and [SHF04].

We assume linear springs, so that, letting \mathbf{q}_i denote the vector from the i 'th foot to hip, force consistency requires:

$$F_{jx} = F_{jx,des} \Rightarrow k_j(l_j(t) - |\mathbf{q}_j|) \frac{q_{jx}}{|\mathbf{q}_j|} = A_{jx} \sin \Omega t, \quad (58)$$

$$F_{jy} = F_{jy,des} \Rightarrow k_j(l_j(t) - |\mathbf{q}_j|) \frac{q_{jy}}{|\mathbf{q}_j|} = A_{jy} \sin C_j \Omega t. \quad (59)$$

Here q_{jx} and q_{jy} are the inertial frame components of q_j and A_{jx} and A_{jy} the force component magnitudes of equations (56) (note $C_j = 2$ for $j = 2$, but

$C_j = 1$ otherwise). The kinematics inherent in Fig 29 allows us to express \mathbf{q}_j in terms of the COM path of (57), the touchdown foot position, and the hip position $d_j(t)$. Then $d_j(t)$ may be derived by dividing the equations (59) to eliminate the common term $k_j(l_j(t) - |\mathbf{q}_j|)/|\mathbf{q}_j|$, and $l_j(t)$ found by inverting the linear force relationship. In order to obtain closed-form expressions, we neglect yawing throughout, incurring errors of up to $\approx 8\%$ in approximating the rotation matrix by the identity. Details are given in [SHF04], and the resulting input functions are shown in Fig. 30.

The unstressed lengths on average obey $l_1 < l_2 < l_3$, echoing leg lengths in the insect. Also, the front and back (ipsilateral) hips move backwards relative to the body during stance, while the middle (contralateral) hip moves forwards. Although the latter varies by over 3 cm, a greater distance than the insect’s body length, the net movement is backwards, as in the bipedal moving COP protocol of Section 5.1.3. Since moving centers of pressure imply torques at the leg joints, this model suggests that the insect generates relatively large middle leg torques.

Equipped with the inputs as explicit functions of time, we may now integrate the fully-coupled equations of motion to obtain gaits. The body coordinate system and state variables used in defining Poincaré maps remain the same as for the bipedal models above (cf. Fig. 29(b)). We first confirm that, even permitting yawing, inputs derived from the idealized preferred speed data of [KF99] do produce gaits with force and velocity variations quantitatively similar to those of the animal. Fig. 31 reproduces the data of Fig. 25 and also shows model results: the match is remarkably good, although the actual average forward speed ($\approx 0.26 \text{ m s}^{-1}$) is slightly higher than the desired (or design) speed V_{des} used to compute the inputs.

These gaits are stable. Indeed, we may produce branches of gaits over a range of speeds, by recomputing inputs for appropriately adjusted desired speeds, leg frequencies, and touchdown positions. As mentioned in §3.2.1, although the insect uses a double tripod pattern throughout the range $0.05\text{--}0.6 \text{ m sec}^{-1}$, it exhibits a gait transition around 0.3 m sec^{-1} : below this speed is regulated by leg cycle frequency, and above it, by stride length. Varying V_{des} and Ω in a piecewise-linear manner to approximate the data of [TBF94, Fig. 2], and additionally changing foot touchdown positions from those of [KF99] by further extending the legs at speeds above 0.25 m s^{-1} , we obtain the branch of stable gaits illustrated in Fig. 32.

As in Fig 28, since the actuated springs supply and extract energy via $l_j(t)$ and $d_j(t)$, along this branch speed is also stabilized, and three of the eigenvalues lie within the unit circle, with only the ‘rotational’ eigenvalue $\lambda_1 = 1$. Moreover the stability boundaries shown in Fig. 32 provide a ratio-

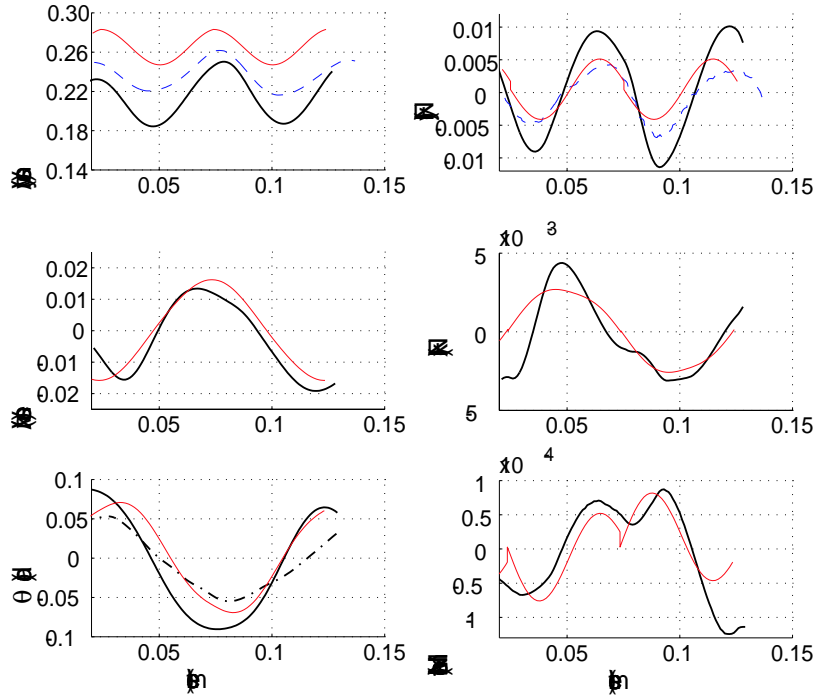


Figure 31: Comparison of insect data of Fig. 25 with the LLS Hexapod model. The model solutions are shown as a red (or light gray) solid line. From [SHF04].

nale for the gait change, since constant frequency or constant stride length protocols would enter unstable regions at either low or high speeds.

In [SHF04] the moments generated at the COM by individual legs are also studied, and it is shown that they sum almost without cancellation to give the net COM moment pattern shown in the lower right panel of Fig. 31, while individual joint moments remain within reasonable bounds. Hence this model also shows that the legs of the stance tripod work together in a relatively efficient manner to produce feedforward force and moment patterns that result in stable running.

5.4 Towards a neuromechanical model

Thus far we have considered rather simple mechanical models, *templates* in the terminology introduced in §1 [FK99], although we have seen that their behaviors are not so easy to derive analytically. Drawing on the material

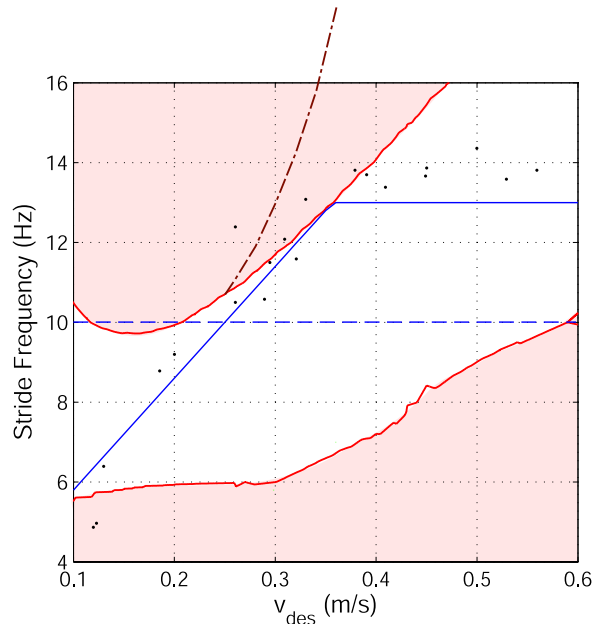


Figure 32: A bifurcation set in design speed-leg cycle frequency space, showing boundaries of the region in which stable gaits exist, and the speed-frequency protocol adopted. Unstable regions are shaded. The fixed frequency protocol (dashed) encounters instability at low and/or high V_{des} , while the piecewise-linear protocol (solid) remains in the stable region, albeit grazing the stability boundary at its break-point. Stability is further improved by adjusting foot placements in this region, as shown by dash-dotted upper boundary above $V_{des} = 0.25$. From [SHF04], with experimental data of [TBF94, Fig. 2] indicated by dots.

summarised in §2.4, we now sketch the elements of a true neuromechanical model, an *anchor* that includes CPG, muscles, six legs and body. This work is still in progress; the first part of it is to appear in [GH04], from which the following is adapted.

5.4.1 The CPG and motoneurons

The model described in this section is based on the work of Pearson and Iles [PI70, PI71, Pea72, PI72] and Ritzmann et al. [WR98a, WR98b, TR00a, TR00b], who studied motoneuron, bursting interneuron, and muscle activity in cockroach locomotion. Pearson and Iles, working with the american

cockroach *Periplaneta americana*, suggest a simplified architecture for the CPG and depressor and levator motoneurons. (Here, since we do not explicitly model the swing phase when the leg is lifted, we shall be concerned only with depressor motoneurons and associated muscles.) Both slow and fast motoneurons, characterised by differing spiking patterns, are involved. The former, with their low level, high frequency spikes, are active during muscle contraction at all speeds, and the latter, with typically 1-5 larger spikes per stride, become increasingly active at high speeds. The motoneuron records presented in [FSAJ98] are from fast cells, while the electromyographs (EMGs) of [WR98a, WR98b, TR00a, TR00b], taken from *Blaberus discoidalis*, primarily reflect slow motoneuron activity, with spikes from fast motoneurons appearing in [TR00b].

Examination of EMGs and both slow and fast motoneuron outputs reveals that they may essentially be described by three parameters: the bursting cycle duration or its inverse, the *bursting frequency*, which coincides with the animal's overall stride frequency (ranging from 2-14 Hz, cf. Fig. 32); the *spiking frequency* within bursts, and the *duty cycle* – the fraction of the bursting cycle occupied by spiking. The latter two modulate the power produced by muscles in a graded fashion, greater spike rates and longer bursts producing greater muscle forces. Fast motoneurons may produce from one to five spikes per cycle, and none at low speeds, while slow motoneurons exhibit significantly faster spike rates, from 50-350 Hz [Pea72, PI72, TR00a, TR00b]. In the absence of detailed information regarding currents and ion channels in cockroach neurons, we choose to model both fast and slow depressor motoneurons by a simplified three-variable ODE of the following form, in which fast gating variables have been removed by assuming instantaneous equilibration, as outlined in §2.3.1:

$$\begin{aligned}
C\dot{v} &= -[I_{Ca} + I_K + I_{KCa} + \bar{g}_L(v - E_K)] + I_{\text{ext}}, \\
\dot{m} &= \frac{\epsilon}{\tau_m(v)} [m_\infty(v) - m], \\
\dot{c} &= \frac{\delta}{\tau_c(v)} [c_\infty(v) - c].
\end{aligned} \tag{60}$$

Here $\delta \ll \epsilon \ll 1/C$, the fast, slow and very slow currents are respectively specified by:

$$I_{Ca} = \bar{g}_{Ca} n_\infty(v)(v - E_{Ca}), \quad I_K = \bar{g}_K m \cdot (v - E_K), \quad I_{KCa} = \bar{g}_{KCa} c \cdot (v - E_{KCa}); \tag{61}$$

the subscripts denote the relevant ions. I_{ext} represents external synaptic and other input currents. As in §2.3.1 the functions $m_\infty(v)$, $n_\infty(v)$ and $c_\infty(v)$

are sigmoids of the forms

$$m_\infty(v) = \frac{1}{1 + \exp[-k_m(v - v_m)]}, \quad (62)$$

and the ‘timescale’ functions are hyperbolic secants:

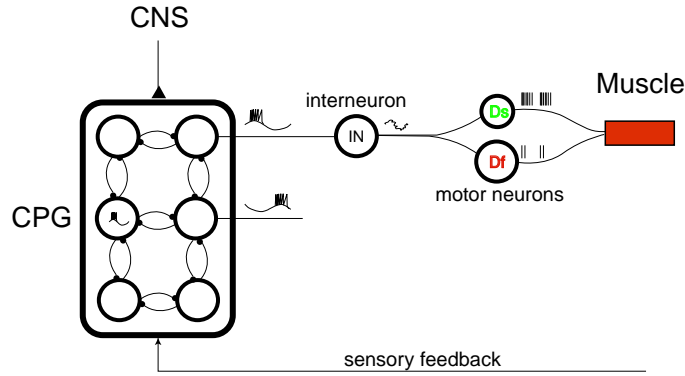
$$\tau_m(v) = \operatorname{sech}(k_m(v - v_m)). \quad (63)$$

Specific parameter values appropriate for fast and slow cockroach motoneurons, as well as CPG (inter-) neurons, may be found in [GH04].

This model, in common with others studied by Rinzel et al. [Rin87, RL86, RL87], has a ‘recovery’ variable c which acts on the fast (v, m) -subsystem as a slowly-varying parameter in I_{KCa} , analogous to an input current. The fast subsystem, which incorporates the membrane voltage v and a collective relatively slow channel variable m , has three branches of equilibria, the upper (w.r.t. v) of which undergoes a supercritical Hopf bifurcation as c increases, producing a branch of periodic orbits. These represent depolarised spiking, and they coexist with a lower branch of stable (hyperpolarised) fixed points. The periodic orbit branch terminates in a homoclinic connection to a middle branch of saddle points [GH90], beyond which only the lower v (hyperpolarised) equilibria are stable. The slow variable c increases, moving toward the homoclinic bifurcation point as long as spiking occurs and membrane voltages are relatively high, but returns toward the Hopf bifurcation point in the absence of spiking, when membrane voltages are lower. At a threshold corresponding to a saddle-node bifurcation in the fast system, the stable hyperpolarised rest point vanishes and the fast subsystem resumes spiking. See [KS98, Chapter 6] for an introduction to such two-timescale bursting models in neurobiology.

The spiking frequency is governed by parameters in the (v, m) subsystem (e.g. ϵ, C , and the conductances \bar{g}_{Ca} etc.), and the burst frequency by parameters in the third z equation, primarily $\delta/\tau_c(v)$. The whole is modulated by the external input current I_{ext} . Following Pearson [Pea72], we suppose that I_{ext} is influenced by ‘external’ inputs from higher brain centers (a tonic excitation level, primarily a speed control), and inhibited by CPG outputs so that the depressor muscle activity is shut off during the swing phase.

Pearson [Pea72, PI72] also found evidence of bursting interneurons that constitute part of (or are driven by) the CPG. Absent detailed knowledge of the neural architecture, we shall again represent each of the six subunits of the CPG by a single bursting neuron of the form (60), with parameters chosen appropriately. We couple each ipsilateral triplet, and each contralateral



Muscle

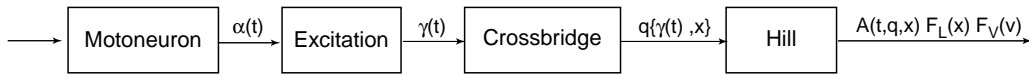


Figure 33: (a) The overall CPG and muscle model structure. Note the fast (D_f) and slow (D_s) depressor motoneurons, inhibited by the CPG output. (b) Elements in the motoneuron muscle model. **Number panels (a) and (b)!! Describe variables in muscle model. Remove interneuron from picture in (a)??.**

pair, by nearest neighbor inhibitory synapses, in the manner characterised in Fig. 33(a). The same overall architecture has been proposed for the stick-insect pattern generator [BB98, Fig. 4]. Following [DA01, p. 180], we model synaptic behavior by the first order dynamics

$$\dot{s} = \frac{s_\infty(v)(1-s) - s}{\tau_{\text{syn}}}, \quad \text{with} \quad s_\infty = \frac{1}{1 + e^{-k_{\text{syn}}(v - E_{\text{syn}}^{\text{pre}})}}, \quad (64)$$

in which v denotes the potential of the presynaptic neuron and τ_{syn} sets the timescale of the postsynaptic potential. The nondimensional synaptic variable s enters the postsynaptic cell in the first of equations (60) as

$$C\dot{v} = -[I_{\text{Ca}} + \dots] + \bar{g}_{\text{syn}} s \cdot (v - E_{\text{syn}}^{\text{post}}), \quad (65)$$

where \bar{g}_{syn} denotes synaptic strength and the current $I_{\text{syn}} = \bar{g}_{\text{syn}} s \cdot (v - E_{\text{syn}}^{\text{post}})$ induced in the postsynaptic cell is typically positive (negative) for excitatory (inhibitory) synapses [JW95].

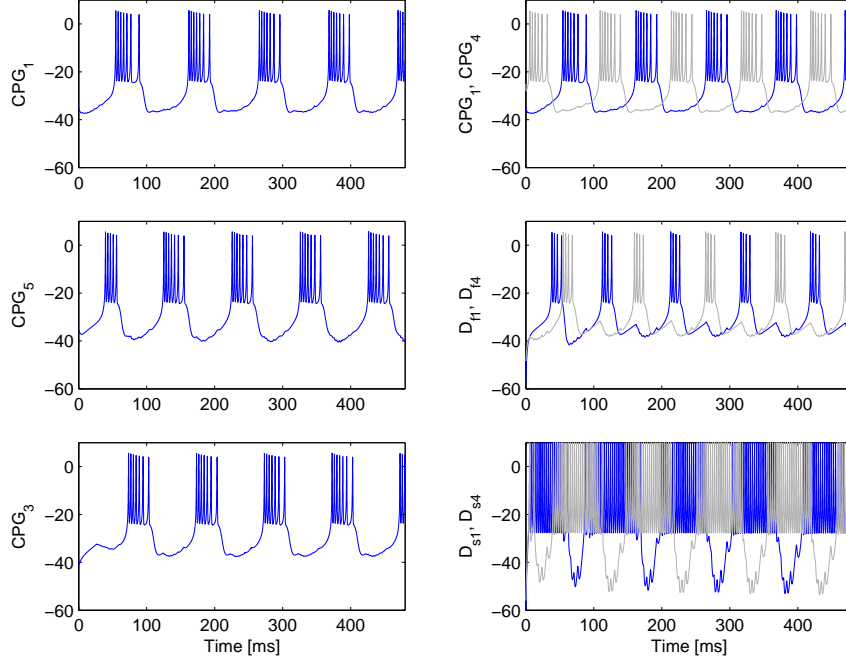


Figure 34: Membrane voltages from a network of six mutually inhibiting bursting neuron models driving slow and fast bursting motoneurons. Left column shows ipsilateral CPG neurons, right column shows contralateral CPG neurons and fast and slow motoneurons for units 1 and 4. Units 1, 2 and 3, and 4, 5 and 6, constituting the left and right tripods respectively, rapidly fall into the appropriate antiphase relationships. From [GH04].

The CPG circuit of Fig. 33(a) produces the requisite 180° (anti)phase difference between the tripods, as shown by simulations illustrated in Fig. 34, which show ipsilateral CPG outputs along the left side, and contralateral CPG and fast and slow motoneuron outputs for the front legs.

In [GH04] it is shown that the three ‘behavioral’ parameters – bursting frequency, spiking frequency and duty cycle – can be individually adjusted by the motoneuron external current I_{ext} , the CPG neuron’s conductance \bar{g}_{KCa} , and the slow timescale parameter $\delta/\tau_c(v)$ respectively. In Fig. 35 we show that variations in δ alone produce duty cycle/stepping frequency variations similar to those measured by Pearson [Pea72], and that a combination of δ and \bar{g}_{KCa} variations can accurately bracket that data. We have likewise been able to find I_{ext} and \bar{g}_{KCa} parameter ranges that reproduce slow motoneuron spike rates and numbers of spikes for fast motoneurons [GH04].

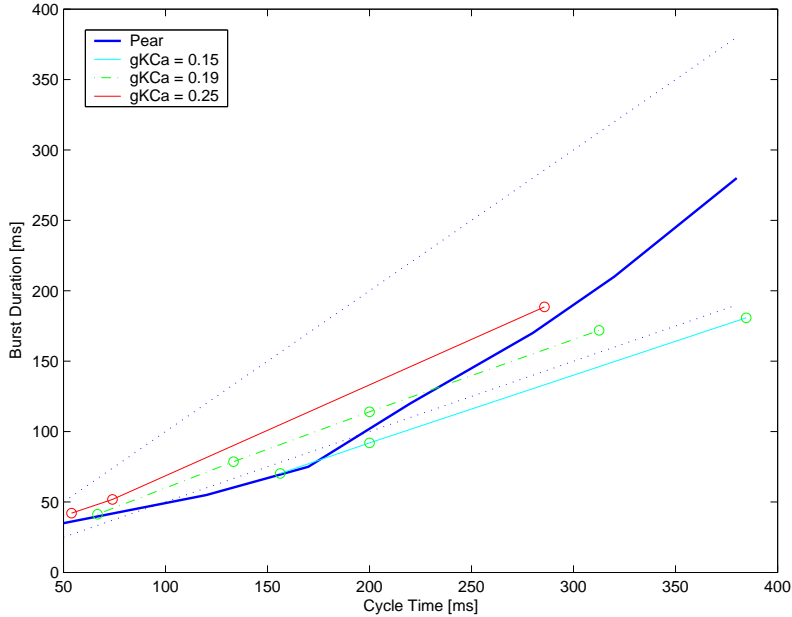


Figure 35: Comparative study of duty cycle versus cycle time (inverse stepping frequency). Data reproduced from Pearson [Pea72, Fig. 5] (bold) and obtained by varying δ from 0.01 to 0.051 and keeping \bar{g}_{KCa} fixed in the CPG model at the values indicated (dashed and broken lines). Dotted lines correspond to 50% and 100% duty cycle. From [GH04].

These motoneuron outputs will be used to innervate Hill type muscle models, but before we consider this we show that the CPG-motoneuron model anchor can be reduced to a phase oscillator template almost as simple as that of Eqn. (18).

We remark that, while each bursting neuron is modelled in some biophysical detail, the circuit of Fig. 33(a) still vastly simplifies the probable architecture of the insect's CPG. A single bursting interneuron represents each 'leg oscillator,' where several neurons are probably involved. Moreover, in studies of slow walking of stick insects, which use more precise foot placement, there is strong evidence of individual *joint* oscillators within the leg units [BB98]. For fast running, however, multiple units are likely to be coordinated in a stereotyped fashion, and so even if more units were included, the phase reduction and symmetry ideas introduced below may still result in considerable simplification.

5.4.2 Reduction to phase oscillators

While substantial analyses can be performed on singularly-perturbed systems such as (60), in the synaptically coupled network of Fig. 33(a) there are sixty ODEs, three each for the six CPG neurons and twelve motoneurons and a further six for the CPG synaptic variables (the coupling to motoneurons is one way, so motoneuron synaptic variables do not appear). This is a formidable system, but for weak coupling, and assuming identical neurons, the six-burster CPG circuit can be reduced, via phase response curve and averaging methods, to ODEs in the relative phases ψ_j of each ‘leg unit.’

As in §2.3.1 we write the ODEs (60) and (64) for a single burster and its synaptic variable as:

$$\dot{\mathbf{x}}_i = \mathbf{f}(\mathbf{x}_i) + \sum_j \bar{g}_{\text{syn},ji} \mathbf{g}_{ji}(\mathbf{x}_i, \mathbf{x}_j); \quad \mathbf{x}_i = (v_i, m_i, c_i, s_i), \quad (66)$$

where \mathbf{g}_{ji} denotes the coupling function (of strength $\bar{g}_{\text{syn},ji}$) from presynaptic cell j to postsynaptic cell i , and the sum is over all cells in the network that synapse onto i . Assuming that (66) has an attracting hyperbolic limit cycle Γ_0 with frequency $\omega_0 = \frac{2\pi}{T_0}$ for $\bar{g}_{\text{syn},ji} = 0$, and extending the analysis of §2.3.1 in the obvious way, we may define a scalar phase variable $\phi(\mathbf{x}_i) \in [0, 2\pi)$ for each unit and derive a coupled set of phase equations of the form:

$$\dot{\phi}_i = \omega_0 + \sum_j \bar{g}_{\text{syn},ji} \mathbf{Z}(\phi_i) \cdot \mathbf{g}_{ji}(\phi_i, \phi_j) + o(\bar{g}_{\text{syn},ji}); \quad \mathbf{Z}(\phi_i(\mathbf{x}_i)) = \frac{\partial \phi_i}{\partial \mathbf{x}_i} \Big|_{\Gamma_0(\phi)} \cdot \quad (67)$$

In deriving (67) we are projecting solutions along *isochronic manifolds* onto the product of the unperturbed limit cycles: for N units, an N -dimensional torus [Win01, Guc75].

As noted in §2.3.1 synaptic dynamics only enters via the variables s_j and v_i in the coupling defined by Equations (64-65), so only the first component of $\mathbf{Z}(\phi_i)$ survives in the dot product of (67). This phase response curve or PRC can be approximated numerically by approach to the limit

$$Z_1(\phi_i) = \lim_{\substack{\Delta v_i \rightarrow 0 \\ t \rightarrow \infty}} \frac{\Delta \phi_i}{\Delta v_i}, \quad (68)$$

or calculated by use of adjoint theory [HI97], as implemented, for example, in the software XPP [Erm02]. Defining the relative phases $\psi_i = \phi_i - \omega_0 t$ and using the fact that the absolute phases ϕ_i evolve faster than $\psi_i(t)$, we

may then average (67) to obtain

$$\dot{\psi}_i = \sum_{j \neq i}^N \bar{g}_{\text{syn},ji} H_{ji}(\psi_i - \psi_j), \quad (69)$$

where

$$H_{ji}(\psi_i - \psi_j) = \frac{1}{T_0} \int_0^{T_0} Z_1(\phi_i) s_j(\Gamma_0(\phi_j)) [v_i(\Gamma_0(\phi_i)) - E_{\text{syn},i}^{\text{post}}] dt \quad (70)$$

(cf. [GH90, Chap. 4] and [HI97, Chap. 9]). As noted in §2.3, pairwise phase differences alone appear in the averaged coupling functions H_{ji} due to periodicity of the integrand in (70).

For mutual coupling between two identical bursters we have $\bar{g}_{\text{syn},ji} H_{ji} = \bar{g}_{\text{syn},ij} H_{ij}$, and the reduced phase equations (69) are

$$\dot{\psi}_1 = \bar{g}_{\text{syn}} H(\psi_1 - \psi_2) \quad \text{and} \quad \dot{\psi}_2 = \bar{g}_{\text{syn}} H(\psi_2 - \psi_1); \quad (71)$$

we may subtract these as in §2.3.3 to further reduce to a single scalar ODE for the phase difference $\theta = \psi_1 - \psi_2$:

$$\dot{\theta} = \bar{g}_{\text{syn}} [H(\theta) - H(-\theta)] \stackrel{\text{def}}{=} \bar{g}_{\text{syn}} G(\theta). \quad (72)$$

Now, since H is 2π -periodic, we have $G(\pi) = H(\pi) - H(-\pi) = H(\pi) - H(\pi) = 0$ and $G(0) = 0$, implying that, *regardless of the form of H* , in-phase and anti-phase solutions *always* exist. For the present burster model and the specific parameters selected in [GH04], these are in fact the *only* fixed points: see Fig. 36. Note that, unless $H(0) = H(\pi) = 0$, we have $\dot{\psi}_1 = \dot{\psi}_2 = \bar{g}_{\text{syn}} H(\bar{\theta})$, so coupling changes the common frequency $\dot{\phi} = \omega_0 + \dot{\psi}_i$ of the units, even when phase locking occurs.

Stability of these phase-locked solutions is determined by the eigenvalues of the 2×2 matrix obtained by linearizing (71) at $\psi_1 - \psi_2 = \bar{\theta}$:

$$\bar{g}_{\text{syn}} \begin{bmatrix} H'(\bar{\theta}) & -H'(\bar{\theta}) \\ -H'(\bar{\theta}) & H'(\bar{\theta}) \end{bmatrix}; \quad (73)$$

these are 0 and $2\bar{g}_{\text{syn}} H'(\bar{\theta}) = \bar{g}_{\text{syn}} G'(\bar{\theta})$, with eigenvectors $(1, 1)^T$ and $(1, -1)^T$ respectively. Hence the dynamics is only neutrally stable to perturbations that advance or retard the phases of both units equally, but since $H'(\pi) < 0$ the anti-phase solution is asymptotically stable to perturbations that disrupt the relative phase $\psi_1 - \psi_2$.

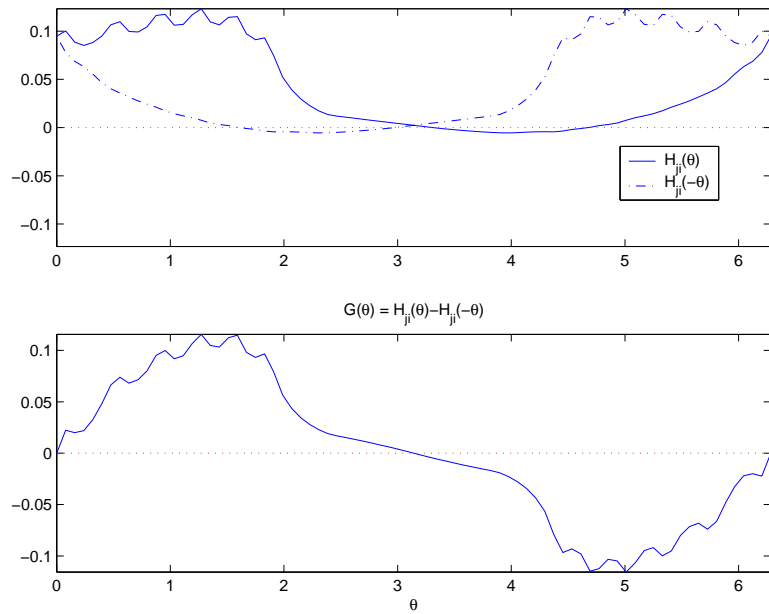


Figure 36: (a) The coupling function $\bar{g}_{\text{syn}}H_{ji}(\theta)$ (solid) for an inhibitory synapse; $\bar{g}_{\text{syn}}H_{ji}(-\theta)$ also shown (dash-dotted). (b) The phase difference coupling function $\bar{g}G(\theta) = \bar{g}_{\text{syn}}[H_{ji}(\theta) - H_{ji}(-\theta)]$. Note that $\bar{g}_{\text{syn}}G'(0) > 0 > \bar{g}_{\text{syn}}G'(\pi)$. From [GH04].

In [GH04], to preserve equal net input to all units, it is assumed that ipsilateral synapses from front and rear leg units to middle ones are half the strength of the remaining ipsilateral and contralateral synapses. The six burster CPG circuit of Fig. 33 then reduces to the system:

$$\begin{aligned}
\dot{\psi}_1 &= \bar{g}_{\text{syn}}H(\psi_1 - \psi_4) + \bar{g}_{\text{syn}}H(\psi_1 - \psi_5) \\
\dot{\psi}_2 &= \frac{\bar{g}_{\text{syn}}}{2}H(\psi_2 - \psi_4) + \bar{g}_{\text{syn}}H(\psi_2 - \psi_5) + \frac{\bar{g}_{\text{syn}}}{2}H(\psi_2 - \psi_6) \\
\dot{\psi}_3 &= \bar{g}_{\text{syn}}H(\psi_3 - \psi_5) + \bar{g}_{\text{syn}}H(\psi_3 - \psi_6) \\
\dot{\psi}_4 &= \bar{g}_{\text{syn}}H(\psi_4 - \psi_1) + \bar{g}_{\text{syn}}H(\psi_4 - \psi_2) \\
\dot{\psi}_5 &= \frac{\bar{g}_{\text{syn}}}{2}H(\psi_5 - \psi_1) + \bar{g}_{\text{syn}}H(\psi_5 - \psi_2) + \frac{\bar{g}_{\text{syn}}}{2}H(\psi_5 - \psi_3) \\
\dot{\psi}_6 &= \bar{g}_{\text{syn}}H(\psi_6 - \psi_2) + \bar{g}_{\text{syn}}H(\psi_6 - \psi_3).
\end{aligned} \tag{74}$$

Seeking left-right tripod solutions of the form $\psi_1 = \psi_2 = \psi_3 \equiv \psi_L(t)$, $\psi_4 = \psi_5 = \psi_6 \equiv \psi_R(t)$, (74) collapses to the pair of equations

$$\dot{\psi}_L = 2\bar{g}_{\text{syn}}H(\psi_L - \psi_R) \text{ and } \dot{\psi}_R = 2\bar{g}_{\text{syn}}H(\psi_R - \psi_L), \tag{75}$$

and the arguments used above may be applied to conclude that $\psi_R = \psi_L + \pi$ and $\psi_R = \psi_L$ are fixed points of (75), again independent of the form of H . For this argument to hold, note that the sums on the right hand sides of the first three and last three equations of (74) must be identical when evaluated on the tripod solutions; hence, net inputs must be equal. If all *synaptic strengths* are assumed equal (replacing $\bar{g}_{\text{syn}}/2$ by \bar{g}_{syn} in (74), then to get antiphase solutions it is *also* necessary that $H(\pi) = 0$, which does, in fact, hold here (Fig. 36).

Linearisation of (74) at fixed points produces the eigenvalues

$$\lambda = 0, \bar{g}_{\text{syn}}H', 2\bar{g}_{\text{syn}}H', 3\bar{g}_{\text{syn}}H', 4\bar{g}_{\text{syn}}H', \tag{76}$$

the third ($2\bar{g}_{\text{syn}}H'$) having algebraic and geometric multiplicity two. Since $\bar{g}_{\text{syn}}H'(\pi) < 0$ (Fig. 36), this establishes asymptotic stability with respect to perturbations that disrupt the tripod antiphase relationships, and instability of the in-phase ('pronking') solution. Moreover, the last and largest negative eigenvalue for the antiphase solution has eigenvector $(1, 1, 1, -1, -1, -1)^T$, indicating that perturbations that disrupt the relative phasing of the left and right tripods recover fastest, before those that affect phases within a tripod.

We note that (71) and (74) provide examples of networks that are forced by their symmetries to possess certain steady state solutions regardless of

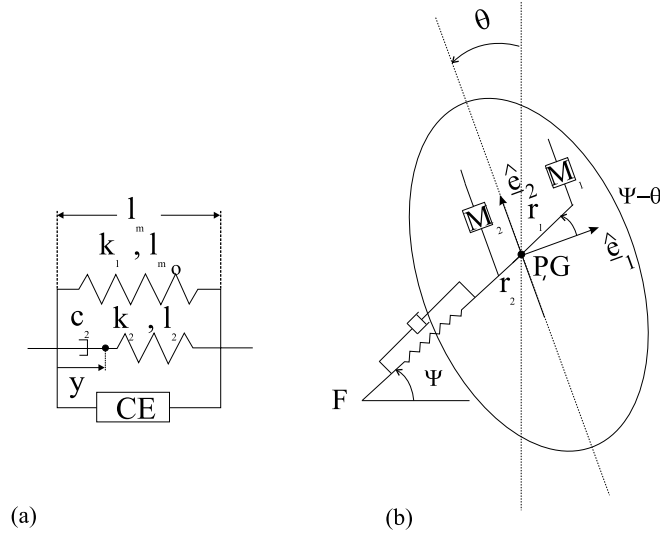


Figure 37: (a) Single muscle complex model: see text for description; (b) bipedal model with two opposing muscles attached at distances r_1 and r_2 from hip; only left leg shown. From [SH03].

the precise forms of the coupling functions. The stability of the solutions, however, does depend on the coupling. This is a typical situation in equivariant bifurcation theory [GS85, GSS88, GSBC99].

5.4.3 Muscles and legs

In [SH03] the bipedal LLS model of Fig. 26 was equipped with agonist-antagonist pairs of muscles, each comprising a contractile element (CE) in parallel with passive visco-elastic elements: Fig. 37(a). The classical Hill model [McM84, Zaj89] was used, adapted to match data from muscle 177c, the main power generator of *Blaberus* hind leg [FA95, Mei01]. Passive stiffness and damping were also estimated by fitting to empirical data [GKP⁺00].

In the Hill model each muscle exerts a force equal to the sum of its passive and active components:

$$F_i = k_1(l_i - l_o) + k_2(l_i - y_i - l_2) + F_{act,i} ; i = 1, 2 . \quad (77)$$

The damper length y_i is determined by an additional differential equation, derived from equality of the damper and series spring forces. The active force $F_{act,i}$ developed in each CE is determined by the product of the isometric force-length, F_l , and force-velocity, F_v , relations and the motoneuronal

activation, F_a . $F_v(\dot{l}_i)$ takes two forms, depending on whether the muscle is shortening or lengthening (cf. [Zaj89, MGK⁺98]), giving:

$$F_{act_i} = \frac{0.52 F_l(l_i) F_a(t) (v_{max} + \dot{l}_i)}{0.52 v_{max} - \dot{l}_i}, \quad \dot{l}_i \leq 0, \quad (78)$$

$$F_{act_i} = \frac{F_l(l_i) F_a(t) (0.114 v_{max} + 1.5 \dot{l}_i)}{0.114 v_{max} + \dot{l}_i}, \quad \dot{l}_i > 0, \quad (79)$$

where $v_{max} = 5.7l_{m_o}$ mmsec⁻¹ is the maximal shortening velocity at which F_{act_i} equals zero. The isometric force-length function for muscle 177c of *Blaberus* is given by

$$F_l(l_i) = F_o [4.435(l_i/l_o)^4 - 16.46(l_i/l_o)^3 + 18.28(l_i/l_o)^2 - 5.333(l_i/l_o) + 0.1150], \quad (80)$$

where $F_o = 0.46$ N is the maximum isometric force and $l_o = .0103$ m the optimal muscle length.

The muscle lengths l_i and velocities \dot{l}_i that appear in (77-80) will be determined by the coupled mechanical (force and moment balance) equations. The motoneuronal excitation function $F_a(t)$ is derived as follows.

Raffaele - NEED YOUR INPUT HERE!!

In [SH03] we showed that the results summarised in §5.2 for the simpler actuated spring LLS of Fig. 26 – the preservation of a branch of stable gaits with the additional property of speed stabilization as per Figs. 27-28 – persist for the Hill muscle pair of Fig. 37(b). We expect that this will hold for hexapedal models, but to properly incorporate muscles we require a more realistic model than the abstracted telescopic leg with a sliding pivot of §5.2. To avoid excessive complexity, we follow Full and Ahn [FA95, Fig. 2] in simplifying the four-component cockroach limbs to a two rigid links, connected to the body at a ‘hip,’ representing the coxa-trochanteral joint, and pivoted at a ‘knee’ or ‘ankle,’ representing the femur-tibia joint. These joints display the greatest angular variations [KWF97]. Similarly, the musculo-apodeme complexes active during the stance phase are collapsed to a single Hill-type element that pulls on the extension of the femur past the coxa-trochanteral joint: see Fig. 38. Rather than including a second (antagonist) element, we rely on passive damping in the knee joint to perform the bulk of the negative work in each stance phase.

NEEDS COMPLETING!!

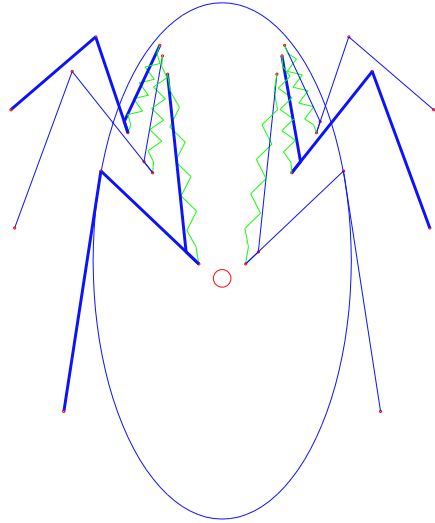


Figure 38: Geometry of the hexapodal model with actuated muscles and two-component legs. For each leg a single Hill type muscle represents the depressor muscle complexes active during stance. The pivots represent the coxa-trochanteral and femur-tibia joints, and torsional stiffness and dissipation can be included in both joints.

5.5 A note on proprioceptive feedback

The neuromechanical model that we have sketched above still lacks reflexive feedback and overall CNS control. In particular, our CPG model is ‘wired’ to produce a stable antiphase tripod gait. (It possesses other periodic gait patterns, but they are unstable [GH04].) Tryba and Ritzmann [TR00a, TR00b] present evidence of different inter- and intra-limb (joint) phase relations during slow walking and searching behaviors, and the extensive work on stick insect locomotion [CKS⁺98, CBMWC98, BB98, Cru02] indicates that proprioceptive feedback from strain sensors (campaniform sensillae) and hair cells [Zil85, RFRZ98] will be important in regulating inter-limb motions in these regimes. Pearson [PI70, Pea72, PI72] shows that campaniform sensillae make excitatory connections to slow depressor motoneurons and inhibitory connections to bursting interneurons, thereby reinforcing the depressor muscle activity during stance, while tonic inputs from other leg receptors exert the opposite effect. It is also known that overall CNS commands excite both CPG neurons and motoneurons, and that, in turn, CPG outputs can signif-

icantly modulate reflexive feedback pathways [CCR00]. The review [Pea95] cites many further references on proprioceptive feedback.

Keep higher level goal-oriented feedback out of it at this stage, except for brief discussions in conclusions and future challenges?

NEEDS COMPLETING!!

6 Conclusions: Open problems and challenges

To be done. Suggestions welcome!!

Acknowledgements: This work was supported by DARPA/ONR: N00014-98-1-0747, DoE: DE-FG02-95ER25238, and **John - Add support details!!**. Raffaele Ghigliazza provided helpful comments and numerous references, and Justin Seipel prepared many of the figures. The work that led to this review was begun in June 1998 at the Institute for Mathematics and its Applications (Minnesota) Workshop on Animal Locomotion and Robotics, which we all attended, and at which some of us first met. We thank the organisers for inviting us.

References

- [01] 2001.
- [Abb94] L. F. Abbott. Single neuron dynamics. In F. Ventriglia, editor, *Neural Modeling and Neural Networks*, chapter 4, pages 57–78. Pergamon Press, Oxford, UK, 1994.
- [ABGB01] T. Akay, U. Bässler, P. Gerharz, and A. Büschges. The role of sensory signals from the insect coxa-trochanteral joint in controlling motor activity of the femur-tibia joint. *J. Neurophysiol.*, 85 (2):594–604, 2001.
- [ADO97] Y. I. Arshavsky, T. G. Deliagina, and G. N. Orlovsky. Pattern generation. *Current Opinion in Neurobiology*, 7:781–789, 1997.
- [AJ78] R.McN. Alexander and A.S. Jayes. Vertical movements in running and walking. *J. Zool. London*, 185:27–40, 1978.

- [AJ83] R.McN. Alexander and A.S. Jayes. A dynamic similarity hypothesis for the gaits of quadrupedal mammals. *J. Zool. London*, 201:135–152, 1983.
- [AKH02] R. Altendorfer, D. E. Koditschek, and P. Holmes. Towards a factored analysis of legged locomotion models. Technical Report CSE-TR-467-02, University of Michigan, 2002.
- [AKH04a] R. Altendorfer, D.E. Koditschek, and P. Holmes. Stability analysis of a clock-driven rigid-body SLIP model for RHex. *Int. J. Rob. Res.*, page (submitted), 2004.
- [AKH04b] R. Altendorfer, D.E. Koditschek, and P. Holmes. Stability analysis of legged locomotion models by symmetry-factored return maps. *Int. J. Rob. Res.*, page (submitted), 2004.
- [Ale03] R.McN. Alexander. *Principles of Animal Locomotion*. Princeton University Press, Princeton, N.J., 2003.
- [AM85] R. Abraham and J. Marsden. *Foundations of Mechanics*. Addison-Wesley, New York, 1985.
- [AMK⁺01] Altendorfer, A.N. Moore, H. Komsuoglu, M. Buehler, H.B. Brown, D. McMordie, U. Saranli, R.J. Full, and D.E. Koditschek. RHex: A biologically inspired hexapod runner. *J. Autonomous Robots*, 11:207–213, 2001.
- [Arn78] V.I. Arnold. *Mathematical Methods of Classical Mechanics*. Springer Verlag, New York, 1978.
- [BB98] U. Bässler and A. Büschges. Pattern generation for stick insect walking movements – multisensory control of a locomotor program. *Brain Research Reviews*, 27(1):65–88, 1998.
- [BBL96] N.A. Borghese, L. Bianchi, and F. Lacquaniti. Kinematic determinants of human locomotion. *J. Physiol.*, 494 (3):863–879, 1996.
- [BF87] R. Blickhan and R.J. Full. Locomotion energetics of the ghost crab: II. Mechanics of the centre of mass during walking and running. *J. Exp. Biol.*, 130:155–174, 1987.
- [BF93] R. Blickhan and R.J. Full. Similarity in multi-legged locomotion: bouncing like a monopode. *J. Comp. Physiol. A*, 173:509–517, 1993.

- [BGM93] A. Back, J. Guckenheimer, and M. Myers. A dynamical simulation facility for hybrid systems. In *Lecture Notes in Computer Science, Vol. 736*, pages 255–267. Springer-Verlag, Berlin, 1993.
- [BH75] A. Bryson and Y. Ho. *Applied Optimal Control*. Taylor and Francis, New York, 1975.
- [Bir27] G.D. Birkhoff. *Dynamical Systems*. American Mathematical Society, Providence, RI, 1927. Colloquium Publications Vol 9, reprinted 1966.
- [BK90] M. Buehler, D.E. Koditschek, and ?? A family of robot control strategies for intermittent dynamical environments. *IEEE Control Systems Magazine*, 10 (2):16–22, 1990.
- [BKMR96] A.M. Bloch, P.S. Krishnaprasad, J.E. Marsden, and T.S. Ratiu. Nonholonomic mechanical systems with symmetry. *Arch. Rat. Mech. Anal.*, 136:21–99, 1996.
- [BL00] I.E. Brown and G.E. Loeb. A reductionist approach to creating and using neuromusculoskeletal movement. In J.M. Winters and P.E. Crago, editors, *Biomechanics and Neural Control of Movement*, pages 148–163. Springer-Verlag, New York, 2000.
- [Bli89] R. Blickhan. The spring-mass model for running and hopping. *J. Biomechanics*, 11/12:1217–1227, 1989.
- [BM98] A. Büschges and A.E. Manira. Sensory pathways and their modulation in the control of locomotion. *Current Opinion in Neurobiology*, 8:733–739, 1998.
- [BMH⁺03] E. Brown, J. Moehlis, P. Holmes, E. Clayton, J. Rajkowski, and G. Aston-Jones. The influence of spike rate and stimulus duration on noradrenergic neurons. Unpublished manuscript, Program in Applied and Computational Mathematics, Princeton University, 2003.
- [BMH04] E. Brown, J. Moehlis, and P. Holmes. On the phase reduction and response dynamics of neural oscillator populations. *Neural Comp.*, 16 (4):673–715, 2004.

- [BPD02] P.J. Beek, C.E. Peper, and A. Daffertshofer. Modeling rhythmic interlimb coordination: Beyond the Haken-Kelso-Bunz model. *Brain and Cognition*, 48:149–165, 2002.
- [BS83] M. Burrows and M. V. S. Siegler. Networks of local interneurons in an insect. In A. Roberts and B. L. Roberts, editors, *Neural Origin of rhythmic movements*, volume 37 of *Symposia of the Society for Experimental Biology*, pages 29–53. Cambridge University Press, Cambridge, UK, 1983.
- [BSL95] I.E. Brown, S.H. Scott, and G.E. Loeb. “Preflexes” – programmable, high-gain, zero-delay intrinsic responses of perturbed musculoskeletal systems. *Soc. Neurosci. Abstr.*, 21:562.9, 1995.
- [BT86] A.A. Biewener and C.R. Taylor. Bone strain: a determinant of gait and speed? *J. Exp. Biol.*, 123:383–400, 1986.
- [BT97] V. Blondel and J.N. Tsitsiklis. NP-hardness of some linear control design problems. *SIAM Journal on Control and Optimization*, 35(6):2118–2127, 1997.
- [BTSD00] E. Bizzi, M.C. Tresch, P. Saltiel, and A. D’Avella. New perspectives on spinal motor systems. *Nature Reviews Neurosci.*, 1:101–108, 2000.
- [Bur80] M. Burrows. The control of sets of motoneurons by local interneurons in the locust. *Journal of Physiology*, 298:213–233, 1980.
- [Bur99] R.E. Burke. Revisiting the notion of ‘motor unit types’. *Prog. Brain Res.*, 123:167–175, 1999.
- [Bur02] R.E. Burke. Some unresolved issues in motor unit research. *Adv. Exp. Med. Biol.*, 508:171–178, 2002.
- [BW91] G. Bowtell and T.L. Williams. Anguilliform body dynamics: modelling the interaction between muscle activation and curvature. *Phil. Trans. Roy. Soc. B*, 334:385–390, 1991.
- [BW94] G. Bowtell and T.L. Williams. Anguilliform body dynamics: a continuum model for the interaction between muscle activation and body curvature. *J. Math Biol.*, 32:83–91, 1994.

- [CBD⁺97] C.C. Canavier, R.J. Butera, R.O. Dror, D.A. Baxter, J.W. Clark, and J.H. Byrne. Phase response characteristics of model neurons determine which patterns are expressed in a ring model of gait generation. *Biol. Cybern.*, 77:367–380, 1997.
- [CBMWC98] G.S. Cymbaluk, R.M. Borisyuk, U. Müller-Wilm, and H. Cruse. Oscillatory network controlling six-legged locomotion: Optimization of model parameters. *Neural Networks*, 11:1449–1460, 1998.
- [CCR97] M.J. Coleman, A. Chatterjee, and A. Ruina. Motions of a rimless spoked wheel: a simple three-dimensional system with impacts. *Dynamics and Stability of Systems*, 12(3):139–159, 1997.
- [CCR00] F. Clarac, D. Cattaert, and D. Le Ray. Central control components of a ‘simple’ stretch reflex. *Trends Neurosci.*, 23(5):199–208, 2000.
- [CGMR01] M.J. Coleman, M. Garcia, K. Mombaur, and A. Ruina. Prediction of stable walking for a toy that cannot stand. *Phys. Rev. E*, 64:022901–1–3, 2001.
- [CH99] M.J. Coleman and P. Holmes. Motions and stability of a piecewise holonomic system: the discrete Chaplygin sleigh. *Regular and Chaotic Dynamics*, 4(2):1–23, 1999.
- [CHR82] A.H. Cohen, P. Holmes, and R.H. Rand. The nature of coupling between segmental oscillators of the lamprey spinal generator for locomotion: a model. *J. Math Biol.*, 13:345–369, 1982.
- [CHT77] G.A. Cavagna, N.C. Heglund, and C.R. Taylor. Mechanical work in terrestrial locomotion: two basic mechanisms for minimizing energy expenditure. *Am. J. Physiol.*, 233 (5):R243–R261, 1977.
- [CJ99] J.M. Camhi and E.N. Johnson. High frequency steering maneuvers mediated by tactile cues: Antennal wall-following in the cockroach. *J. Exp. Biol.*, 202:631–643, 1999.
- [CK93] A.H. Cohen and T. Kiemel. Intersegmental coordination: lessons from modeling systems of non-linear oscillators. *Amer. Zool.*, 33:54–65, 1993.

- [CKS⁺98] H. Cruse, T. Kindermann, M. Schumm, J. Dean, and J. Schmitz. Walknet – a biologically inspired network to control six-legged walking. *Neural Networks*, 11:1435–1447, 1998.
- [CR98] M.J. Coleman and A. Ruina. An uncontrolled walking toy that cannot stand still. *Phys. Rev. Lett.*, 80 (16):3658–3661, 1998.
- [CRE88] A.H. Cohen, S. Rossignol, and S. Grillner (Eds). *Neural Control of Rhythmic Movements in Vertebrates*. Wiley, 1988.
- [CRH88] A.H. Cohen, R.H. Rand, and P. Holmes. Systems of coupled oscillators as models of central pattern generators. In A.H. Cohen, S. Rossignol, and S. Grillner, editors, *Neural Control of Rhythmic Movements in Vertebrates*, pages 333–367. Wiley, 1988.
- [Cru02] H. Cruse. The functional sense of central oscillations in walking. *Biol. Cybern.*, 86 (4):271–80:271–8, 2002.
- [CS93] J.J. Collins and I. Stewart. Hexapodal gaits and coupled nonlinear oscillator models. *Biol. Cybern.*, 68:287–298, 1993.
- [CTZ76] G.A. Cavagna, H. Thys, and A. Zamboni. The sources of external work in level walking and running. *J. Physiol. Lond.*, 262:639–657, 1976.
- [CW80] A.H. Cohen and P. Wallén. The neuronal correlate of locomotion in fish. “Fictive swimming” induced in an in vitro preparation of the lamprey spinal cord. *Exp. Brain. Res.*, 41:11–18, 1980.
- [CWB98] J. Carling, T.L. Williams, and G. Bowtell. Self-propelled anguilliform swimming: simultaneous solution of the two-dimensional Navier-Stokes equations and Newton’s laws of motion. *J. Exp. Biol.*, 201:3143–3166, 1998.
- [DA01] P. Dayan and L.F. Abbott. *Theoretical Neuroscience*. MIT Press, Cambridge, MA, 2001.
- [DCC00] J. Duysens, F. Clarac, and H. Cruse. Load-regulating mechanisms in gait and posture: Comparative aspects. *Physiol. Rev.*, 80 (1):83–13, 2000.

- [DCF⁺97] E. Doedel, A. Champneys, T. Fairgrieve, B. Sandstede, Y. Kuznetsov, and X. Wang. Auto 97: Continuation and bifurcation software for ordinary differential equations. Technical report, Concordia University, 1997. Available via FTP from directory /pub/doedel/auto at ftp.cs.concordia.ca; software available from <http://indy.cs.concordia.ca/auto/> and <http://sourceforge.net/projects/auto2000>.
- [Del80] F. Delcomyn. Neural basis of rhythmic behaviours in animals. *Science*, 210:492–498, 1980.
- [Del85] F. Delcomyn. Walking and running. In G.A. Kerkut and L.I. Gilbert, editors, *Comprehensive Insect Physiology Biochemistry and Pharmacology*, pages 439–466. Pergamon Press, New York, 1985.
- [Del91] F. Delcomyn. Perturbation of the motor system in freely walking cockroaches II. The timing of motor activity in leg muscles after amputation of a middle leg. *J. Exp. Biol.*, 156:503–517, 1991.
- [DFF⁺00] M.H. Dickinson, C.T. Farley, R.J. Full, M.A.R. Koehl, R. Kram, and S. Lehman. How animals move: an integrative view. *Science*, 288:100–106, 2000.
- [EG99] Ö. Ekeberg and S. Grillner. Simulations of neuromuscular control in lamprey swimming. *Phil. Trans. Roy. Soc. B*, 354:895–902, 1999.
- [EK86] G.B. Ermentrout and N. Kopell. Symmetry and phase locking in chains of weakly coupled oscillators. *Comm. Pure Appl. Math.*, 39:623–660, 1986.
- [EK90] G.B. Ermentrout and N. Kopell. Oscillator death in systems of coupled neural oscillators. *SIAM J. on Appl. Math.*, 50:125–146, 1990.
- [EK91] G.B. Ermentrout and N. Kopell. Multiple pulse interactions and averaging in systems of coupled neural oscillators. *J. Math. Biol.*, 29:195–217, 1991.
- [Eke93] Ö. Ekeberg. A combined neuronal and mechanical model of fish swimming. *Biol. Cybernetics*, 69:363–374, 1993.

- [Erm96] B. Ermentrout. Type I membranes, phase resetting curves, and synchrony. *Neural Comp.*, 8:979–1001, 1996.
- [Erm02] G.B. Ermentrout. *Simulating, Analyzing, and Animating Dynamical Systems: A Guide to XPPAUT for Researchers and Students*. SIAM, Philadelphia, 2002.
- [FA95] R.J. Full and A.N. Ahn. Static forces and moments generated in the insect leg: comparison of a three-dimensional musculoskeletal computer model with experimental measurements. *J. Exp. Biol.*, 198:1285–1298, 1995.
- [FBT91] R.J. Full, R. Blickhan, and L.H. Ting. Leg design in hexapedal runners. *J. Exp. Biol.*, 158:369–390, 1991.
- [FF00] R.J. Full and C.T. Farley. Musculoskeletal dynamics in rhythmic systems - A comparative approach to legged locomotion. In J.M. Winters and P.E. Crago, editors, *Biomechanics and Neural Control of Movement*, pages 192–205. Springer-Verlag, New York, 2000.
- [Fit60] R. Fitzhugh. Thresholds and plateaus in the Hodgkin-Huxley nerve equations. *J. of General Physiol.*, 43:867–896, 1960.
- [Fit61] R. Fitzhugh. Impulses and physiological states in theoretical models of nerve membrane. *Biophys. J.*, 1:455–466, 1961.
- [FK99] R.J. Full and D.E. Koditschek. Templates and anchors: neuromechanical hypotheses of legged locomotion on land. *J. Exp. Biol.*, 202:3325–3332, 1999.
- [FKS⁺02] R.J. Full, T. Kubow, J. Schmitt, P. Holmes, and D. Koditschek. Quantifying dynamic stability and maneuverability in legged locomotion. *Integ. and Comp. Biol.*, 42:149–157, 2002.
- [FSAJ98] R.J. Full, D. Stokes, A.N. Ahn, and R.K. Josephson. Energy absorption during running by leg muscles in a cockroach. *J. Exp. Biol.*, 201:997–1012, 1998.
- [FT90] R.J. Full and M.S. Tu. Mechanics of six-legged runners. *J. Exp. Biol.*, 148:129–146, 1990.

- [FT91a] C.T. Farley and C.R. Taylor. A mechanical trigger for the trot-gallop transition in horses. *Science*, 253:306–308, 1991.
- [FT91b] R.J. Full and M.S. Tu. Mechanics of a rapid running insect: two-, four- and six-legged locomotion. *J. Exp. Biol.*, 156:215–231, 1991.
- [Ful89] R.J. Full. Mechanics and energetics of terrestrial locomotion: From bipeds to polypeds. In W. Weiser and E. Gnaiger, editors, *Energy Transformation in Cells and Animals*, pages 175–182. Georg Thieme Verlag, Stuttgart, Germany, 1989.
- [Ful91] R.J. Full. Animal motility and gravity. *Physiologist*, 34:S15–18, 1991.
- [Ful97] R.J. Full. Invertebrate locomotor systems. In W. Dantzler, editor, *The handbook of comparative physiology*, pages 853–930. Oxford University Press, New York, 1997.
- [FYJ95] R.J. Full, A. Yamauchi, and D.L. Jindrich. Maximum single leg force production: cockroaches righting on photoelastic gelatin. *J. Exp. Biol.*, 198:2441–2452, 1995.
- [GAHK03] R. Ghigliazza, R. Altendorfer, P. Holmes, and D. Koditschek. A simply stabilized running model. *SIAM J. on Applied Dynamical Systems*, 2 (2):187–218, 2003.
- [GCRC98] M. Garcia, A. Chatterjee, A. Ruina, and M.J. Coleman. The simplest walking model: Stability, complexity and scaling. *ASME J. Biomech. Eng.*, 120 (2):281–288, 1998.
- [Get88] P. A. Getting. Comparative analysis of invertebrate central pattern generators. In A. H. Cohen, S. Rossignol, and S. Grillner, editors, *Neural Control of Rhythmic Movements in Vertebrates*, chapter 4, pages 101–128. John Wiley, New York, NY, 1988.
- [GGMA01] M.S. Goldman, J. Golowasch, E. Marder, and L.F. Abbott. Global structure, robustness, and modulation of neuronal models. *J. Neurosci.*, 21 (14):5229–5238, 2001.
- [GH90] J. Guckenheimer and P. Holmes. *Nonlinear Oscillations, Dynamical Systems, and Bifurcations of Vector Fields*. Springer-Verlag, New York, NY, 1990.

- [GH04] R.M. Ghigliazza and P. Holmes. A minimal model of bursting pacemakers and motoneurons for insect locomotion. *????*, *??:??*, 2004.
- [Gil97] C. Gilbert. Visual control of cursorial prey pursuit by tiger beetles (Cicindelidae). *J. Comp. Physiol. A*, 181 (3):217–230, 1997.
- [GJM⁺96] A. Griewank, D. Juedes, H. Mitev, J. Utke, O. Vogel, and A. Walther. Adol-c: A package for the automatic differentiation of algorithms written in c/c++. *ACM TOMS*, 22 (2):131–167, 1996. Algor. 755, see also <http://www.math.tu-dresden.de/wir/project/adolc/>.
- [GKP⁺00] M. Garcia, A. Kuo, A. Peattie, P. Wang, and R.J. Full. Damping and size: Insights and biological inspiration. *The Intl. Symp. on Adaptive Motion of Animals and Machines*, 2000.
- [GM00] J. Guckenheimer and B. Meloon. Computing periodic orbits and their bifurcations with automatic differentiation. *SIAM J. Sci. Stat. Comp.*, 22:951–985, 2000.
- [Gol80] H. Goldstein. *Classical Mechanics*. Addison Wesley, Reading, MA, 1980. Second edition.
- [Gov85] P.B. Gove, editor. *Webster's Third New International Dictionary of the English Language unabridged*. Merriam, Springfield, MA., 1985.
- [Gri85] S. Grillner. Neurobiological bases of rhythmic motor acts in vertebrates. *Science*, 228:143–149, 1985.
- [Gri99] S. Grillner. Bridging the gap - from ion channels to networks and behaviour. *Current Opinion in Neurobiology*, 9:663–669, 1999.
- [Gri00] A. Griewank. *Evaluating Derivatives: Principles and Techniques of Algorithmic Differentiation*. SIAM Press, Philadelphia, PA, 2000.
- [GS85] M. Golubitsky and D. G. Schaeffer. *Singularities and Groups in Bifurcation Theory, Volume I*. Springer-Verlag, New York, 1985.

- [GSBC98] M. Golubitsky, I. Stewart, P.L. Buono, and J.J. Collins. A modular network for legged locomotion. *Physica D*, 115:56–72, 1998.
- [GSBC99] M. Golubitsky, I. Stewart, P.L. Buono, and J.J. Collins. The role of symmetry in locomotor central pattern generators and animal gaits. *Nature*, 401:693–695, 1999.
- [GSS88] M. Golubitsky, I. Stewart, and D. G. Schaeffer. *Singularities and Groups in Bifurcation Theory, Volume II*. Springer-Verlag, New York, 1988.
- [GTM02] M.S.A. Graziano, C.S.R. Taylor, and T. Moore. Complex movements evoked by microstimulation of prefrontal cortex. *Neuron*, 34:841–851, 2002.
- [Guc75] J. Guckenheimer. Isochrons and phaseless sets. *J. Math. Biol.*, 1:259–273, 1975.
- [GWBL91] S. Grillner, P. Wallén, L. Brodin, and A. Lansner. Neuronal network generating locomotor behavior in lamprey. *Annual Review in Neuroscience*, 14:169–199, 1991.
- [HH52] A. Hodgkin and A. Huxley. A quantitative description of membrane current and its application to conduction and excitation in nerve. *J. Physiol.*, 117:500–544, 1952.
- [HHB85] J.A. Kelso H. Haken and H. Bunz. A theoretical model of phase transitions in human hand movements. *Biol. Cybern.*, 51 (5):347–356, 1985.
- [HI97] F.C. Hoppensteadt and E.M. Izhikevich. *Weakly Connected Neural Networks*. Springer-Verlag, New York, 1997.
- [Hol90] P. Holmes. Poincaré, celestial mechanics, dynamical systems theory and “chaos”. *Physics Reports*, 193 (3):137–163, 1990.
- [HR84] J.L. Hindmarsh and R. Rose. A model of neuronal bursting using three coupled first order differential equations. *Proc. Roy. Soc. Lond. B*, 221:87–102, 1984.
- [HT81] D.F. Hoyt and C.R. Taylor. Gait and the energetics of locomotion in horses. *Nature*, 292:239–240, 1981.

- [HT88] N.C. Heglund and C.R. Taylor. Speed, stride frequency and energy cost per stride. How do they change with body size and gait? *J. Exp. Biol.*, 138:301–318, 1988.
- [HW91] E. Hairer and G. Wanner. *Solving Ordinary Differential Equations II: Stiff and Differential Algebraic Problems*. Springer-Verlag, New York, 1991.
- [IGML02] Y.P. Ivanenko, R. Grasso, V. Macellari, and F. Lacquaniti. Two-thirds power law in human locomotion: role of ground contact forces. *Neuroreport*, 13 (9):1171–1174, 2002.
- [Ijs01] A.J. Ijspeert. A connectionist central pattern generator for the aquatic and terrestrial gaits of a simulated salamander. *Biol. Cybern.*, 84:331–348, 2001.
- [JF02] D. Jindrich and R.J. Full. Dynamic stabilization of rapid hexapedal locomotion. *J. Exp. Biol.*, 205:2803–2823, 2002.
- [JKC96] R. Jung, T. Kiemel, and A.H. Cohen. Dynamic behavior of a neural network model of locomotor control in the lamprey. *J. Neurophysiol.*, 75 (3):1074–1086, 1996.
- [Jon94] C.K.R.T. Jones. *Geometric Singular Perturbation Theory*, volume 1609 of *Lecture Notes in Mathematics*. Springer Verlag, Heidelberg, 1994. C.I.M.E. Lectures.
- [JW95] D. Johnston and S.M-S. Wu. *Foundations of Cellular Neurophysiology*. MIT Press, Cambridge, MA, 1995.
- [Kaw99] M. Kawato. Internal models for motor control and trajectory planning. *Current Opinion in Neurobiology*, 9:718–72, 1999.
- [KB91] D.E. Koditschek and M. Buehler. Analysis of a simplified hopping robot. *Int. J. Robotics Res.*, 10 (6):587–605, 1991.
- [KC98] T. Kiemel and A.H. Cohen. Estimation of coupling strength in regenerated lamprey spinal cords based on a stochastic phase model. *J. Comp. Neurosci.*, 5:267–284, 1998.
- [KE90] N. Kopell and G.B. Ermentrout. Phase transitions and other phenomena in chains of coupled oscillators. *SIAM J. on Appl. Math.*, 50:1014–1052, 1990.

- [KEW91] N. Kopell, G.B. Ermentrout, and T.L. Williams. On chains of oscillators forced at one end. *SIAM J. on Appl. Math.*, 51:1397–1417, 1991.
- [KF99] T.M. Kubow and R.J. Full. The role of the mechanical system in control: a hypothesis of self-stabilization in hexapedal runners. *Phil. Trans. Roy. Soc. Lond. B*, 354:849–861, 1999.
- [KFDC01] J.A.S. Kelso, P. W. Fink, C.R. DeLaplain, and R.G. Carson. Haptic information stabilizes and destabilizes coordination dynamics. *Proc. Roy. Soc. Lond. B*, 268:1207–1213, 2001.
- [KFK03] T. Kubow, R.J. Full, D. Koditschek, and ???. A posture principle in cockroach running. (in preparation), 2003.
- [KK02] E. Klavins and D.E. Koditschek. Phase regulation of decentralized cyclic robotic systems. *Int. J. Robotics Res.*, 3:257–275, 2002.
- [KKK01] E. Klavins, H. Komsuoglu, and D.E. Koditschek. Coordination and control for locomotion. In A. Rudolph, editor, *Neurotechnology for Biomimetic Robots*, pages ??–?? MIT Press, Boston, MA, 2001.
- [KL94] N. Kopell and G. LeMasson. Rhythmogenesis, amplitude modulation, and multiplexing in a cortical architecture. *Proc. Natl. Acad. Sci. U S A*, 91 (22):10586–10590, 1994.
- [Kop88] N. Kopell. Toward a theory of modelling generators. In A.H. Cohen, S. Rossignol, and S. Grillner, editors, *Neural Control of Rhythmic Movements in Vertebrates*, pages 369–413. Wiley, 1988.
- [KS98] J. Keener and J. Sneyd. *Mathematical Physiology*. Springer, New York, 1998.
- [Kuo02] A.D. Kuo. The relative roles of feedforward and feedback in the control of rhythmic movements. *Motor Control*, 6 (2):129–145, 2002.
- [KWF97] R. Kram, B. Wong, and R.J. Full. Three-dimensional kinematics and limb kinetic energy of running cockroaches. *J. Exp. Biol.*, 200:1919–1929, 1997.

- [LBC99] G.E. Loeb, I.E. Brown, and E.J. Cheng. A hierarchical foundation for models of sensorimotor control. *Exp. Brain Res.*, 126 (1):1–18, 1999.
- [LGZ99] F. Lacquaniti, R. Grasso, and M. Zago. Motor patterns in walking. *News Physiol. Sci.*, 14 (4):168–174, 1999.
- [LPSB01] C-S.R. Li, C. Padoa-Schioppa, and E. Bizzi. Neuronal correlates of motor performance and motor learning in the primary motor cortex of monkeys adapting to an external force field. *Neuron*, 30:593–607, 2001.
- [LTV83] F. Lacquaniti, C. Terzuolo, and P. Viviani. The law relating the kinematic and figural aspects of drawing movements. *Acta Psychol.*, 54 (1-2):115–130, 1983.
- [Mal49] I.G. Malkin. *Methods of Poincaré and Linstedt in the Theory of Nonlinear Oscillations*. Gostexisdat, Moscow, 1949. In Russian.
- [Mal56] I.G. Malkin. *Some Problems in Nonlinear Oscillation Theory*. Gostexisdat, Moscow, 1956. In Russian.
- [Mar76] R. Margaria. *Biomechanics and Energetics of Muscular Exercise*. Oxford University Press, Oxford, UK, 1976.
- [Mar00a] E. Marder. Motor pattern generation. *Current Opinion in Neurobiology*, 10:691–698, 2000.
- [Mar00b] E. Marder. Motor pattern generation. *Current Opinion in Neurobiology*, 10 (6):691–698, 2000.
- [MB83] T.A. McMahon and J. Bonner. *On Size and Life*. Scientific American Books/W.H. Freeman and Co., New York, NY, 1983.
- [MC90] T.A. McMahon and G.C. Cheng. The mechanics of running: how does stiffness couple with speed? *J. Biomechanics*, 23 (suppl 1):65–78, 1990.
- [McG75] R. McGehee. Triple collisions in newtonian gravitational systems. In J. Moser, editor, *Dynamical Systems, Theory and Applications*, pages 550–572. Springer-Verlag, Berlin, 1975. Lecture Notes in Physics, Vol. 38.

- [McG90] T. McGeer. Passive bipedal running. *Proc. Roy. Soc. Lond.*, B 240:107–134, 1990.
- [McM84] T. McMahon. *Muscles, Reflexes and Locomotion*. Princeton University Press, Princeton, NJ, 1984.
- [Mei01] Kenneth Meijer. Personal communication, 2001.
- [MGK⁺98] K. Meijer, H.J. Grootenboer, H.F.J.M. Koopman, B.J.J.J. van der Linden, and P.A. Huijing. A Hill type model of rat medial gastrocnemius muscle that accounts for shortening history effects. *J. of Biomech.*, 31(6):555–564, 1998.
- [MI99] F.A. Mussa-Ivaldi. Modular features of motor control and learning. *Current Opinion in Neurobiology*, 9:713–717, 1999.
- [MLBS02] K.D. Mombaur, R.W. Longman, H.G. Bock, and J.P. Schlöder. Stable one-legged hopping without feedback and with a point foot. In *IEEE International Conference on Robotics and Automation*, volume 4, pages 3978–3983, 2002.
- [MM80] S. Mochon and T.A. McMahon. Ballistic walking. *J. Biomechanics*, 13:49–57, 1980.
- [MM81] S. Mochon and T.A. McMahon. Ballistic walking: an improved model. *Math. Biosci.*, 52:241–260, 1981.
- [Mur01] J.D. Murray. *Mathematical Biology, 3rd. Ed.* Springer, New York, 2001.
- [NF72] J.I. Neĭmark and N.A. Fufaev. *Dynamics of Nonholonomic Systems*. American Mathematical Society, Providence, RI, 1972.
- [NFK00] J. Nakanishi, T. Fukuda, and D.E. Koditschek. A brachiating robot controller. *IEEE Trans. Rob. Aut.*, 16(2):109–123, 2000.
- [Pea72] K.G. Pearson. Central programming and reflex control of walking in the cockroach. *J. Exp. Biol.*, 56:173–193, 1972.
- [Pea93] K.G. Pearson. Common principles of motor control in vertebrates and invertebrates. *Ann. Rev. Neurosci.*, 16:265–297, 1993.

- [Pea95] K.G. Pearson. Proprioceptive regulation of locomotion. *Current Opinion in Neurobiology*, 5:786–791, 1995.
- [Pea00] K.G. Pearson. Motor systems. *Current Opinion in Neurobiology*, 10:649–654, 2000.
- [Phi03] E. Phipps. *Taylor series integration of differential-algebraic equations: automatic differentiation as a tool for simulating rigid body mechanical systems*. PhD thesis, Cornell University, 2003.
- [PI70] K.G. Pearson and J.F. Iles. Discharge patterns of coxal levator and depressor motoneurons in the cockroach *periplaneta americana*. *J. Exp. Biol.*, 52:139–165, 1970.
- [PI71] K.G. Pearson and J.F. Iles. Innervation of the coxal depressor muscles in the cockroach *periplaneta americana*. *J. Exp. Biol.*, 54:215–232, 1971.
- [PI72] K.G. Pearson and J.F. Iles. Nervous mechanisms underlying intersegmental co-ordination of leg movements during walking in the cockroach. *J. Exp. Biol.*, 58:725–744, 1972.
- [PSB04] I. Poulakakis, A. Smith, and M. Buehler. Experimentally validated bounding models for the Scout II quadruped robot. In *International Conference on Robotics and Automation*, page (in press). IEEE, Sep. 2004.
- [Rai86] M. Raibert. *Legged Robots that Balance*. MIT Press, Cambridge, MA, 1986.
- [RE99] J. Rinzel and G. B. Ermentrout. Analysis of excitability and oscillations. In C. Koch and I. Segev, editors, *Methods in neuronal modeling: From ions to networks*, chapter 7, pages 251–291. MIT Press, Cambridge, MA, 1999.
- [Ree04] M.C. Reed. Why is mathematical biology so hard? *AMS Notices*, 51 (3):338–342, 2004.
- [RF02] M.J. Richardson and T. Flash. Comparing smooth arm movements with the two-thirds power law and the related segmented-control hypothesis. *J. Neurosci.*, 22 (18):8201–8211, 2002.

- [RFRZ98] A.L. Ridgel, S.F. Frazier, R.A.DiCaprio, and S.N. Zill. Encoding of forces by cockroach tibial campaniform sensilla: implications in dynamic control of posture and locomotion. *J. Comp. Physiol. A*, 186:359–374, 1998.
- [RH89] R. Rose and J.L. Hindmarsh. The assembly of ionic currents in a thalamic neuron I: The three-dimensional model. *Proc. Roy. Soc. Lond. B*, 237:267–288, 1989.
- [Rin87] J. Rinzel. A formal classification of bursting mechanisms in excitable systems. In E. Teramoto and M. Yamaguti, editors, *Mathematical Topics in Population Biology, Morphogenesis, and Neurosciences*, Lecture Notes in Biomathematics, pages 267–281. Springer Verlag, 1987.
- [RK94] A.A. Rizzi and D.E. Koditschek. Further progress in robot juggling: Solvable mirror laws. In *Int. Conf. Rob. and Aut.*, pages 2935–2940, 1994.
- [RL86] J. Rinzel and Y.S. Lee. On different mechanisms for membrane potential bursting. In H. Othmer, editor, *Nonlinear Oscillations in Biology and Chemistry*, pages 19–33. Springer Verlag, 1986. Lecture Notes in Biomathematics, Vol 66.
- [RL87] J. Rinzel and Y.S. Lee. Dissection of a model for neuronal parabolic bursting. *J. Math. Biol.*, 25:653–675, 1987.
- [Rui98] A. Ruina. Non-holonomic stability aspects of piecewise holonomic systems. *Reports on Mathematical Physics*, 42(1/2):91–100, 1998.
- [SBK95] P.J. Swanson, R.R. Burridge, and D.E. Koditschek. Global asymptotic stability of a passive juggler: a parts feeding strategy. *Mathematical Problems in Engineering*, 1:193–224, 1995.
- [SBK01] U. Saranli, M. Buehler, and D.E. Koditschek. Rhex: A simple and highly mobile hexapod robot. *The International Journal of Robotics Research*, 20(7):616–631, 2001.
- [Sch98] W.J. Schwind. *Spring Loaded Inverted Pendulum Running: A Plant Model*. PhD thesis, University of Michigan at Ann Arbor, 1998.

- [SER⁺98] A. Selverston, R. Elson, M. Rabinovich, R. Huerta, and H. Abarbanel. Basic principles for generating motor output in the stomatogastric ganglion. In O. Kiehn, R. M. Harris-Warrick, and N. Kudo L. M. Jordan H. Hultborn, editors, *Neuronal Mechanisms for Generating Locomotor Activity*, volume 860, pages 35–50. New York Academy of Sciences, 1998.
- [SG02] A. Seyfarth and H. Geyer. Natural control of spring-like running – optimized self-stabilization. In *Proceedings of the Fifth International Conference on Climbing and Walking Robots (CLAWAR 2002)*, pages 81–85. Professional Engineering Publishing Limited, 2002.
- [SGBH02] A. Seyfarth, H. Geyer, R. Blickhan, and H. Herr. Does leg retraction simplify control in running? In *IV. World Congress of Biomechanics*, Calgary, Canada, 2002.
- [SGGB02] A. Seyfarth, H. Geyer, M. Günther, and R. Blickhan. A movement criterion for running. *J. Biomech.*, 35:649–655, 2002.
- [SGH03] A. Seyfarth, H. Geyer, and H. Herr. Swing leg retraction: a simple control model for stable running. *J. Exp. Biol.*, 206:2547–2555, 2003.
- [SGR⁺02] J. Schmitt, M. Garcia, R.C. Razo, P. Holmes, and R.J. Full. Dynamics and stability of legged locomotion in the horizontal plane: A test case using insects. *Biol. Cybern.*, 86(5):343–353, 2002.
- [SH00a] J. Schmitt and P. Holmes. Mechanical models for insect locomotion: Dynamics and stability in the horizontal plane – Application. *Biol. Cybern.*, 83(6):517–527, 2000.
- [SH00b] J. Schmitt and P. Holmes. Mechanical models for insect locomotion: Dynamics and stability in the horizontal plane – Theory. *Biol. Cybern.*, 83(6):501–515, 2000.
- [SH01] J. Schmitt and P. Holmes. Mechanical models for insect locomotion: Stability and parameter studies. *Physica D*, 156(1-2):139–168, 2001.
- [SH03] J. Schmitt and P. Holmes. Mechanical models for insect locomotion: Active muscles and energy losses. *Biol. Cybern.*, 89(1):43–55, 2003.

- [SHF04] J. Seipel, P. Holmes, and R.J. Full. Dynamics and stability of insect locomotion: A hexapedal model for horizontal plane motions. *????, ??:??-??*, 2004. In preparation.
- [Sin78] D. Singer. Stable orbits and bifurcations of maps of the interval. *SIAM J. on Appl. Math.*, 35:260–267, 1978.
- [Sin91] Y. Sinai. Hyperbolic billiards. In *Proceedings of the International Congress of Mathematicians*, pages 18–??, Berlin, 1991. Springer-Verlag.
- [SK97] W.J. Schwind and D.E. Koditschek. Characterization of monopod equilibrium gaits. In *Proc. IEEE Int. Conf. on Rob. and Aut.*, pages 1986–1992, Albuquerque, NM, 1997.
- [SK00] W.J. Schwind and D.E. Koditschek. Approximating the stance map of a 2 dof monopod runner. *J. Nonlin. Sci.*, 10(5):533–568, 2000.
- [SK03] U. Saranli, D.E. Koditschek, and ??. Template based control of hexapedal running. In *IEEE Int. Conference on Robotics and Automation, Taiwan*, 2003.
- [SM99] A.B. Schwartz and D.W. Moran. Motor cortical activity during drawing movements: population representation during lemniscate tracing. *J. Neurophysiol.*, 82 (5):2705–2718, 1999.
- [SS01] S. Schaal and D. Sternad. Origins and violations of the 2/3 power law in rhythmic three-dimensional arm movements. *Exp. Brain Res.*, 136 (1):60–72, 2001.
- [SSA96] S. Schaal, D. Sternad, and C.G. Atkeson. One-handed juggling: A dynamical approach to a rhythmic movement task. *J. Motor Behavior*, 28:165–183, 1996.
- [SSK98] U. Saranli, W.J. Schwind, and D.E. Koditschek. Toward the control of a multi-jointed, monopod runner. In *Proc. IEEE Int. Conf. on Rob. and Aut.*, pages 2676–2682, Leuven, Belgium, 1998.
- [SWDA⁺01] P. Saltiel, K. Wyler-Duda, A.D’Avella, M.C. Tresch, and E. Bizzi. Muscle synergies encoded within the spinal cord: Evidence from focal intraspinal NMDA iontophoresis in the frog. *J. Neurophysiol.*, 85 (2):605–619, 2001.

- [Swi02] S. P. Swinnen. Intermanual coordination: from behavioural principles to neural-network interactions. *Nature Neurosci.*, 3 (5):348–359, 2002.
- [TBF94] L.H. Ting, R. Blickhan, and R.J. Full. Dynamic and static stability in hexapedal runners. *J. Exp. Biol.*, 197:251–269, 1994.
- [TJ98] E. Todorov and M.I. Jordan. Smoothness maximization along a predefined path accurately predicts the speed profiles of complex arm movements. *J. Neurophysiol.*, 80 (2):696–714, 1998.
- [TJ02] E. Todorov and M.I. Jordan. Optimal feedback control as a theory of motor coordination. *Nature Neurosci.*, 5 (11):1226–1235, 2002.
- [Tod00] E. Todorov. Direct cortical control of muscle activation in voluntary arm movements: a model. *Nature Neurosci.*, 3 (4):391–398, 2000.
- [TR00a] A.K. Tryba and R.E. Ritzmann. Multi-joint coordination during walking and foothold searching in the Blaberus cockroach. I. Kinematics and electromyograms. *J. Neurophysiol.*, 83:3323–3336, 2000.
- [TR00b] A.K. Tryba and R.E. Ritzmann. Multi-joint coordination during walking and foothold searching in the Blaberus cockroach. II. Extensor motor patterns. *J. Neurophysiol.*, 83:3337–3350, 2000.
- [Utk77] V. Utkin. Variable structure systems with sliding modes. *IEEE Transactions on Automatic Control*, AC-22(2):212–231, 1977.
- [Wal86] K.J. Waldron. Force and motion management in legged locomotion. *IEEE J. Robotics and Automation*, RA-2 (4):214–220, 1986.
- [WKG03] E. Westervelt, J. Grizzle, and D. Koditschek. Hybrid zero dynamics of planar biped walkers. *IEEE Transactions on Automatic Control*, 48:42–56, 2003.

- [WHCM03] S.J. Wickl, D.F. Hoyt, E.A. Cogger, and G. Myers. The energetics of the trot-gallop transition. *J. Exp. Biol.*, 206:1557–1564, 2003.
- [Win01] A. Winfree. *The Geometry of Biological Time*. Springer, New York, 2001.
- [WR98a] J.T. Watson and R.E. Ritzmann. Leg kinematics and muscle activity during treadmill running in the cockroach, *blaberus discoidalis*. I. Slow running. *J. Comp. Physiol. A*, 182:11–22, 1998.
- [WR98b] J.T. Watson and R.E. Ritzmann. Leg kinematics and muscle activity during treadmill running in the cockroach, *blaberus discoidalis*. II. Transition to fast running. *J. Comp. Physiol. A*, 182:23–33, 1998.
- [Wri02] P. Wriggers. *Computational Contact Mechanics*. Wiley, New York, 2002.
- [WV84] K. J. Waldron and V. J. Vohnout. Configuration design of the adaptive suspension vehicle. *Int. J. Rob. Res.*, 3 (2):37–48, 1984.
- [Zaj89] F.E. Zajac. Muscle and tendon: properties, models, scaling, and application to biomechanics and motor control. *Critical Rev. in Biomed. Eng.*, 17(4):359–411, 1989.
- [Zil85] S.N. Zill. Proprioceptive feedback and the control of cockroach walking. In W.J.P. Barnes and M.H. Galden, editors, *Feedback and Motor Control in Invertebrates and Vertebrates*, pages 187–208. Croom Helm, London, UK, 1985.
- [ZS99] E.P. Zehr and R.B. Stein. What functions do reflexes serve during human locomotion?”. *Prog. Neurobiol.*, 58 (2):185–205, 1999.